Analysis of Flow Reversal under Two-Phase Natural Circulation in CANDU9 during Small Loss of Coolant Accident with Loss of Class IV Power

ANALYSIS OF FLOW REVERSAL UNDER TWO-PHASE NATURAL CIRCULATION IN CANDU9 DURING SMALL LOSS OF COOLANT ACCIDENT WITH LOSS OF CLASS IV POWER

BY

CHANGRUI YU, B.Eng.

A THESIS

SUBMITTED TO THE DEPARTMENT OF ENGINEERING PHYSICS

AND THE SCHOOL OF GRADUATE STUDIES

OF MCMASTER UNIVERSITY

IN PARTIAL FULFILMENT OF THE REQUIREMENTS

FOR THE DEGREE OF

MASTER OF APPLIED SCIENCE

Master of Applied Science (2016) McMaster University

(Engineering Physics) Hamilton, Ontario, Canada

TITLE:	Analysis of Flow Reversal under Two-Phase Natural Circulation in CANDU9 during Small Loss of Coolant Accident with Loss of Class IV Power
AUTHOR:	Changrui Yu B.Eng., (Nuclear Engineering and Technology) University of Science and Technology of China
SUPERVISOR:	Dr. John C. Luxat
NUMBER OF PAGES:	xi, 144

Abstract

A thermal hydraulic analysis has been conducted to investigate the conditions leading to the channel flow reversal and the subsequent effects that may have on the Primary Heat Transfer System(PHTS) thermohydraulic parameters during the natural circulation under the specific accident scenarios for a generic CANDU 900 MW plant model similar to Darlington NGS. The assumed initiating events are the combination of a small Loss Of Coolant Accident (LOCA) with a loss of Class IV power, as well as the unavailability of Emergency Coolant Injection (ECI) system. No makeup inventory is taken into account in this study, and there is no fuel sheath temperature excursion or fuel centerline melting, i.e., the integrity of fuel is always maintained.

A one-dimensional quasi-steady state Homogeneous Equilibrium Model(HEM) has been constructed for the study. A specific node-link structure is adopted to represent the primary heat transfer loop: The whole loop and different components in HTS are represented by a series of nodes that have quasi-static thermal hydraulic characteristics such as pressure and enthalpy, etc. Dynamic characteristics are delivered by the links between nodes, e.g., flow rate and pressure drop. The channel powers (decay heat), the secondary side pressure and the pressure at Reactor Inlet Header(RIH) are chosen as boundary conditions to describe the assumed initiating incidents for the

model.

With ongoing loss of inventory and system depressurization, vapor lock occurs in Steam Generator(SG), and it increases the pressure drop from Reactor Outlet Header(ROH) to RIH across SG and forms an increasingly negative RIH-to-ROH pressure differential. Flow reversal occurs in the channel due to the counter force balance between negative RIH-to-ROH pressure difference and the driving force derived from the density difference between the hot and cold legs. It is found that channels in row A have the highest reversal preference, then followed by the channels in row B, and in that order subsequently. Row A reverses when inventory decreases to about 79.5% of initial value, with following boundary conditions: decay heat is 1.5% of Full Power(FP) and secondary side pressure is 5.070 MPa. In addition, it is found that the decrease in channel power accelerates the depressurization process and brings forward the occurrence of flow reversal in fuel channels.

Acknowledgements

First and foremost I wish to express my deepest appreciation to my supervisor Dr. Luxat for his long-standing support and guidance throughout this project. I would also like to thank Dr. Nagasaki and Dr. Jackson for their generous help and suggestions on my thesis and defence.

I would like to thank Dr. Rouben and Dr. Popov for their brilliant courses that helped me improve my understanding of nuclear engineering and industry. And I appreciate the chance to work with Dr. Nagasaki and Barry as a TA on EP 4U04, in which I have learned a lot.

I am grateful to my fellow colleagues and friends, Kurt, Shlomi, Izaak, Alex, Zack, Shaun, Hummel, James, Fred, Feng, Ahmad, Yang, Mengmeng, Travis, Dave, Matt, Chris, Garik, Kendall, Jay, Remon, Wesley, Salma, Andrew, Jared, Xiaopan, Justin, Mohammed and everyone else who I might have forgotten. It is my pleasure to work, study and play with you guys in past two years. I would also like to thank my friends Puzhen, Dong, Shan and all other nice fellows in Canada.

Last but not least, I am greatly grateful to the understanding and support from my family.

Notation and abbreviations

Acronyms

PHTS Primary Heat Transfer System

CANDU CANada Deuterium Uranium

LOCA Loss Of Coolant Accident

ECI Emergency Cooling Injection

HEM Homogeneous Equilibrium Model

FP Full Power

SG Steam Generator

RIH Reactor Inlet Header

ROH Reactor Outlet Header

UST Unit Service Transformer

SST Station Service Transformer

SDS	Shutdown System
EPS	Emergency Power System
PHTP	Primary Heat Transport Pump
PT	Pressure Tube
CT	Calandria Tube
LWR	Light Water Reactor
FE	Fuel Element
EF	End Fitting
IF	Inlet Feeder
OF	Outlet Feeder
IBIF	Intermittent Buoyancy Induced Flow

Letters

P	Pressur
H	Enthalpy
ϵ	Tube surface roughness
S	Slip rate
ρ	Density
ν	Special volume
μ	Viscosity
x_e	Thermal quality
x	Flow quality
α	Void fraction
Re	Reynolds Number
f	Friction factor
ϕ_{lo}^2	Two phase multiplier for friction pressure drop, liquid only
g	Gravity acceleration
int	mass inventory

Contents

List of Figures

Chapter 1

Introduction

In safety analysis for CANada Deuterium Uranium (CANDU) reactor, understanding the thermal hydraulic behavior of the PHTS during potential accident scenarios is an important research subject. In some accident scenarios, the HTS inventory is reduced to the level that can lead to the flow reversal in some channels. Flow reversal creates a new flow path that bypasses the intended heat sink, SG. This may jeopardize the safety of PHTS. The aim of this study is to investigate the conditions leading to channel flow reversal and the subsequent effects that may have on PHTS thermohydraulic parameters during the natural circulation under specific accident scenarios.

The assumed initiating events are the combination of a small LOCA with a loss of Class IV power, as well as the unavailability of ECI system. In addition, no makeup of HTS inventory is credited in this study. A turbine trip is assumed to occur simultaneously with loss of Class IV power. There is no fuel sheath temperature excursion or fuel centerline melting during the initial phases of the accident sequence, i.e., the integrity of fuel is always maintained.

A small LOCA in a CANDU is conventionally defined as the break in any pipe within PHTS, with an area up to the size of twice the cross-section of the largest feeder pipe. (Spurious opening of a Liquid Relief Valve is also included in this category.) Without makeup inventory, a small LOCA can lead to the slow loss of coolant inventory and depressurization of the PHTS. The pressure controller action is rendered ineffective due to the loss of electrical power to the pressurizer immersion heaters.

Table 1.1: Classification of power sources[17]

Class of power	System load characteristics
Class I	Power can never be interrupted under postulated conditions
Class II	Power can be interrupted up to 4 milliseconds
Class III	Power can be interrupted up to 5 minutes
Class IV	Power can be interrupted indefinitely

According to the design of CANDU electrical system, all power sources of a CANDU unit are divided into four levels based on the allowed duration of interruption that can be tolerated by the loads they supply, as shown in Table 1.1. Table 1.2 shows the partial lists of the systems and equipment that are powered by Class III and IV power supply systems. It can be seen that Class IV power supports many important process systems in a CANDU plant including main heat transport circulating pumps and main boiler feed pumps.

Table 1.2: Equipments supported by each Class III and IV power supplies.[17]

Class	Equipments
III	Auxiliary boiler feed pumps
	Auxiliary condensation extraction pumps
	Shutdown system cooling pumps
	Turbine turning gear
	Heat transport feed pumps
	Moderator circulating pumps
	Class I power rectifiers
	Fire water pumps
	Emergency core coolant injection pumps
	Instrument air compressors
	End shield cooling pumps
	Service water pumps
IV	Main boiler feed pumps
	Main heat transport circulating pumps
	Condenser cooling water pumps
	Generator excitation
	Heating and ventilation equipment
	Normal lighting systems

As shown in Fig. 1.1, Class IV supplies come from two sources. During normal operation, Class IV power is obtained from the main generator through the Unit

Service Transformers (USTs), using the power generated internally by the plant's own generator. Class IV power can also be obtained from the grid through the Station Service Transformers (SSTs) when the USTs are unavailable.

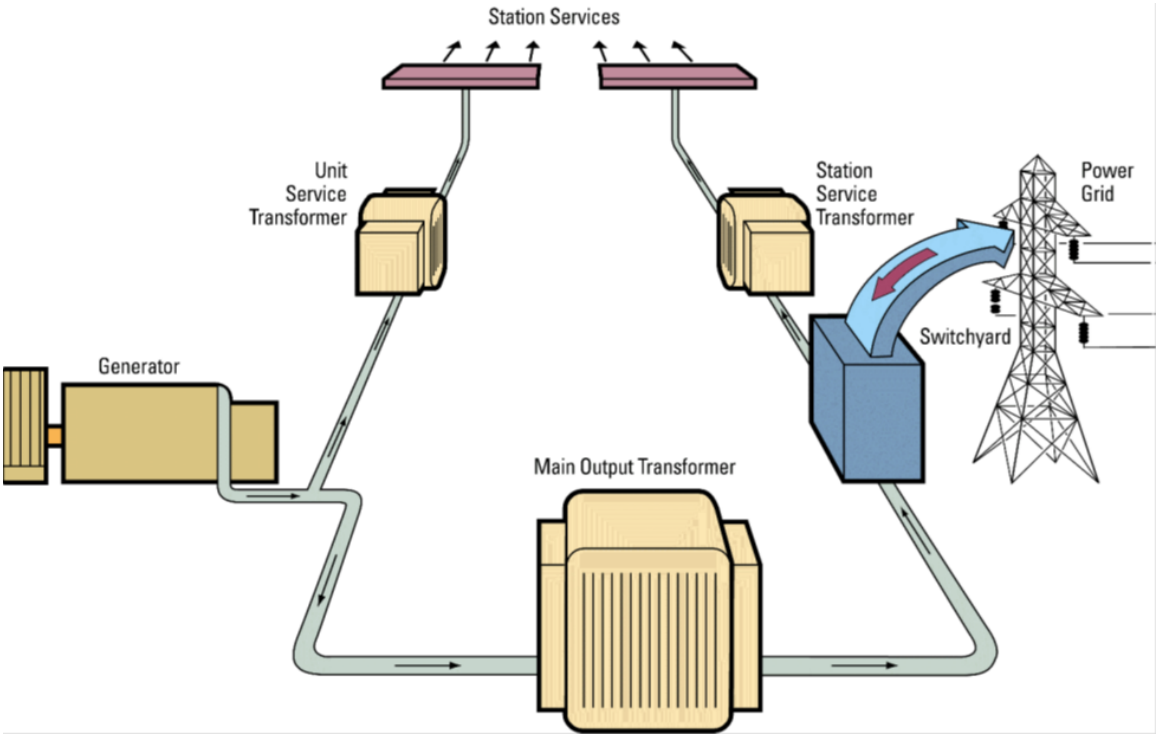

Figure 1.1: Class IV power is supplies by USTs and SSTs.[17]

If failures occur to USTs and SSTs, Class IV power supplies are lost, and forced circulation within the primary loop will cease due to the rundown of PHTS pumps, and the main boiler feed pumps are tripped as well. According to the design operation logic, once experiencing the loss of Class IV power source, the unit will be shut down immediately by one of its two Shutdown systems (SDS1 and SDS2), so the heat generation rate in fuel channels will fall to the decay heat level with an exponential

trend, as shown in Fig. 1.2.

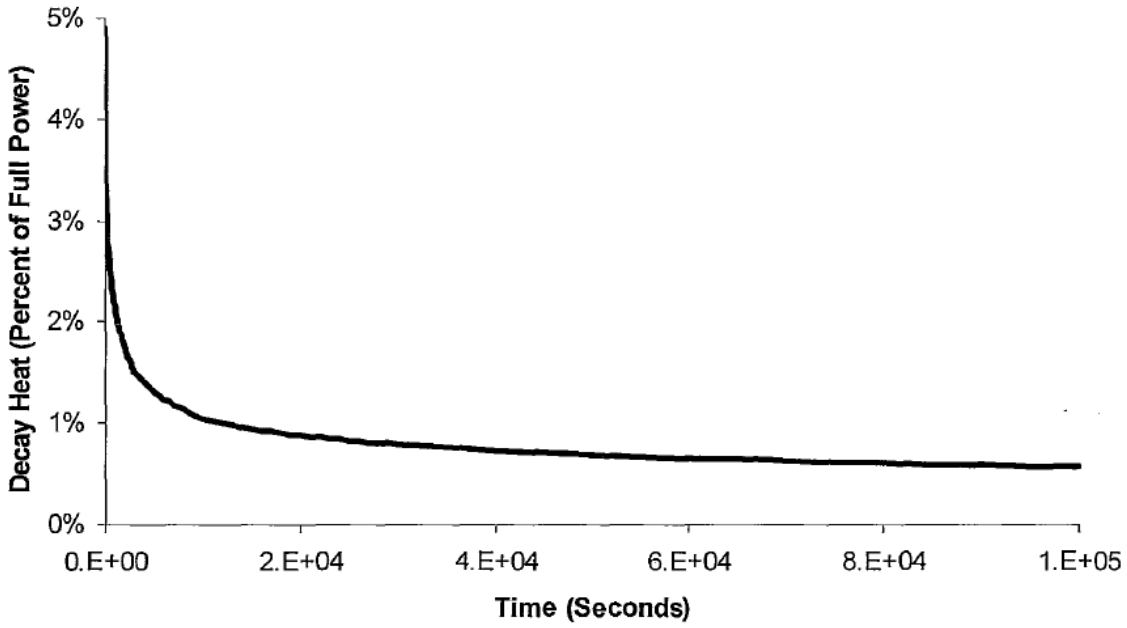

Figure 1.2: After reactor trip, heat generation rate falls with an exponential trend.

If Class III power, supplied by on-site standby diesel generators and/or Emergency Power System (EPS), is available, auxiliary boiler feed pumps and shutdown system cooling pumps that are supported by Class III power are still operational. So the primary heat sinks are kept on shutdown level, and the decay heat in the primary loop can be removed to the secondary loop by SGs.

It should be noted that, although ECI pumps are supported by Class III power, there is a possibility that it is not initiated due to random failures. Therefore, ECI system is assumed not to be available in this study, and as a result, there is no crash

cooldown of the SGs .

Because of the special layout of CANDU PHTS, the primary heat sinks are located above primary heat sources, and natural circulation can be established. The heat transfer capability to remove decay heat is maintained by single- or two-phase natural convection driven by the density difference between the hot and cold legs of PHTS in the absence of forced circulation. However, with the ongoing loss of coolant inventory from HTS, two-phase natural circulation may at some point be interrupted. Flow reversal phenomena may occur in some channels under two-phase conditions.

The loss of the primary coolant inventory and the depressurization of PHTS may result in the generation and/or the accumulation of void within the inverted U-tubes of SG, when inventory and system pressure have decreased below certain level. The appearance of void in boiler tubes can partially block the flow path through SG and consequently increase the flow resistance across it. This effect is referred to as vapor lock in this report. With the occurrence of vapor lock, a large negative pressure differential can be formed between RIH and ROH. The negative RIH-to-ROH pressure difference can trigger the occurrence of flow reversal in some channels when it is negative enough to overcome the forward driving forces derived from the density differences across these channels.

Based on the assumption that small LOCA is a relatively slow process, a quasi-steady state model has been built to analyze the results of the assumed initiating accidents. A specific node-link structure is adopted to represent the primary heat

transfer loop: The whole loop and different components in HTS are represented by a series of nodes that have quasi-static thermal hydraulic characteristics such as pressure and enthalpy, etc. Dynamic characteristics are generated by the links between nodes, e.g., flow rate and pressure drop. Once the boundary conditions are provided, with the help of the conservation equations of mass, energy and momentum, as well as the equation of state of coolant fluid, the thermal hydraulic properties of the whole loop can be simulated. In this study, the channel powers (decay heat), the secondary side pressure and the pressure at RIH are chosen as boundary conditions. With hypothetical flow rate of the loop, information regarding pressure and enthalpy is delivered from node to node, and updated iteratively until a converged flow rate is obtained. Once the convergence is achieved, all thermal hydraulic properties of each node can be calculated with equation of state, using pressure and enthalpy as input variables. At this point, the distributions of all thermal hydraulic parameters, including pressure and flow, are known. They are used to analyze PHTS thermal hydraulic behavior and to predict the occurrence of flow reversal by changing different boundary conditions.

Despite local thermal hydraulic features in each node, global features of HTS can also be inspected by summing the values in each node. For example, with the density and volume of each node, the total mass inventory can be calculated. It is a key thermal hydraulic parameter that influences all HTS behavior. So total inventory is calculated to understand macro-behavior of HTS for each change of boundary conditions. It is chosen as the independent variable to investigate other thermal hydraulic parameters for the assumed accident scenarios.

Some useful results have been collected in the study, and they provide good insights into understanding the behavior and consequences of the loss of inventory and the occurrence of flow reversal.

The plant chosen for the analysis in this report is a generic CANDU 900 MW plant model similar to Darlington NGS. The geometry parameters are from Sabouri[21].

This report consists of six chapters. Chapter Two briefly introduces the important design features and the key components of CANDU 9 reactor that are related to the thermal hydraulic analysis in this study. Chapter Three provides a literature review of the previous work that is related to the concerning problems in this study, and it presents good insights into understanding flow reversal phenomenon and its related research methods. Chapter Four introduces the necessary theoretical background of the current topic, and an approach to build simulation model is also presented in this chapter. The analysis and discussions of simulation results have been provided in Chapter Five. The last chapter of the report summarizes the important conclusions of the study, and some expectations on future work have also been proposed in the chapter.

Chapter 2

Overview of CANDU 9 reactor

A CANDU reactor is pressurized heavy water reactor that utilizes natural uranium as fuel. The whole CANDU system is shown in Fig. 2.1, and its detailed parameters are presented in various technology manuals [3].

2.1 Global View

As shown in Fig. 2.1, CANDU system is huge and complicated, and it contains a lot of sub-systems for different functions. This report will just focus on PHTS that concerns natural circulation and flow reversal. The key function of PHTS is to transfer fission heat from the primary heat source, reactor channels, to the primary heat sink, steam generators, via a circulation loop that consists of a series of piping components. It is presented in Fig. 2.2.

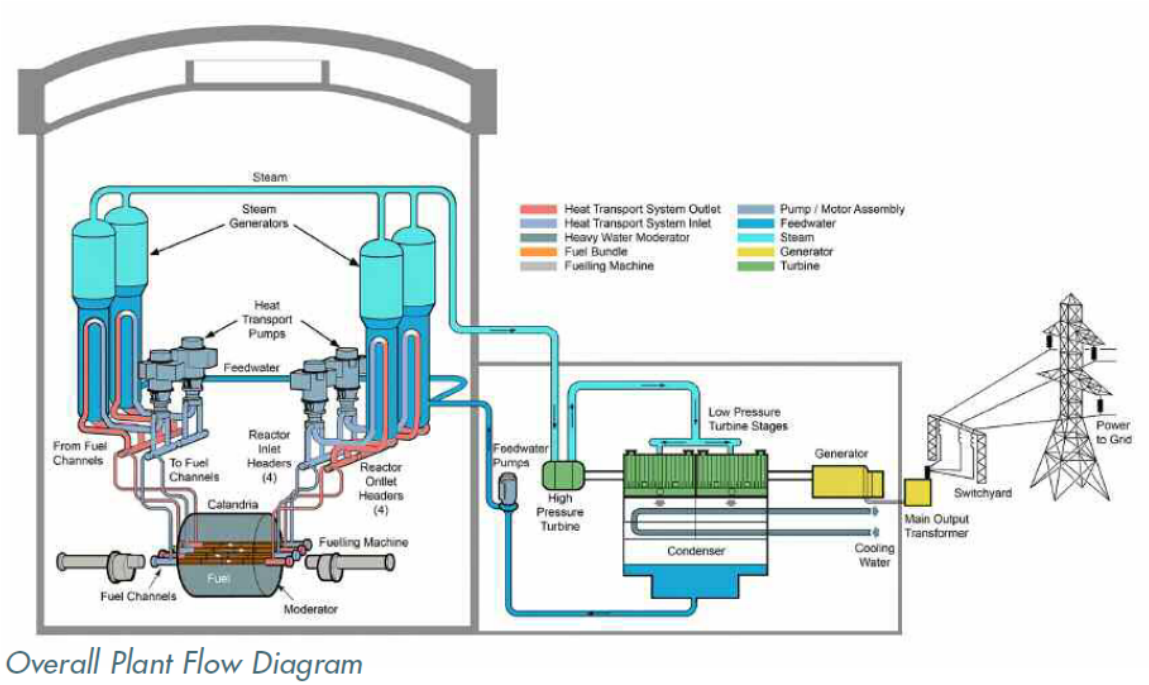

Figure 2.1: overview of CANDU system [3]

2.2 PHTS

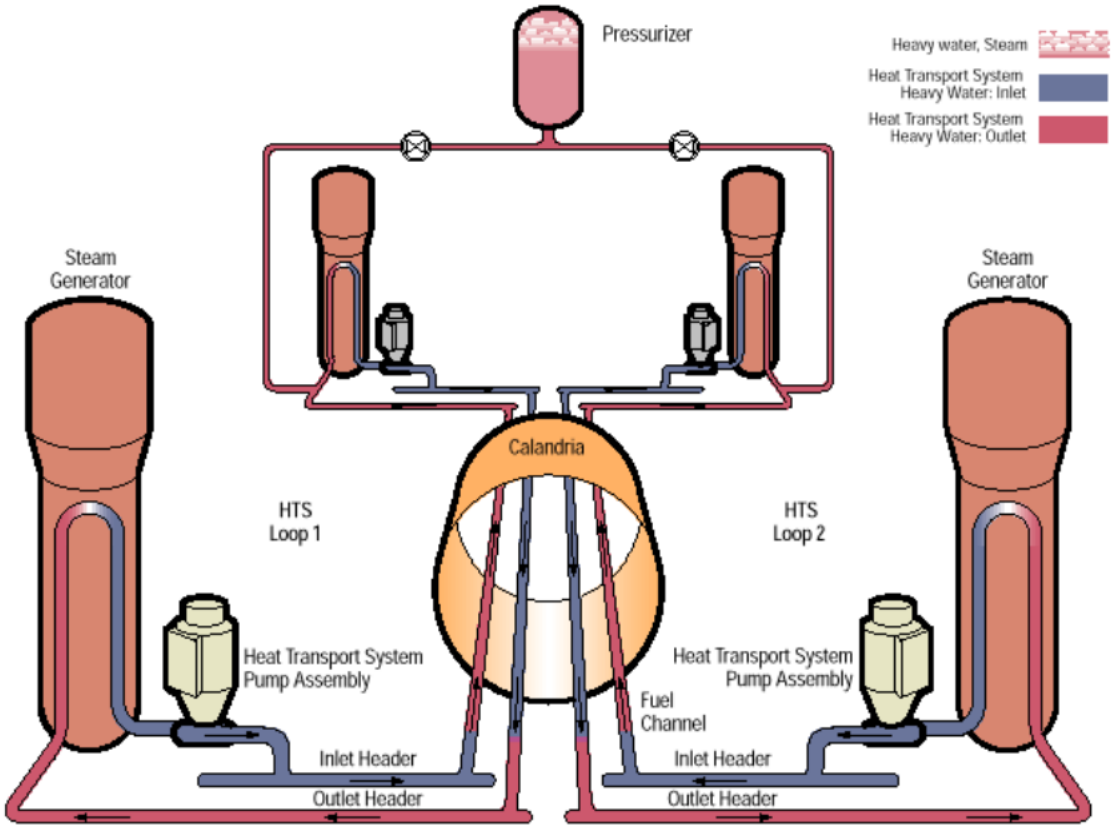

Figure 2.2: Primary Heat Transfer System for CANDU 9 [3]

As shown in Fig. 2.2, a typical CANDU PHTS has two separate loops, and each loop contains 2 SGs, 2 Primary Heat Transport Pumps (PHTPs), and 2 pairs of RIHs and ROHs. These components are divided into two flow passes and are arranged in a Figure-of-Eight configuration. Low-temperature coolant flows from RIH-1 to ROH-1 through the core, where it is heated to high temperature. Then this high-temperature coolant leaves the ROH-1 and goes through SG-1, through which heat is transferred to

the secondary side with the coolant temperature being reduced to close to secondary side saturated temperature. The lower-temperature coolant flows through pump-1 and enters into RIH-2 on the other side of reactor face. This coolant flow is referred to as a flow pass. In second flow pass, the high-temperature coolant flows from ROH-2 and to SG-2, where heat is extracted, and lower-temperature coolant goes across pump-2 and finally goes back to RIH-1. The two flow passes form a complete flow loop.

The following paragraphs will introduce individual components that are important for PHTS. They include reactor core, end fittings, feeders, headers as well as steam generator.

2.3 Reactor Core

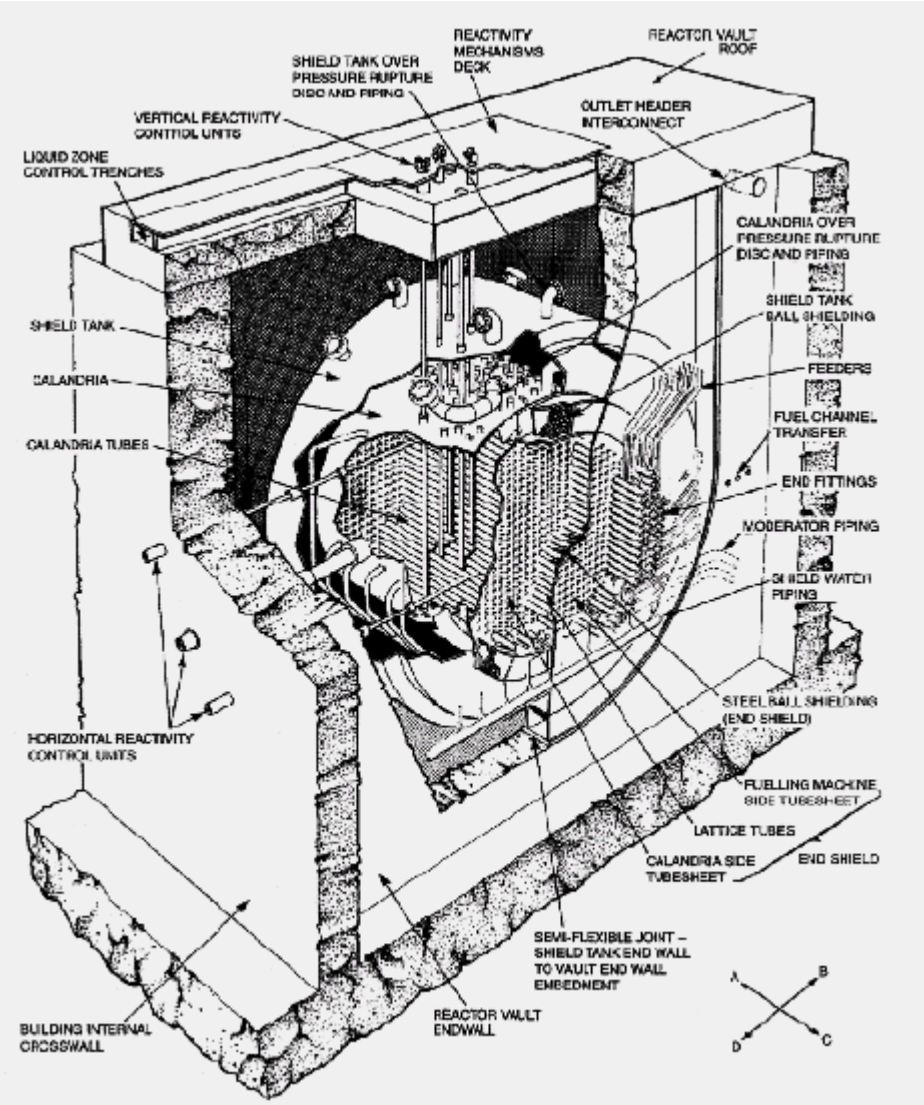

Figure 2.3: CANDU reactor core [3]

As a pressurized heavy water reactor, CANDU reactor core has many special features that make it a unique reactor type. Fig. 2.3 illustrates some of its essential design features:

1. The reactor contains individual fuel channels consisting of a pressure tube contained within a calandria tube. The annulus between the two tubes is filled with carbon dioxide gas that insulates the hot, high pressure coolant in the pressure tube from the low pressure and temperature heavy water moderator surrounding the calandria tubes.

2. All fuel channels are arranged in horizontal direction.

3. Large horizontal cylinder-shaped stainless steel Calandria Vessel acts as the key structural component that holds fuel channels and contains heavy water moderator within the space between fuel channels and Calandria Vessel inner surface.

4. In CANDU 9, the Calandria Vessel is submerged in the light water that is held by Shield Tank and End Shields, which provide both thermal and biological shielding.

5. It should be noted that CANDU6 has 380 fuel channels, while CANDU9 has 480 fuel channels. So within CANDU9, each flow pass has 120 channels, through which coolant flows around the loop. The details of fuel channels are described below.

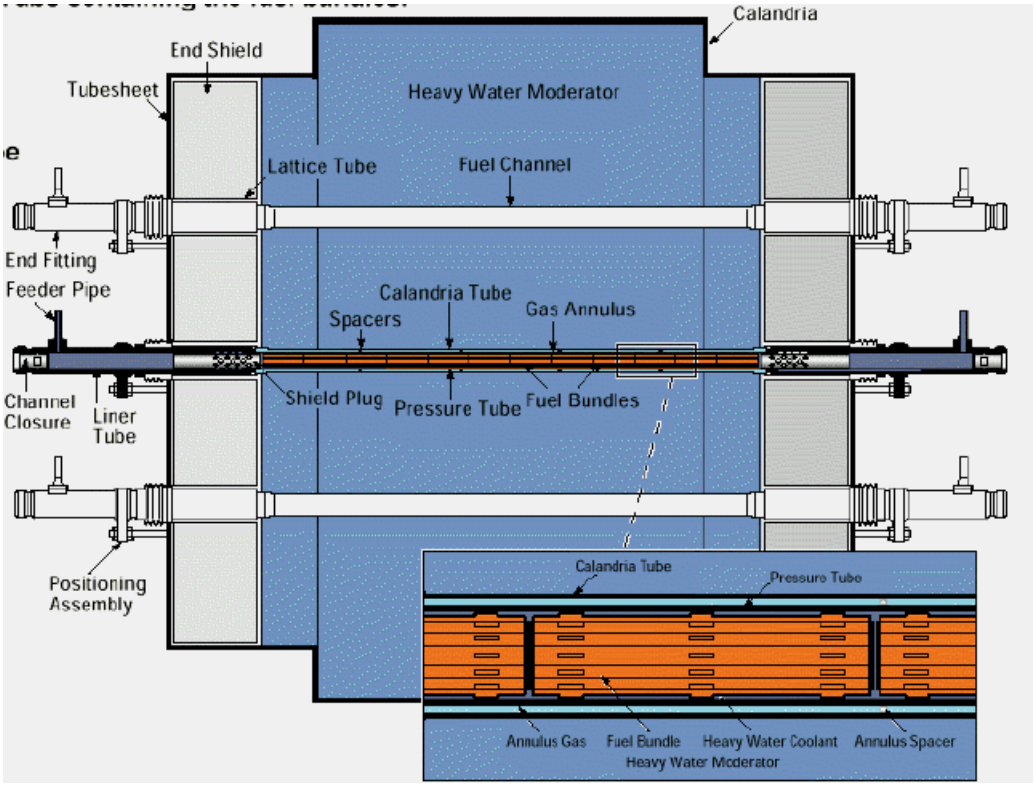

Figure 2.4: Cross section of CANDU 9 reactor core [3]

Fig. 2.4 shows a cross section of Calandria, End Shield and fuel channel assemblies, and Fig. 2.5 illustrates the design details of fuel channel assembly. It can be seen that the whole fuel channel assembly is divided into three sections: the pressure tube section containing the fuel bundles and two End Fitting sections at either end of the pressure tube.

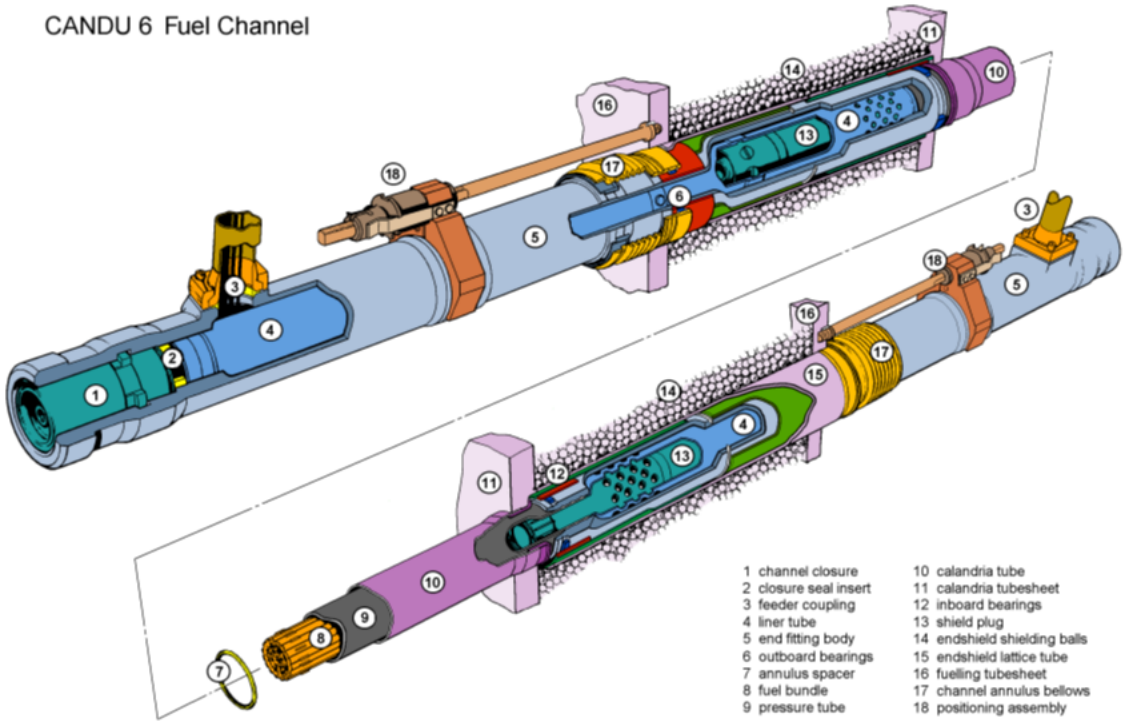

Figure 2.5: Fuel Channel for CANDU [3]

2.4 Fuel Section

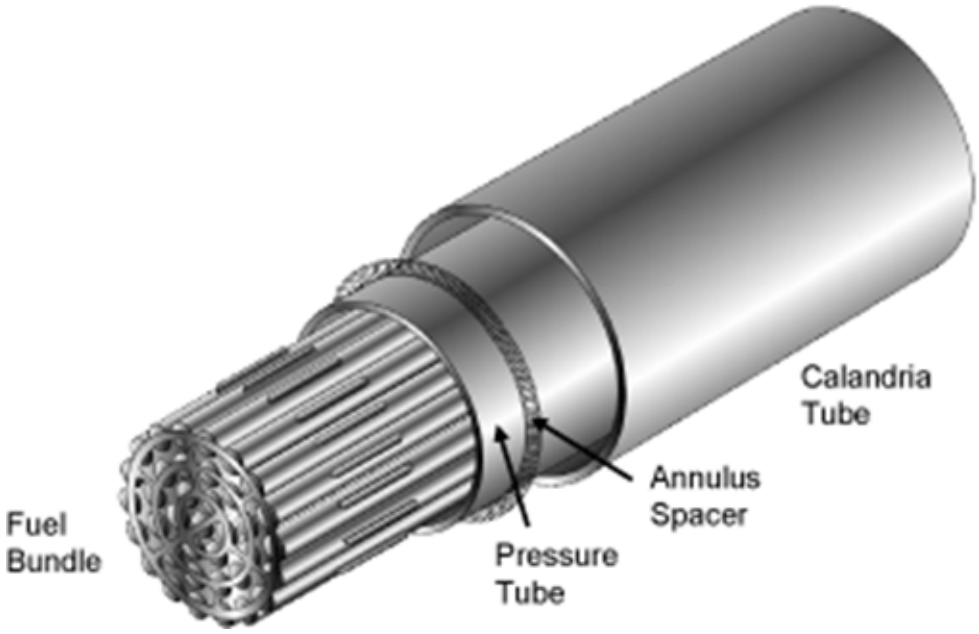

Figure 2.6: Fuel channel has a structure of fuel bundle, pressure tube and calandria tube.

The fuel section consists of fuel bundles, Pressure Tube(PT) and Calandria Tube(CT). As indicated in Fig. 2.6, fuel bundles are installed into PT. The annulus spacers provide support to ensure that pressure tube does not contact the calandria tube. The free volume within the fuel bundles and the space between fuel bundles and the PT provides paths for coolant flow. This flow through PT removes the fission heat generated by fuel bundles. PT is made of Zr-2.5%Nb alloy and provides high pressure environment for coolant. This kind of high-pressure-tube design makes CANDU HTS different from the high-pressure-vessel design adopted in Light Water Reactor(LWR). As indicated in Fig. 2.6, PT is surrounded by CT, and annual space between them

is supported by spacers and is filled with carbon dioxide gas, which provides heat insulation that improves reactor thermal efficiency and limits PT material degradation associated with hydrogen ingress into the Zirconium alloy.

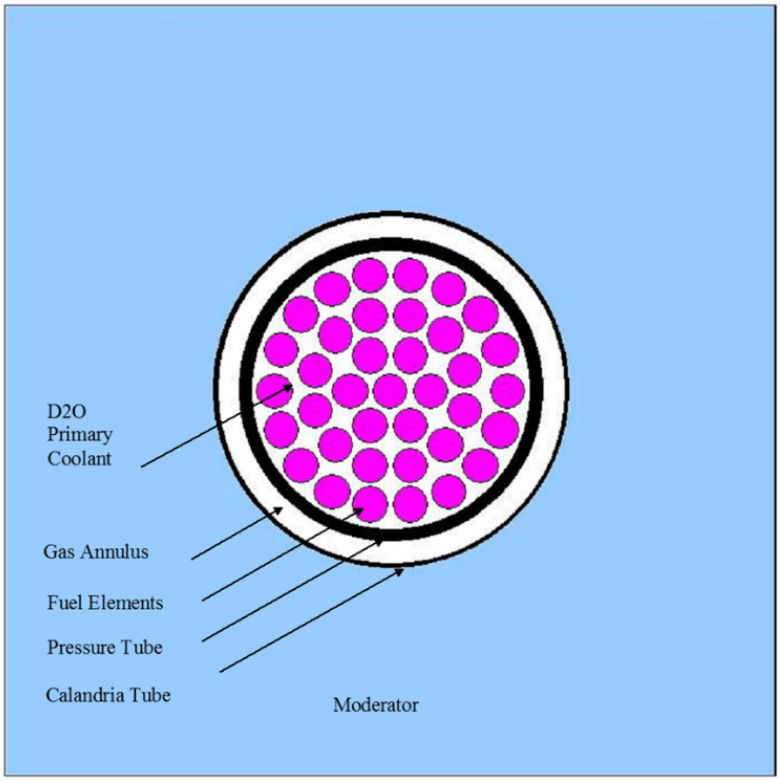

Figure 2.7: Cross section of fuel channel [3]

Each CANDU fuel bundle contains 37 Fuel Elements(FEs), and FE consists of UO2 fuel pellets, which are enclosed in fuel cladding tubes made of Zircaloy-4. All 37 FEs are held in fixed positions by welding them to two End Plates at either end of the bundle. These elements are fixed at specific positions and are spaced from each other by the End Plates and by Inter Element Spacers at the middle of the bundle. Fig. 2.7 shows a cross section of fuel channel, and the radial details, including FEs,

PT, CT, moderator and other components. The outer elements of the bundle have bearing pads brazed to the elements that support the bundle on the pressure tube and limit contact between the outer elements and the pressure tube inner wall.

2.5 End Fittings

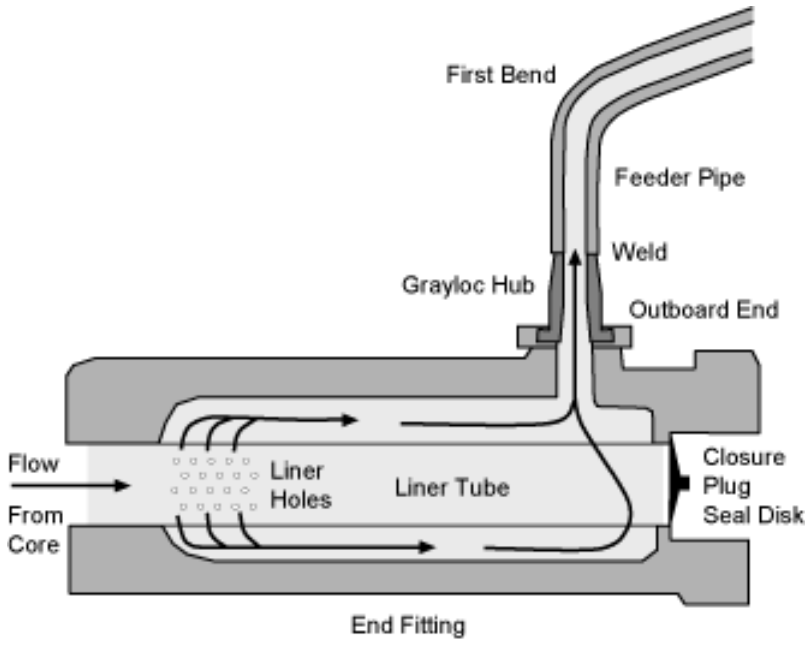

Figure 2.8: Cross section of end fitting

End Fittings(EFs) are located on both ends of fuel channel, and they are important components that have many functions. Regarding thermal hydraulics, they are the connections between PT and feeders, allowing coolant flow in or out fuel channels through them. Regarding refueling, EFs are the structure whereby fueling machine opens Closure Plug and loads fuel bundles, as shown in Fig. 2.8. There is a Liner

Tube internal to the EF body. A stainless steel shield plug within the liner tube provides radiation shielding in axial direction, and in some fuel channel designs, it provides support for the fuel string.

2.6 Feeders

Feeders are groups of pipes that connect EFs and RIH/ROH, as labeled with the number 2 in Fig. 2.8. Each channel is connected with an Inlet Feeder(IF) on inlet side and with an Outlet Feeder(OF) on outlet side via the two EFs.

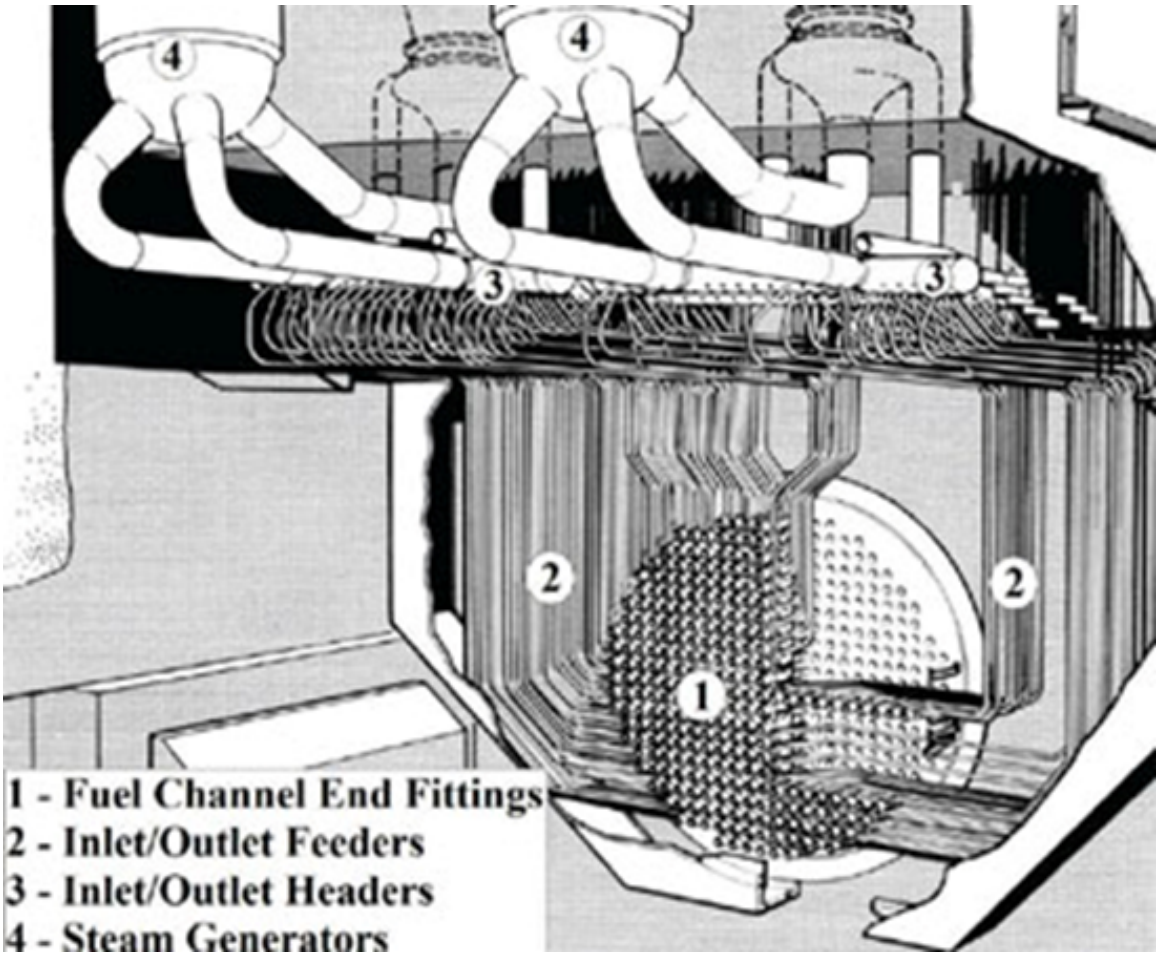

Figure 2.9: Feeders connect headers and end fittings in HTS.

Within a flow pass, all IFs connect to one RIH, and all OFs connect to one ROH. To make fully use of the limited space around reactor core, and to match with the individual channel flow conditions, feeder pipes are forged into different types and are arranged in different configurations. As shown in Fig. 2.9, each feeder pipe has many bends and this results in different pressure distributions within different feeder pipes.

Sabouri [21] developed a simplified model of feeder pipes distributed into six representation groups, as shown in Table 2.1. In other models, the feeders are sometimes lumped into one or more "average" channel groups. However, in natural circulation analysis the channel flows are strongly dependent on the elevation difference between the headers and channels(ΔZ).

Table 2.1: Average hydraulic parameters for lumped feeder groups [21]

Group	Feeder	Length(m)	Area(m^2)	ΔZ(m)	K(Pa/Pa)	HD(m)
1	Inlet	9.90	0.0337	-5.24	1.058	0.0426
1	Outlet	13.35	0.0482	+5.62	0.845	0.0518
2	Inlet	11.35	0.0572	-6.22	1.155	0.0470
2	Outlet	14.81	0.0787	+6.59	0.572	0.0578
3	Inlet	11.25	0.0635	-6.20	1.206	0.0544
3	Outlet	14.62	0.0872	+6.57	0.561	0.0525
4	Inlet	16.01	0.0713	-8.18	1.229	0.0547
4	Outlet	19.50	0.0968	+8.55	0.446	0.0525
5	Inlet	17.27	0.0629	-9.04	0.891	0.0535
5	Outlet	20.81	0.0865	+9.42	0.383	0.0598
6	Inlet	17.52	0.0326	-9.64	0.614	0.0423
6	Outlet	21.06	0.0521	10.01	0. 826	0.0523

2.7 Headers

Reactor Header is a large-diameter cylindrical structure that acts as a manifold to either collect or redistribute coolant flow from or to the feeders that connect to the header. Within a flow pass, there are two kinds of reactor headers: Reactor Inlet Header (RIH) and Reactor Outlet Header (ROH). RIH is located at upstream of IFs, whereby coolant flow is distributed into different IFs to match with different heat removal demands of channels. On the other side, ROH is located at downstream of OFs, where all flows from different channels merge together to form a flow with the same enthalpy. Fig. 2.10 is a schematic diagram of Inlet Header 6 and Outlet Header 7 of RD-14M test facility (Note that the feeders connect to headers at or below the horizontal centre-line of the header, refer to Fig. A.1), and real CANDU reactors have the similar design.

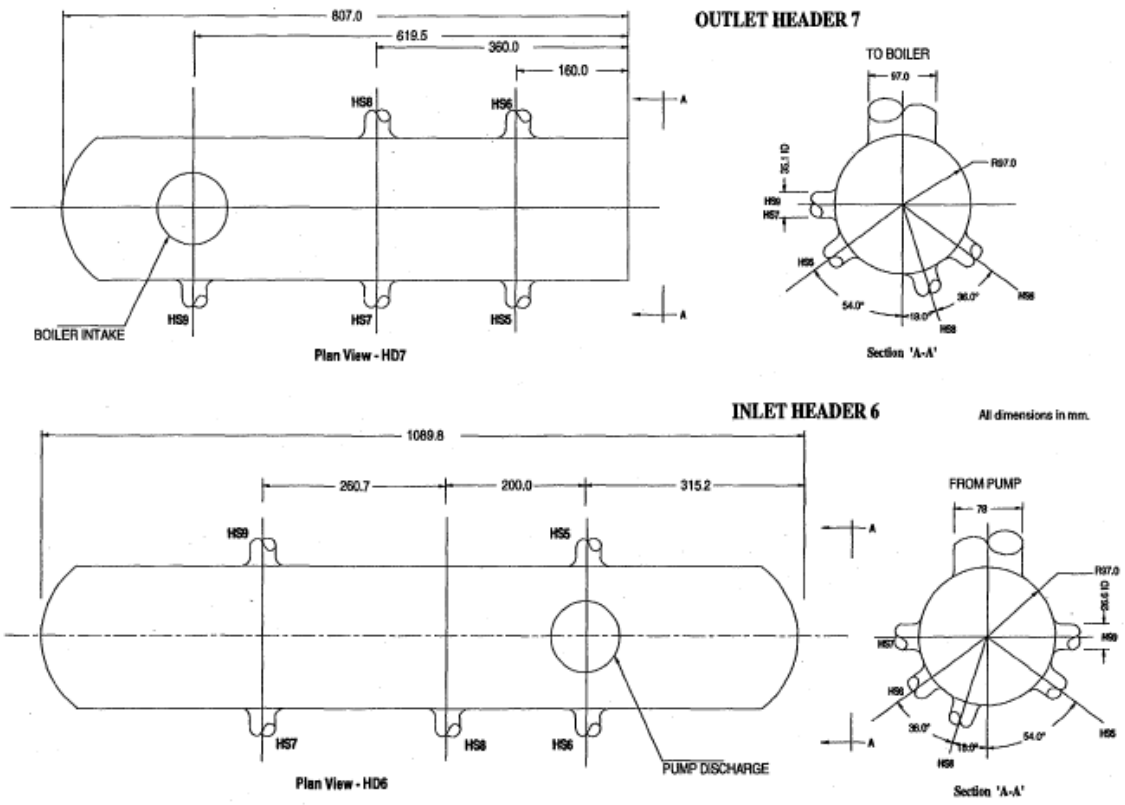

Figure 2.10: Outlet Header 7 and Inlet Header 6 in RD-14M

As shown in Fig. 2.10, on the upper side of Headers, there are two large nozzles, through which ROH connects to SG inlet head on outlet side, and RIH connects to Pump Discharge on inlet side. On the lower side of Headers, there are many small nozzles that connect to feeder pipes. These nozzles are located in different angles asymmetrically. This makes the flow condition within Headers complicated. A simplified Reactor Header model is proposed by Sabouri [21], as illustrated in Fig. 2.11. It has a length of 9.02 m, and an inner diameter of 0.41 m. All nozzles on the lower side are supposed to be the same and are located in the same angle with the vertical

direction.

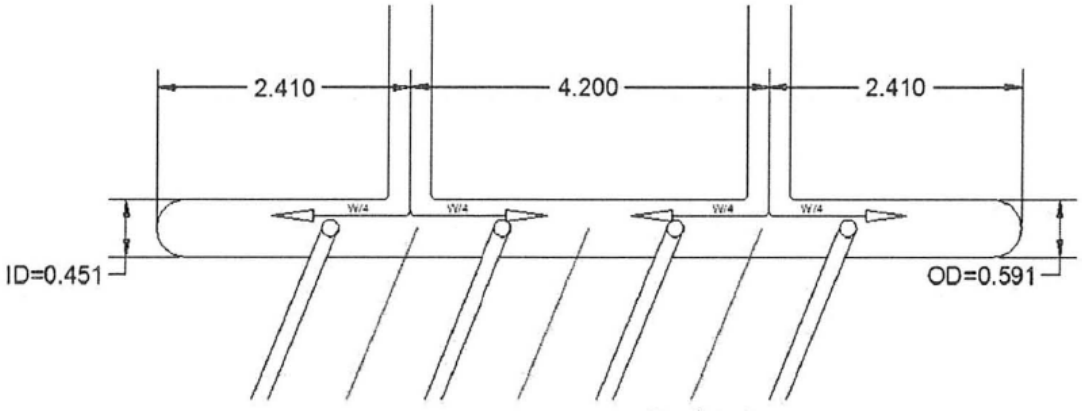

Figure 2.11: Simplified Header Model [21]

2.8 Steam Generator

Figure 2.12: Main internal structure in steam generator is a series of parallel inverted U-tubes.

Steam Generator (SG) is a key component in PHTS that acts as the heat sink for the primary loop and as the heat source for the secondary loop. The main internal structure of SG is a bunch of inverted U-tubes, as shown in Fig. 2.12. These tubes are the boundary between the primary loop and the secondary loop. In CANDU 9, each SG contains 4663 inverted U-tubes.

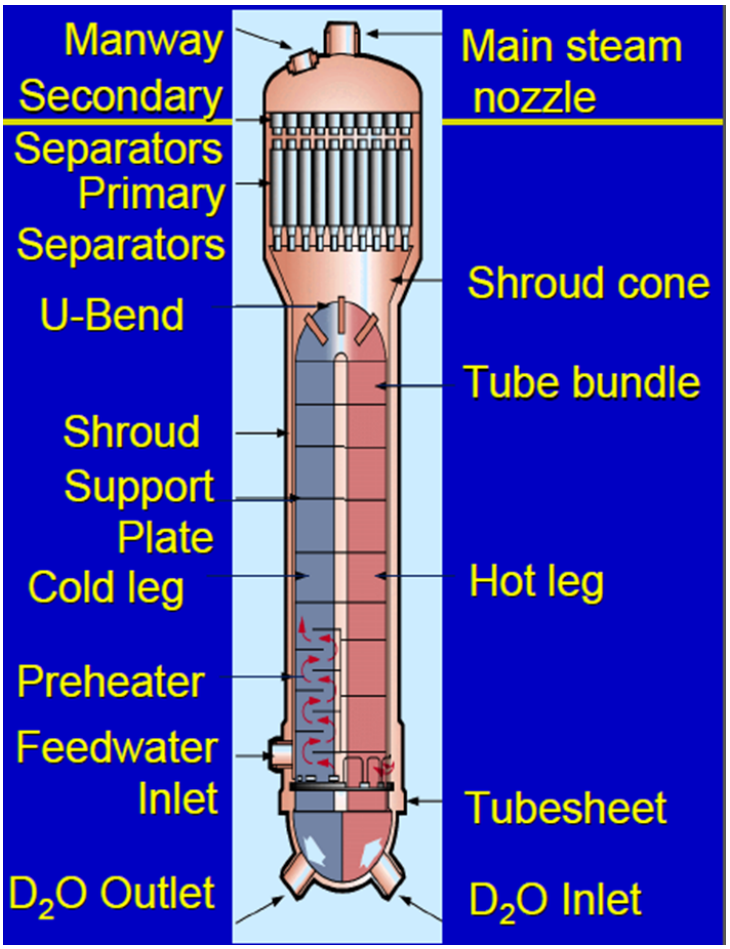

Figure 2.13: Cross section of steam generator [3]

A cross section diagram of the whole SG is presented in Fig. 2.13. Heavy water coolant, working fluid of the primary side, flows from ROH into hemispherical SG inlet head, where the flow is distributed into 4663 inverted U-tubes made of Inconel 800 alloy.The heat contained in the heavy water is transferred to the secondary side through the walls of the inverted U-tubes. As a result, the temperature of fluid decreases and the density of fluid increases as it flows through a U-tube. This leads to the formations of hot leg (of high-temperature lower-density flow) and cold leg (of

low-temperature higher-density flow) within the SG. Finally, subcooled heavy water leaves SG through SG outlet head and flows to the pump suction.

On the secondary side, light water is chosen as working fluid. It is pumped into SG by main boiler feed pumps during normal operation or by auxiliary boiler feed pumps during the event of loss of Class IV power. This subcooled flow is firstly heated to the saturation state within preheater, and then it flows upwards and covers the outer surface of the inverted U-tubes. The light water absorbs the heat from the primary side and evaporates to steam. Because of buoyancy, the steam moves upwards to steam separators, in which liquid droplets are seperated out by centrifugal action to yield pure dry vapor that will be transported to turbine that drives the electrical generator. The steam exits the turbine into the lower turbine condenser volume where heat is extracted by flowing condense cooling water. The condensate that collects is pumped out and returned to the main feedwater system for delivery to the SG's. This closed loop system consists of the main steam supply system and main feedwater system.

2.9 Pumps

Pumps provide the driving pressure head for the whole PHTS to maintain forced circulation under normal condition. In CANDU PHTS, each loop has two pumps that are arranged between SGs and RIHs in two separate flow passes. They are driven by electrical power from Class IV power supply system under normal state. When Class IV power supply is lost, PHTPs lose driving power and run down, therefore forced circulation around the primary loop is lost.

Until now, all important components in HTS have been introduced. Based on these information, a model will be built to simulate and analyze the behavior of HTS under small LOCA with loss of Class IV power accident scenario, and ECI system is assumed unavailable.

Chapter 3

Literature Review

3.1 Natural circulation in CANDU

Natural circulation is one mode of heat removal that can occur in the absence of forced pump flow. The flow is a result of the buoyancy effects associated with the density difference between heat source and heat sink in the absence of any forced circulation. According to Wan et al [28], in the heat transfer loop like that in CANDU, the primary heat sinks, SGs, are located at a higher elevation than the heat sources in the horizontal fuel channels. As a result of the density difference between coolant in the hot and cold legs of the loops, a buoyancy-induced flow develops. These natural circulation flows are capable of removing decay heat in the absence of forced circulation when power is at decay heat level. Natural circulation in CANDU encompasses a wide range of boundary conditions covering reactor power, the secondary side temperature (or pressure) and the primary inventory (or pressure). However, a reactor power at decay level and loss of pumping of the primary loop are two common features in this kind of heat removal mode [24].

According to the development of flow conditions, natural circulation in PHTS of CANDU can be divided into at least three transition stages:

1. Transition from forced circulation to thermosyphoning;
2. Transition from thermosyphoning to the onset of flow reversal;
3. Breakdown of two-phase natural circulation.

3.1.1 Transition from forced circulation to thermosyphoning

Thermosyphoning is a particular form of natural circulation that can maintain a unidirectional coolant flow around the heat transfer loop, driven by the force from the density difference between the hot and cold legs of the circulation loop. The flow can be single-phase or two-phase, steady or oscillatory, but it is always unidirectional [28].

From the results of previous experiments, analysis and actual reactor operating experience [28], the period of the transition from forced circulation to thermosyphoning can be divided into three time phases: Pump Rundown Phase, Flow-Power Adjustment Phase and Thermosyphoning Establishment Phase. The following paragraphs will introduce these three phases in details.

Pump Rundown Phase

As a result of the loss of pumping in the primary loop, forced circulation cooling in PHTS is ceased. Immediately after the loss of AC power to the pump motors, the

reactor is tripped by SDS1 and/or SDS2 to protect the reactor from potential fuel failures.

Right after the trip of pumps, while the pump is running down, the coolant flow behavior is still largely influenced by the pump design characteristics, e.g., inertia. With pumps running down, the driving force from circulation pumps declines and is no longer the dominant factor to decide the flow rate, as a consequence, the flow across loop will keep decreasing to a level that is too small to remove all decay heat out of the primary loop. The resultant changes are that temperature and density distribution of coolant are rearranged across the loop.

Flow-Power Adjustment Phase

At the end of pump rundown phase, the driving force from pumps is negligible. In contrast, the driving force derived from the density difference between the hot and cold legs becomes the dominant factor that decides the flow rate in the loop.

However, the flow during this period is not high enough to take all the decay heat away from channels. There exists a mismatch between the heat transported by the flow and the heat transfered from the fuel to the coolant. Coolant in the heated sections, i.e., fuel channels, will heat up, forming lower-density coolant flow because of coolant temperature increase or the development of a two-phase mixture. As the flow remains in the initial forward direction, newly-generated lower-density coolant will go into the hot leg of the natural circulation loop and will further increase the

density difference between the hot and cold legs. Through this flow-power adjustment process, the flow driven by this density difference will increase and the heat rejection capability of the loop will increase as well.

It should be noted that, after this phase, the average temperature of the primary side increases, and the improved heat rejection capability is the result of the larger temperature difference between the primary and secondary sides of the primary heat transfer loop. [28]

Thermosyphoning Establishment Phase

After Flow-Power adjustment phase, an effective density driving head is established that is large enough to maintain relatively steady thermosyphoning that is sufficient to remove all the generated and stored decay heat in the channel section. A new heat balance is built up to maintain the system temperature-flow condition at a relatively steady state if there is no significant external perturbation. And during this phase, the primary side average temperature is kept at a constant level that can maintain a relatively fixed primary-secondary temperature difference to transfer all the decay heat to the secondary side in SGs. Many experiments and simulations have been conducted to study the thermosyphoning in CANDU-type heat transfer loops.[28][24][15][19]

It should be noted that the flow conditions in thermosyphoning vary based on the specific loop conditions such as HTS pressure and inventory. When HTS pressure

and inventory are relatively high, the fluid in the hot leg is kept as single-phase, as depicted in Fig. 3.1. The low density is probably due to the high temperature and the volumetric swell of fluid. Thermosyphoning is maintained under single-phase coolant conditions. However, with ongoing loss of inventory and simultaneous depressurization due to the assumed accident conditions, void will appear in the heated section and hot leg, so the fluid in the hot leg becomes two-phase mixture, as shown in Fig. 3.2. The low density in the hot leg arises from the appearance of void, and two-phase thermosyphoning continues.

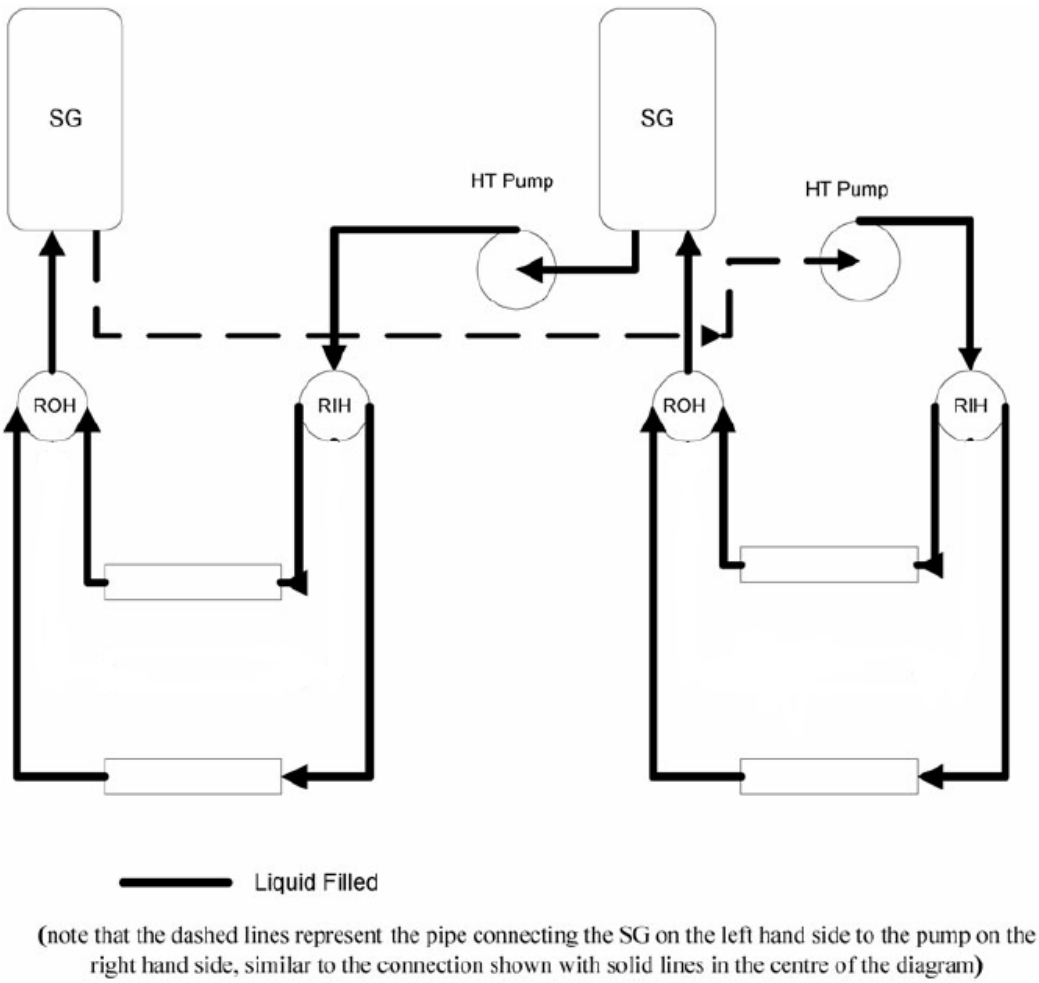

Figure 3.1: Single-phase thermosyphoning in CANDU [18].

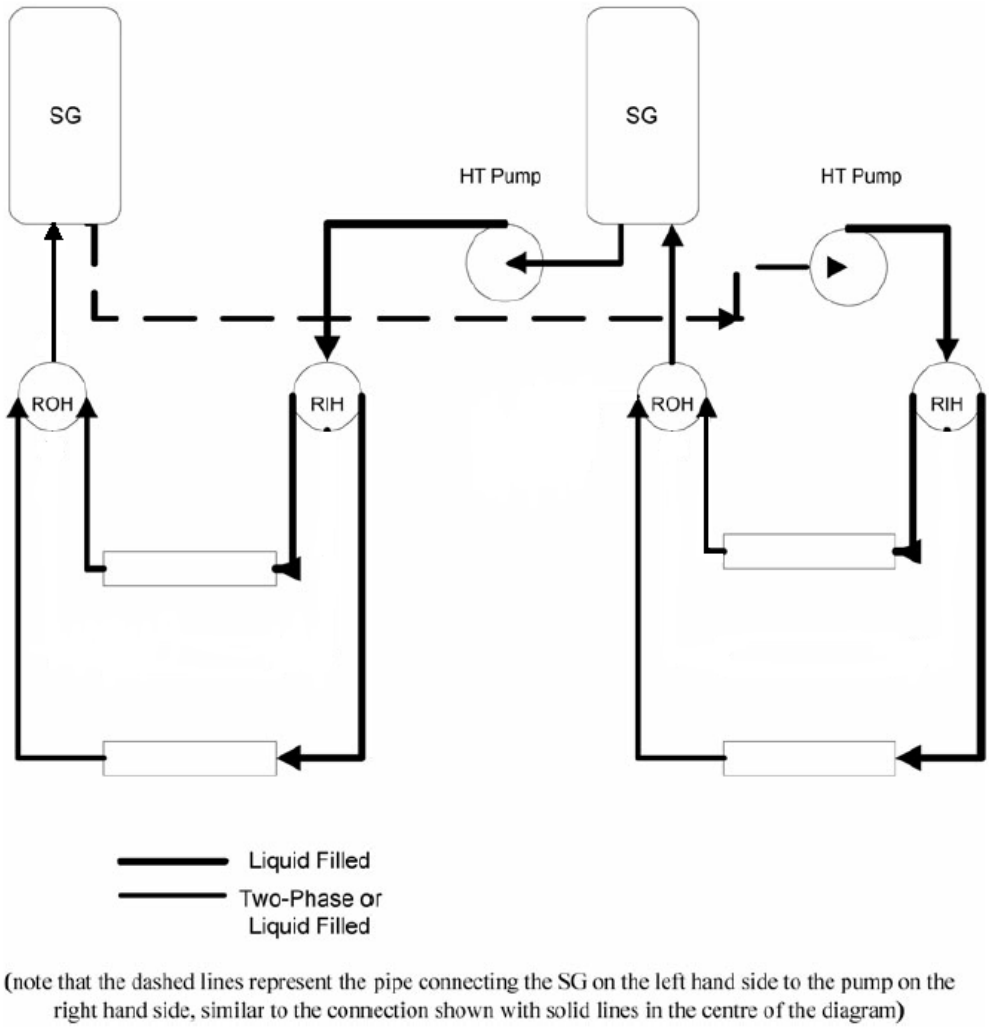

Figure 3.2: Two-phase thermosyphoning in CANDU [18].

The conditions of the secondary side are determined by the initial accident. If there is no damage or disturbance on the secondary side, the cooling function of the secondary side is maintained by normal feedwater system. If the secondary side is influenced by the initial accident, e.g., station blackout, the cooling capability of

the secondary side might be jeopardized. In this analysis, although main boiler feed pumps are tripped due to the loss of Class IV power, the auxiliary boiler feed pumps powered by Class III power are still available to provide feedwater for SGs at decay heat level.

3.1.2 Transition from thermosyphoning to the onset of flow reversal in some channels

Once thermosyphoning is built up across the loop, if there is no external perturbation, it can maintain sufficient heat transfer capability to reject all the heat added by the heat source(decay heat) for the system. A long-term quasi-steady state can be achieved based on this natural circulation mechanism. However, in an accident such as a small LOCA, the HTS is continuously depressurized as a result of loss of coolant inventory. These variations will introduce perturbations into the system that make the system depart from thermosyphoning to other modes of natural circulation cooling. Therefore, thermosyhoning can not last for a long term and will eventually break down.

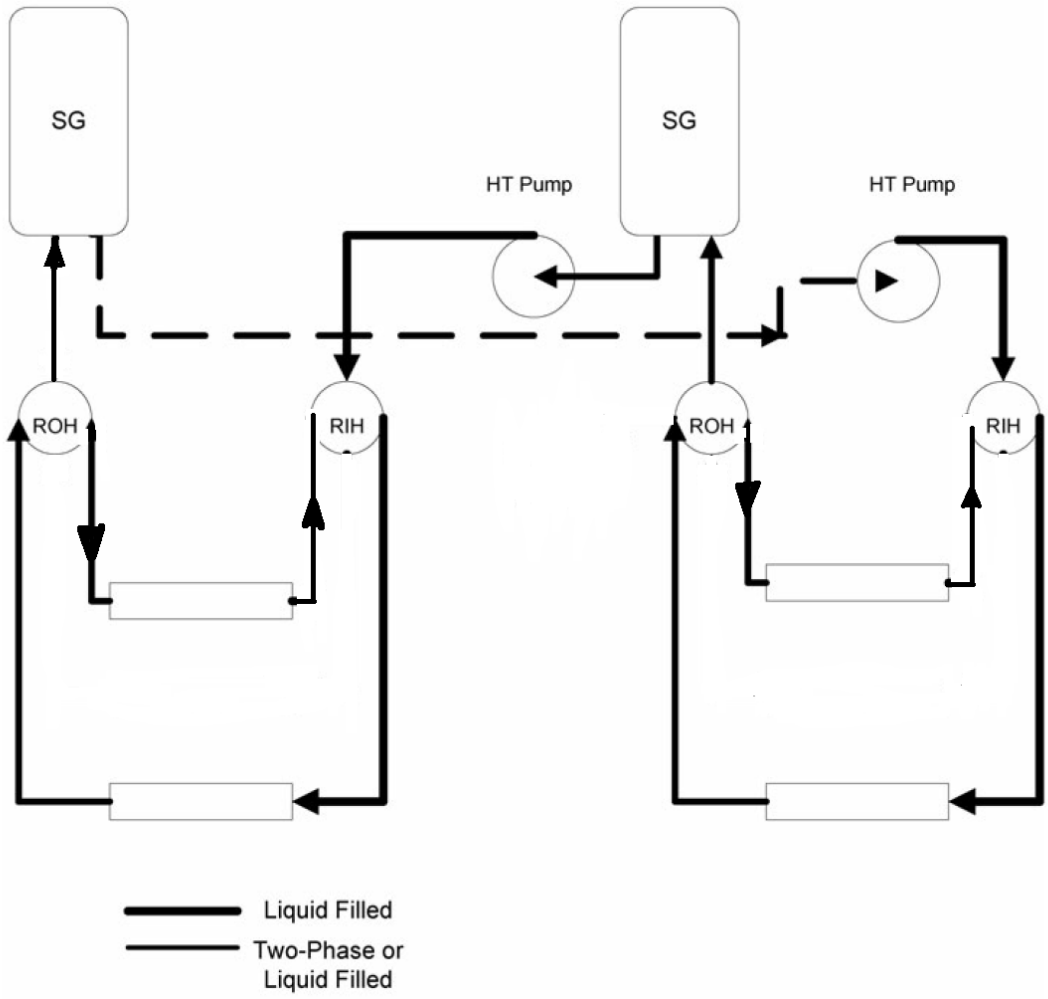

Figure 3.3: Flow reversal in CANDU

One possible departure path from thermosyphoning is the onset of flow reversal in the loop. It is one mode of heat transfer controlled behaviour in which some flow directions in part of channels reverse as a result of change of force balance, as depicted in Fig. 3.3. Wan et al [26] and Gulshani et al [12] have proposed a criterion to determine the occurrence of flow reversal. In thermosyphoning, a forward-direction

flow is kept as ROH-to-RIH pressure difference is smaller than the pressure head due to density difference, i.e.,

$$P_{RIH} - P_{ROH} < [(\rho h)_{cold} - (\rho h)_{hot}]g \tag{3.1}$$

Where :

P_{RIH} is the pressure value at RIH;

P_{ROH} is the pressure value at ROH;

ρ is the average density;

h_{IF} is the elevation change between heat sink and heat source;

Subscripts, *cold* and *hot*, represent the cold leg and the hot leg;

g is the gravitational acceleration constrant.

However, with ongoing loss of inventory and system depressurization, two-phase thermosyphoning breaks down, and the competition of two kinds of force will reverse: The header-to-header pressure difference will become more and more negative as a result of increased two-phase flow resistances in the hot leg piping, and finally its absolute value will be large enough to counteract the buoyancy head due to the density difference between hot and cold legs, i.e.,

$$P_{ROH} - P_{RIH} > [(\rho h)_{cold} - (\rho h)_{hot}]g \tag{3.2}$$

$$P_{RIH} - P_{ROH} < [(\rho h)_{OF} - (\rho h)_{IF}]g \tag{3.3}$$

Where :

ρ_{OF} or ρ_{hot} is the average density in the hot leg of vertical piping in the Outlet Feeder;

ρ_{IF} or ρ_{cold} is the average density in the cold leg of vertical piping in the Inlet Feeder;
h_{OF} is the elevation difference from the channel to ROH across the corresponding outlet feeder;
h_{IF} is the elevation difference from the channel to RIH across the corresponding inlet feeder.

Flow reversal may occur under this force imbalance condition. Eq. 3.2 is a good statement of the force comparison, which has been chosen as a criterion that determines the condition under which flow reversal occurs [12].

According to the observations from previous experiments and reactor operating experience, the flow reversal behavior can be classified into three categories [28]:
a. Flow reversal under relatively steady conditions;
b. Flow reversal under highly oscillatory conditions;
c. Hybrid flow reversal that combines the category a & b.

Flow reversal under relatively steady conditions

Because of specific characteristics of the heat transfer loop, individual flow conditions and detailed operation procedures prior to the occurrence of flow reversal, some systems have relatively stable response to the perturbation of the loop. With the reduction of coolant inventory and the depressurization of the loop, its transition process is relatively steady. Even though there may be some minor fluctuations in the system parameters during the transition process, their magnitude are not large

enough to counteract the inequality between header-to-header pressure difference and the density-difference driving head. This will make the system behave in a quasi-steady fashion, i.e., time-average assumption can be utilized to investigate this kind of transient process. Time-averaged values can be used in Eq. 3.2 to predict the occurrence of flow reversal.

Flow reversal under highly oscillatory conditions

In this category, the system response to the inventory decrease and system depressurization is drastic, and the transition process does not follow the gradually changing trend that is followed in the first category. Significant oscillation can be observed in system parameters. This oscillation includes the inequality between the header-to-header pressure difference and the static pressure head derived from the density difference within hot and cold legs. The period and the magnitude of oscillation are sometimes large enough to make the pressure distribution in some channels fulfill the criterion of Eq. 3.2, so flow reversal can occur in these channels. The reason that causes flow oscillation might be the delayed response of buoyancy force to flow change.

However, it should be noted that this kind of oscillation-introduced flow reversal is not as stable as that in category a. It is somewhat temporary, and flow directions in reversed channels may reverse back to normal forward direction because of some subtle perturbation. Therefore, this instability increases the complexity of the flow behavior. Many studies have investigated the stability of figure-of-eight loop like that in CANDU, and it has been an independent detailed [5][7][8][9][10][13]. This

behaviour is not further discussed in this thesis.

Hybrid flow reversal

Flow reversal in hybrid case shows the features of both category a & b, and the different mechanisms that creates the flow reversals in the first two categories all project influences on the formation of flow reversal in this category. On the one hand, the system transition derived from inventory decrease create adverse RIH-to-ROH pressure differential whose absolute value is large enough to offset the effect from forward density difference head. On the other hand, inherent instability of the system leads to the oscillation of pressure and flow distributions across the loop, and this contributes to the imbalance of force that generates the flow reversal.

3.1.3 Breakdown of two-phase natural circulation

With continuous loss of HTS inventory, the existing two-phase natural circulation might break down in the loop due to:

1. Total vapor lock: It may occur at the top of the inverted U-tubes in SG, i.e., no flow goes through SG line and all flows are circulated within heated sections below headers [22];

2. Reduced inventory: Natural circulation requires a minimum coolant level to allow a flow path in the loop. [23]

This can lead to a flow phenomenon called Intermittent Buoyancy Induced Flow

(IBIF), a heat transfer pattern developed after the breakdown of natural circulation. It can be described as a serious of stages [23]:

1. Channel stagnation: Flow will stagnate in a channel after the breakdown of natural circulation.

2. Channel heatup: The fluid is heated in the channel by decay heat, and liquid is stratified. A slug of hot liquid or a steam bubble may form at the center of channel, as shown in Fig. 3.4

3. The bubble or slug growth: With continuous heating, the bubble or slug at the center will expand and contact one or both of end fittings, as shown in Fig. 3.5

4. End fitting penetration: The bubble or slug will enter one or two end fittings and continue to feeders. Since end fitting has a large mass and typically lower temperature than the saturated bubble/slug, heat of bubble/slug can transfer to end fitting body. The subcooled inventory in end fittings can also help lower the temperature of bubble/slug. (Fig. 3.6)

5. Venting: The bubble/slug will finally reach one feeder at one end, setting up a pressure differential across the whole channel. A venting process ensues, with bubble/slug rising up feeder and cold fluid entering the channel from the other end, as shown in Fig. 3.7. Through venting, heat is transfered to SG, in which it is transfered to the secondary side.

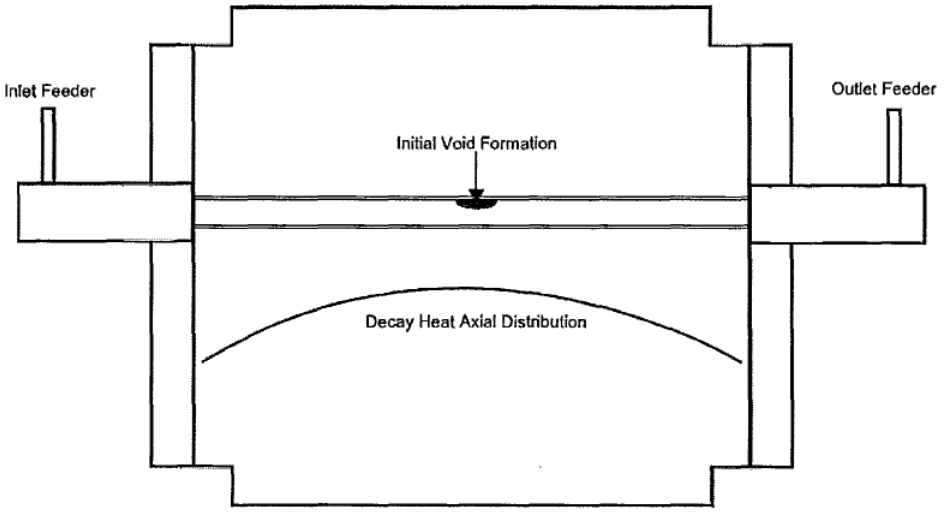

Figure 3.4: IBIF Phase1[23]

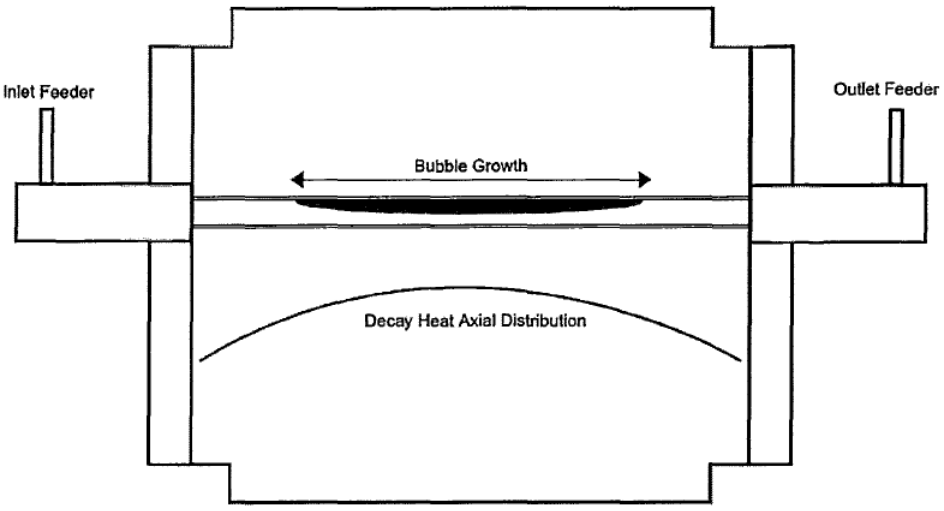

Figure 3.5: IBIF Phase2[23]

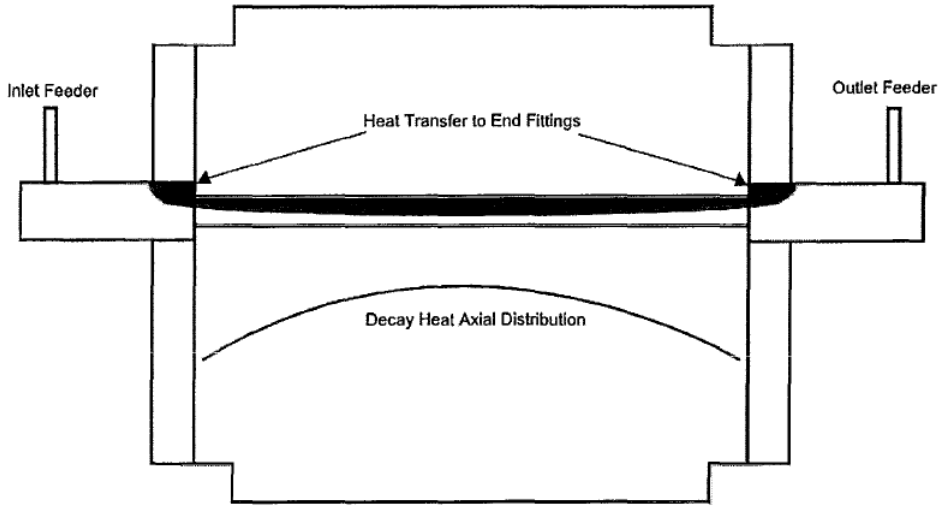

Figure 3.6: IBIF Phase3[23]

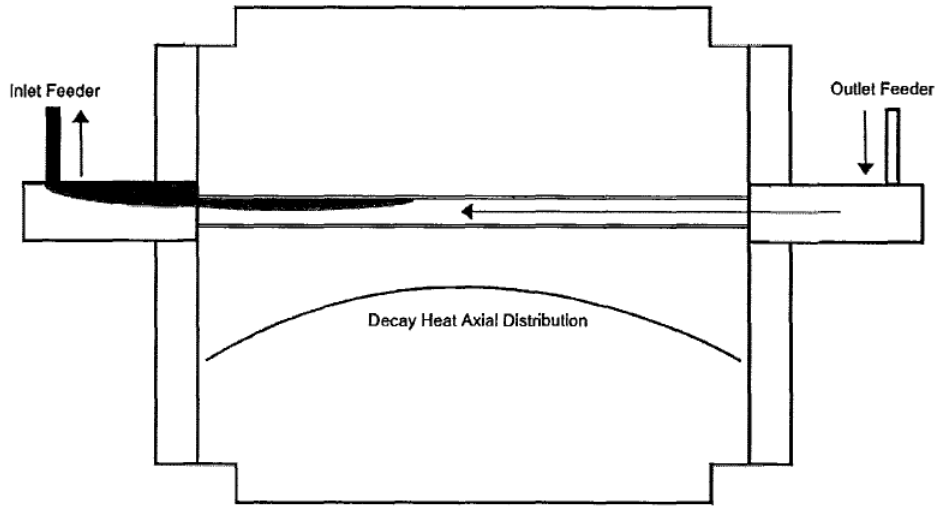

Figure 3.7: IBIF Phase4[23]

IBIF cycles can be repeated as long as loop conditions (such as inventory, heat

generation, stagnated flow, etc.) remain favourable. The local pressure and temperature are important concerns for IBIF, since they can impact channel and fuel integrity and safety.

Until now, main development process of natural circulation in CANDU has been described. It provides good insight into understanding thermal hydraulic behavior in HTS for postulated accident events.

3.2 The consequences of flow reversal to HTS

The issues of interest are what are the consequences of flow reversal in one or more channels, and whether adequate fuel cooling can be maintained to guarantee the integrity of fuel channels, and hence the integrity of the HTS as well as the whole reactor.

As other analysis shows [24, 27, 1], the onset of flow reversal creates a new pathway within CANDU heat transfer loop — the flow leaving ROH enters the reversed channels instead of entering the path to the intended heat sink, steam generators. Therefore, except for the initially-designed circulation loop (from RIH to RIH via IFs, channels, OFs, ROH, SGs), a new circulation loop (from RIH to RIH through normal IFs, forward-direction channels, normal OFs, ROH, reversed OFs, reversed channels, reversed IFs) is formed because of the onset of flow reversal. This actually results in a reduction of flow rate that goes through the above-headers-path, and makes part of flow bypass the intended dominant heat sinks. For example, if one channel is reversed, the flows in equivalent two channels actually need not go through

SG, since the flow in these two channels can form a closed loop to circulate entirely within it. The reduction in flow across SG is the double size of reduction in number of forward-direction channels.

It may cause a potential degradation of heat rejection capability for the whole HTS, since the heat carried by the reversed flow cannot be rejected out of the primary circulation loop. The global primary loop average temperature may increase, and part of loop, e.g., reversed channels, may undergo local temperature excursion as a result of lack of effective cooling. Moreover, the increase in local or overall temperature may jeopardize the integrity and safety of fuel and HTS. So it is of significant interest to investigate the behavior of flow reversal and its subsequent development and influences to HTS.

Some experiments [1, 12, 20, 16, 11] and simulations have been conducted, and different test facilities and thermal hydraulic codes have been utilized in this study. For example, P.T. Wan et al [26] used RD-14M test facility to investigate the onset of flow reversal, and P. Gulshani et al [11] studied two-phase thermosyphoning in RD-14M and compared experiments with CATHENA simulations. They adopted a similar way to drain the inventory in RD-14M loop and inspected the loop parameters. Gulshani et al [12] proposed a steady state model as a function of the loop integrated void fraction, steam generator secondary side pressure and the heat losses, and the cold flashing at the top of SG and in the cold leg is thought to lead to the flow reversal. Soedijono et al [22] utilized a mechanistic quasi-steady state model to analysis the variation of RIH-to-ROH pressure difference with inventory decreasing,

and proposed a mechanistic approach to decide the vapor lock at the top of SG.

However, many assumptions and simplifications to different degrees have been applied to the tests and models. Some drawbacks, e.g. over-simplified models or boundary conditions, have offset the accuracy of the predictions. Since HTS of CANDU is a complex system, keeping a reasonable complexity of the model is a necessary requirement for the validity of results. Therefore, a new, more complex model following the parametric approach has been constructed in this study to analyze the problems. A node-link structure is used to represent HTS, and channel power, RIH pressure and the secondary-side pressure are set as boundary conditions. The loop conditions are investigated based on different coolant inventory levels.

This model is used to investigate the thermal hydraulic behavior of HTS, and the formation and development of flow reversal. Several questions below will be analyzed in this study:

1. What are the variations of system parameters during the assumed accidents?
2. Is it possible that flow reversal will occur under the hypothetical initiating events?
3. If flow reversal occurs in fuel channels, what is the reversal preference for each row of channels?
4. What is the inventory level at which the flow reversal will occur?
5. To what extent do the system parameters, e.g. decay power level, influence flow reversal behavior?

3.3 Some special assumptions

To guarantee the efficiency of the investigation and to understand the key mechanism that determines the occurrence of flow reversal, several extra assumptions are utilized in the analysis:

3.3.1 Quasi-steady state

It is assumed that the flow reversal being investigated in this study is under quasi-steady state conditions, and no oscillation or instability will be considered. The actual simulations follow a parametric approach. The development of the initiating events is characterized by the variable RIH pressures and resultant inventory levels. Since the model is quasi-steady state, no time-dependent variables(such as discharge rate) are used in the simulation.

3.3.2 HEM

Homogeneous Equilibrium Model(HEM) is applied to simulate the two-phase flow in this study. It implies that the velocities of liquid and vapor phases are equal in any cross section, so there is no friction or slip, and hence no exchanges of energy or momentum due to the relative stress forces between the two phases. The coolant is treated as a homogeneous fluid. In addition, HEM assumes a thermodynamic equilibrium in fluid, i.e., there is no temperature difference between two phases. This implies that there is no heat transfer in radial direction within coolant, or that the heat transfer coefficient of the coolant is infinitely large in a cross section that is perpendicular to the flow direction. This assumption avoids the potential of occurrence

of subcooled boiling in the loop. In conclusion, a quasi-steady-state Homogeneous Equilibrium Model (HEM) is developed to analyze the thermal hydraulic behavior of HTS.

3.3.3 Flow resistance in SG

A review of previous studies [22, 27, 20] indicate that, it is not enough to get an effective negative RIH-ROH pressure differential, if a two-phase flow pressure drop is thought to be the only source to contribute to the pressure drop in SG. With the decreasing of coolant inventory in the loop, some other flow behavior must have happened within SG to introduce larger pressure drop across SG. This behavior is related to partial boiler-tube blockage/vapor lock due to the appearance of void at the top of SG invert-U tubes. This vapor lock/boiler tubes blockage behaviour decreases the flow area and increase the pressure drop across SG line, so that the RIH-ROH pressure difference continually becomes more negative to the level that is negative enough to counterbalance the pressure differential from density difference between the hot and cold legs. Finally, flow reversal occurs as a result of large negative ΔP_{HH}.

3.3.4 Unavailability of ECI system

According to the design of CANDU electrical system, Emergency Coolant Injection(ECI) system is supplied by Class III power. Although Class III power is still available in this analysis based on the assumed initiating accidents, there is a possibility that ECI system is not initiated due to random failures. Therefore, ECI system is assumed not to be available in tis study, subsequently, there is no crash cooldown

of the SGs.

Chapter 4

Methology

4.1 Theory Background

To fulfill different demands, reactor thermo-hydraulics analysis can be of various levels of complexity. For the application in flow reversal analysis, a system analysis is used to simulate the macro-behavior of loop during a small LOCA with a loss of Class IV power. At this level, as the dominant goal is to obtain the distributions of flow and pressure, some simplifications to HTS modelling can be made during the analysis. It should not be surprising that a large degree of empiricism is applied, as the flow behavior is inherently chaotic.

4.1.1 HEM Model

During the development of natural circulation, it is inevitable that two-phase flow will be involved. Two-phase flow is a condition in which the fluid is a mixture of both liquid and vapor phases, and this alters fluid properties as the vapor fraction

increases. In this work, a straightforward and effective fluid model, HEM, is applied to address two-phase flow.

In HEM, the mixture of two phases can be treated as a special single-phase flow with the averaged flow properties. These properties are calculated as follows[2]:

Mixture Density, ρ_m

$$\rho_m = \alpha\rho_v + (1-\alpha)\rho_l \tag{4.1}$$

where:

α is void fraction;

ρ_v is the saturation vapor density at current pressure;

ρ_l is the saturation liquid density at current pressure;

Mixture Specific Volume, ν_m

$$\nu_m = x\nu_v + (1-x)\nu_l \tag{4.2}$$

where:

x is coolant flow quality;

ν_v is the saturation vapor specific volume at current pressure;

ν_l is the saturation liquid specific volume at current pressure;

Mixture Viscosity, μ_m

$$\mu_m = (\frac{x}{\mu_v} + \frac{1-x}{\mu_l})^{-1} \tag{4.3}$$

where:

μ_v is the saturation vapor viscosity at current pressure;

μ_l is the saturation liquid viscosity at current pressure;

4.1.2 Coolant Conservation Equations

To develop quasi-steady state HEM for the case of flow reversal, a series of one-dimensional equations will be formulated to describe the loop behavior. These equations are the mathematical reflections of fundamental fluid dynamics features, e.g., the conservations of mass, energy and momentum. They will be introduced in detail in following paragraphs.

Mass Equations

According to transport theory, the mass conservation is expressed as below:

$$\frac{\partial}{\partial t}\rho + \nabla \cdot \rho\vec{v} = 0 \tag{4.4}$$

where:

t is time derivative;

ρ is local density of fluid;

$\vec{v}$ is velosity of fluid;

Since the analysis is one-dimensional, and the fluid simulated is two-phase mixture, Eq. 4.4 becomes as below:

$$\frac{\partial}{\partial t}\rho_m + \frac{\partial}{\partial z}G_m = 0 \tag{4.5}$$

Where:

z is along the flow direction;

G_m is mass flow flux, defined as $G_m = \rho v$;

Because of the quasi-steady-state assumption, the time-dependent term on the left-hand side can be removed, and Eq. 4.5 becomes as follow:

$$\frac{\partial}{\partial z}G_m = 0 \tag{4.6}$$

Eq. 4.6 can be integrated across the cross section along different piping branches, it becomes

$$\sum_{n=1}^{N} G_{m,n}A_n = \sum_{n=1}^{N} W_n = W_{total} = constant \tag{4.7}$$

where:

W is the flow rate in a specific piping branch;

A is cross section area;

Subscript, n, is the label of different flow branches.

Energy Equations

The transport equation for energy is as below:

$$\rho_m \frac{\partial h_m}{\partial t} + G_m \frac{\partial h_m}{\partial l} + \frac{\partial P}{\partial t} = \frac{q" P_h}{A} + \frac{G_m}{\rho_m}(\frac{\partial P}{\partial l} + \frac{f G_m |G_m|}{2 D_e \rho_m}) \tag{4.8}$$

where:

ρ_m is mixture density;

h_m is mixture enthalpy;

l is length derivative;

P is local pressure;

$q"$ is power in unit area;

P_h is the perimeter of the tube;

f is friction factor;

D_e is the hydraulic diameter of the tube;

For quasi-steady state, all terms containing time-dependent variables can be removed, so Eq. 4.8 is simplified to:

$$G_m \frac{\partial h_m}{\partial l} = \frac{q" P_h}{A} + \frac{G_m}{\rho_m}(\frac{\partial P}{\partial l} + \frac{f G_m |G_m|}{2 D_e \rho_m}) \tag{4.9}$$

It is assumed that the influence of pressure terms is negligible, so Eq. 4.9 becomes as below:

$$G_m \frac{\partial h_m}{\partial l} = \frac{q" P_h}{A} \tag{4.10}$$

Rearrange Eq. 4.10 and integrate it along the flow direction as shown below:

$$W_m \int_{up}^{i} dh_m = \int_{up}^{i} q' dl = \int_{up}^{i} dQ \tag{4.11}$$

where:

Subscript i represents current point along flow direction;

Subscript up is the upsteam of point i;

Finally, energy conservation equation has the following form:

$$W_m(h_i - h_{up}) = Q_i \quad \text{or} \quad h_i = h_{up} + \frac{Q_i}{W_m} \tag{4.12}$$

where:

W_m is the flow rate of the mixture;

h_i is the enthalpy in current point i;

h_{up} is the enthalpy in the upstream of point i;

Q_i is the heat injected into the flow in current point i.

Momentum Equations

The momentum conservation equation plays a dominant role in the formulation of the model, since based on it, the pressure gradient across the loop is calculated. According to momentum transport, the momentum equation is as below:

$$\rho \frac{D\vec{v}}{Dt} = \frac{\partial}{\partial t}\rho\vec{v} + \nabla \cdot \rho\vec{v}\vec{v} = -\nabla P + \nabla \cdot \bar{\bar{\tau}} + \rho\vec{f} \tag{4.13}$$

where:

τ is shear force;

$\vec{f}$ is volume force to flow.

Because of the quasi-steady-state HEM assumption, the time term is removed, the shear force is from wall friction, and the volume force is gravity force, so Eq. 4.13 becomes as below:

$$\nabla \cdot \rho \vec{v}\vec{v} = -\nabla P + \nabla \cdot \frac{\vec{F}_{wall}}{V} + \rho \vec{g} \tag{4.14}$$

where:

$\vec{F}_{wall}$ is friction force from the wall of pipe;

V is volume of fluid in one point of pipe;

$\vec{g}$ is gravity acceleration;

Rearrange Eq. 4.14 and integrating along the flow direction, $\vec{z}$:

$$\int -\nabla P \cdot d\vec{z} = \int \nabla \cdot \rho \vec{v}\vec{v} \cdot d\vec{z} - \int \frac{\vec{F}_{wall}}{V} \cdot d\vec{z} - \int \rho \vec{g} \cdot d\vec{z} \tag{4.15}$$

Eq. 4.15 is for one-dimensional two-phase mixture in HEM model, so for any point i along flow direction, it is as below:

$$\int_{up}^{i} -\frac{dP}{dz} dz = \int_{up}^{i} d(\frac{G_m^2}{\rho_m}) - \int_{up}^{i} -\frac{f G_m |G_m|}{2 D_e \rho_m} dz - \int_{up}^{i} -\rho g \cos\theta dz \tag{4.16}$$

where:

Subscript, i, is the label for current point;

Subscript, up, is the label for upstream point;

f in the second term on the right-hand side is friction factor of the pipe;

D_e is the hydraulic diameter of the pipe;

θ is the angle between the flow direction and the upwards direction;

Now analyze Eq. 4.16 term by term.

On the left-hand side:

$$\int_{up}^{i} -\frac{dP}{dz}dz = P_{up} - P_i = \Delta P \tag{4.17}$$

where:

ΔP is the pressure difference between the upstream point to current point i.

On the right-hand side, more terms are involved.

- Acceleration term:

$$\Delta P_{acc} = \int_{up}^{i} d(\frac{G_m^2}{\rho_m}) = (\frac{G_m^2}{\rho_m})_i - (\frac{G_m^2}{\rho_m})_{up} = W_m^2[(\frac{1}{\rho_m A_z^2})_i - (\frac{1}{\rho_m A_z^2})_{up}] \tag{4.18}$$

  This term comes from the changes of mass flux and density.

- Friction term:

$$\Delta P_{fric} = -\int_{up}^{i} -\frac{fG_m|G_m|}{2D_e\rho_m}dz = \int_{up}^{i} \frac{fW_m^2}{2D_e A_z^2 \rho_m}dz \tag{4.19}$$

This term is due to the friction from pipe wall.

There is another term that is related to the flow area change such as pipe contraction and expansion, or to the flow direction change like elbow. This term is called form or local term.

- Form term:

$$\Delta P_{form} = \sum_j (\frac{K_j W_m^2}{2\rho_m A_z^2})_j \tag{4.20}$$

where:

Subscript j labels number of local form pressure drop;

K_j is flow resistance coefficient.

- Gravity term:

$$\Delta P_{grav} = -\int_{up}^{up} -\rho g \cos\theta dz = (\rho g h)_i - (\rho g h)_{up} = g[(\rho h)_i - (\rho h)_{up}] \tag{4.21}$$

This term is derived from gravity pressure difference, and h_i is the vertical height from arbitrary set point.

In conclusion, one-dimensional pressure drop can be expressed as below:

$$P_{up} - P_i = \Delta P_{acc} + \Delta P_{fric} + \Delta P_{grav} + \Delta P_{form} \quad \text{or} \quad P_i = P_{up} - (\Delta P_{acc} + \Delta P_{fric} + \Delta P_{grav} + \Delta P_{form}) \tag{4.22}$$

The paragraphs above introduce the conservation equations of mass, energy and momentum used in one-dimensional quasi-steady-state flow simulation.

4.1.3 Heat Transfer in SG

Within SG, The heat is transferred from the primary side to the secondary side across the inverted U-tubes as below:

$$\Delta Q = NU\Delta A\Delta T \tag{4.23}$$

where:

ΔQ is the heat transfer rate of a specific section in SG, in W;

N is the number of inverted U-tubes in one SG;

U is the lumped heat transfer coefficient across the wall of one inverted U-tube, in $W/m^{2\circ}$C;

ΔA is the heat transfer area of the wall for a chosen section of one inverted U-tube, in m^2;

ΔT is the temperature difference across the inverted U-tubes, in °C.

The overall lumped heat transfer coefficient for single U-tube is calculated as below:

$$UA = [\frac{1}{h_{in}A_{in}} + \frac{1}{2\pi kL}ln(\frac{r_{out}}{r_{in}}) + \frac{1}{h_{out}A_{out}} + \frac{R_{f,in}}{A_{in}} + \frac{R_{f,out}}{A_{out}}]^{-1} \tag{4.24}$$

where:

Subscript in refers to inner surface of the wall;

Subscript *out* refers to outer surface of the wall;

h is the heat transfer coefficient of the working fluid(note that it is not enthalpy in this equation);

A is the heat transfer area;

k is the thermal conductivity of the wall;

L is the length of the chosen section of the pipe;

r_{in} is the inner radius of pipe;

r_{out} is the outer radius of pipe;

R_f is the thermal resistance due to the fueling;

As the thickness of the inverted U-tube wall ($\tau = r_{out} - r_{in}$) is small, using first-order Taylors Formula, the second term on the right-hand side can be simplified as below:

$$ln(\frac{r_{out}}{r_{in}}) = ln(1 + \frac{r_{out} - r_{in}}{r_{in}}) = ln(1 + \frac{\tau}{r_{in}}) \approx \frac{\tau}{r_{in}} \tag{4.25}$$

So Eq. 4.24 becomes as below:

$$UA = [\frac{1}{h_{in}2\pi r_{in}L} + \frac{1}{2\pi kL}(\frac{\tau}{r_{in}}) + \frac{1}{h_{out}2\pi r_{out}L} + \frac{R_{f,in}}{2\pi r_{in}L} + \frac{R_{f,out}}{2\pi r_{out}L}]^{-1} \tag{4.26}$$

$$= 2\pi L(\frac{1}{h_{in}r_{in}} + \frac{\tau}{kr_{in}} + \frac{1}{h_{out}r_{out}} + \frac{R_{f,in}}{r_{in}} + \frac{R_{f,out}}{r_{out}})^{-1} \tag{4.27}$$

Linear heat transfer coefficient for one SG is as below:

$$q' = \frac{\Delta Q}{\Delta L} = \frac{NU\Delta A\Delta T}{\Delta L} \tag{4.28}$$

Substitute Eq. 4.26 into Eq. 4.28, it becomes

$$q' = 2\pi\Delta T N(\frac{1}{h_{in}r_{in}} + \frac{\tau}{kr_{in}} + \frac{1}{h_{out}r_{out}} + \frac{R_{f,in}}{r_{in}} + \frac{R_{f,out}}{r_{out}})^{-1} \tag{4.29}$$

Where:

h_{in}: U-tube inner surface condensing heat transfer coefficient;

h_{out}: U-tube outer surface boiling heat transfer coefficient;

k: Thermal conductivity of the wall;

R_f: Fouling factors;

Now the object becomes finding the proper correlations or values of the terms in Eq. 4.29. Some assumptions have been made by reviewing previous documents, and they are discussed in the following paragraphs.

Secondary side: h_{out}

It is supposed that fully developed nucleate boiling occurs on the secondary side of the inverted U-tubes, Jens-Lottes correlation is valid for both local and bulk boiling under such circumstance [25].

$$h_{out} = exp(\frac{4P_{sec}}{6.2})(\frac{1}{25^4})(T_w - T_{sec})^3 * 10^6 \tag{4.30}$$

where:

h_{out} is in $W/(m^{2\circ}\mathrm{C})$;

P_{sec} is the secondary side pressure in MPa;

T_w is wall temperature in °C;

T_{sec} is secondary side saturation temperature;

Wall thermal conductivity: k

Temperature	Electrical Resistivity	Thermal Conductivity	Coefficient of Expansion[a]
°F	ohm•circ mil/ft	Btu•in/ft²•h°F	10^{-6} in/in/°F
70	595	80	-
100	600	83	-
200	620	89	7.9
400	657	103	8.8
600	682	115	9.0
800	704	127	9.2
1000	722	139	9.4
1200	746	152	9.6
1400	758	166	9.9
1600	770	181	10.2
1800	776	214	-
2000	788	-	-
°C	µΩ•m	W/m°C	µm/m/°C
20	0.989	11.5	-
100	1.035	13.0	14.4
200	1.089	14.7	15.9
300	1.127	16.3	16.2
400	1.157	17.9	16.5
500	1.191	19.5	16.8
600	1.223	21.1	17.1
700	1.251	22.8	17.5
800	1.266	24.7	18.0
900	1.283	27.1	-
1000	1.291	31.9	-

[a]Between 70°F (21°C) and temperature shown.

Figure 4.1: Properties of Inconel 800[4]

The inverted U-tubes are made of Inconel 800. According to the properties of Inconel 800 in Fig. 4.1, it can be fitted as

$$k_w = 0.016 * T_w + 11.5 \tag{4.31}$$

where:

k_w is the wall thermal conductivity in $W/m°\mathrm{C}$;

T_w is the wall temperature in °C;

Eq. 4.31 is used to calculate the thermal conductivities of the wall at different temperatures.

Fouling factor: R_f

Table 4.1: Fouling factors for several common fluids [14], $R_f = 0.001/5.6783(m^{2^\circ}\mathrm{C})/W$, is adopted as fouling factor for both sides of inverted U-tubes.

Types of Fluid	Fouling Factor $(hr - ft^2 - F/Btu)$
Sea water below 125 F	0.0005
Sea water above 125 F	0.001
Treated boiler feedwater above 125 F	0.001
Fuel oil	0.005
Quenching oil	0.004
Alcohol vapors	0.0005
Steam, non-oil bearing	0.0005
Industrial air	0.002
Refrigerating liquid	0.001

With time, the surface of inverted U-tubes may be covered by a layer of impurities from working fluid or corrosion. These kinds of impurities will accumulate on both sides of U-tubes and will introduce extra thermal resistance for the overall heat transfer capability. Thus a fouling factor, R_f, is used to modify the lumped heat transfer coefficient. The recommended values for fouling factors are given in Table 4.1 for some common fluids.

Primary side: h_{in}

On the primary side of SG, there exist both single-phase and two-phase flows over the whole span of the inverted U-tubes.

For single-phase section, Dittus-Boelter correlation is used to calculate heat transfer coefficient in tubes as below.

$$Nu = 0.023 Re^{0.8} Pr^{n} \tag{4.32}$$

where:

$Nu = \frac{hD}{k}$, Nusselt number;

$Re = \frac{GD}{\mu}$, Reynolds number;

$Pr = \frac{C_p \mu}{k}$, Prandtl number;

$n = 0.4$ when the fluid is heated, and n=0.3 when the fluid is cooled.

Rearrange Eq. 4.32, it becomes

$$h_{in} = 0.023 (\frac{k}{D_{in}}) (\frac{G_{in} D_{in}}{\mu})^{0.8} (\frac{C_p \mu}{k})^{0.3} \tag{4.33}$$

where:

h_{in} is the heat transfer coefficient for the primary side;

k is the thermal conductivity of the primary working fluid, i.e., heavy water;

D_{in} is the hydraulic diameter of the inverted U-tube, is equal to geometric diameter;

G_{in} is the flow flux of the primary fluid;

μ is the viscosity of the primary working fluid;

C_p is the heat capacity of the primary working fluid;

For two-phase section, condensing occurs and it is difficult to find a proper correlation to cover various heat transfer mechanisms. This makes the problem more complicated, so some semi-empirical assumptions are adopted when dealing with this situation.

4.1.4 Mechanism of vapor-lock

As referred in Chapter 3, the two-phase pressure drop calculation alone cannot lead to the negative header-to-header pressure differential whose magnitude is large enough to reverse the flows in channels.[22] There exists some extra mechanism that might increase the flow resistance across the loop and lead to the negative pressure differential between RIH and ROH. According to previous researches and investigations, this mechanism may be attributed to the blockage of the inverted U-tubes due to the presence or the accumulation of void at the very top of SG boiler tubes. In this report, this phenomenon is named as vapor lock [22].

Two potential approaches are proposed in previous documents that might result in void-lock. One is that void in the hot leg expands over the top of boiler tubes and enters the cold leg of SG [15]. Under some situation, e.g., Station Blackout, the heat transfer capacity of SG deteriorates to a low level. Since it is unable to transfer enough heat to the secondary side, two-phase flow in the hot leg cannot be cooled down to single-phase flow before it goes into the cold leg. Because of buoyancy, the

void in two-phase flow may accumulate at the top of the inverted U-tubes and result in the blockage in these tubes.

Another potential approach is called cold flash [12]. Under the natural circulation conditions, the top of inverted U-tubes is the specific point that has the lowest pressure within the whole loop. During a loop depressurization resulting from either loop cooldown or loss of inventory, the pressure at the top of U-tubes may decrease to a level that is slightly lower than the saturation pressure of local temperature. This will result in a rapid flashing process, during which void is generated in a short period. With the depressurization proceeding, the volume of void keeps expanding, and more and more tubes are blocked.

The vapor-lock phenomena will increase the flow resistance in the loop by decreasing the flow area that is initially available to transport coolant. This is shown to cause large pressure drop across the steam generator and to result in the negative header-to-header pressure differential. In this report, the second approach, cold flashing, is adopted as the mechanism of vapor-lock, as it is more appropriate for the case of the slow depressurization due to small LOCA that is the subject in this work.

Until now, some important theory backgrounds and the corresponding derivations have been introduced. They will be used in the following model construction and calculation process.

4.2 Modeling

In this Chapter, a quasi-steady-state model is developed to simulate two-phase natural circulation of coolant within HTS in a CANDU 9 reactor. Parameters from the full power normal operation conditions are used to test and benchmark the model, and then this model is applied to analyze the flow and pressure distributions across the loop under the circumstance of small LOCA with loss of Class IV power (ECI system is also assumed out of work).

4.2.1 Model construction

As shown in Fig. 2.2 in Chapter 2, the two loops within one CANDU HTS are arranged in a symmetric configuration, and they are relatively independent with each other except for the connection through pressurizer. Under the concerned accident scenario, the two loops are isolated from each other due to the closure of valve on the connection pipe, so it is valid to just investigate one single loop to understand the dominant behavior of HTS.

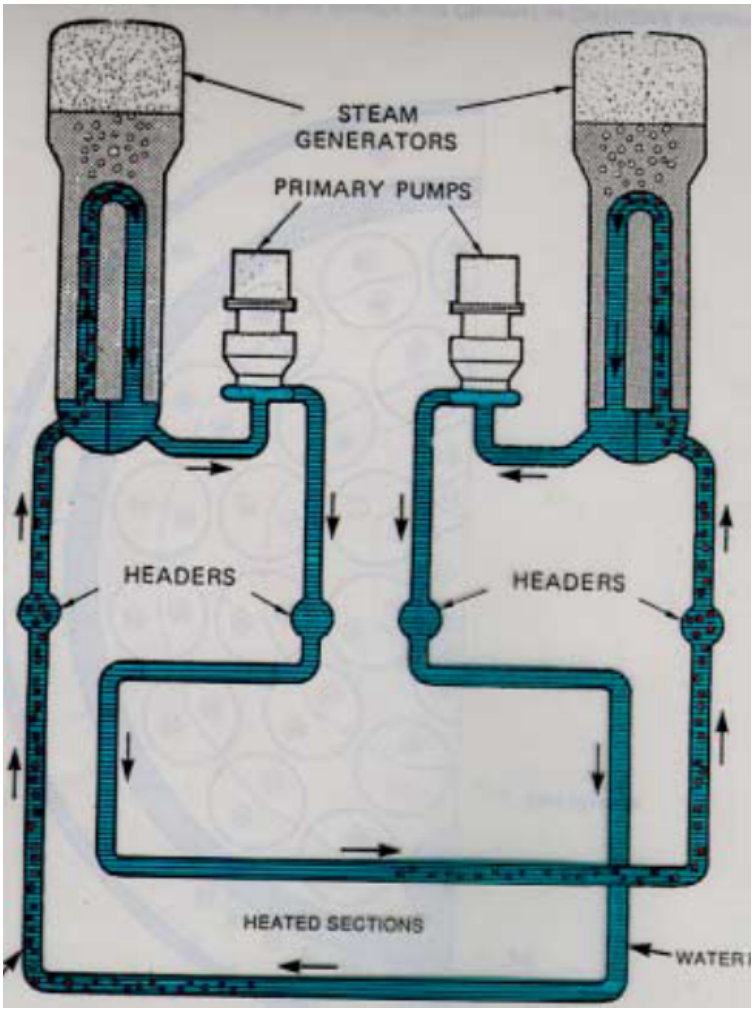

Figure 4.2: Heat transfer loop of CANDU

As illustrated in Fig. 4.2, a single simplified heat transfer loop has been extracted to show the coolant circulation process in HTS. Though it just presents one fuel channel in each flow pass, it has clearly outlined the unique figure-of-eight configuration of CANDU HTS. As shown in Fig. 4.2, the two flow passes within one loop are laid out in a symmetric fashion that make them behave similarly in the aspects of flow and pressure distributions. To focus on the important characteristics of HTS and to

investigate the key mechanisms that make the flow reverse, a simplified figure-of-zero configuration is adopted in the model, and all important components in HTS are represented by different calculation modules, as presented in Fig. 4.3.

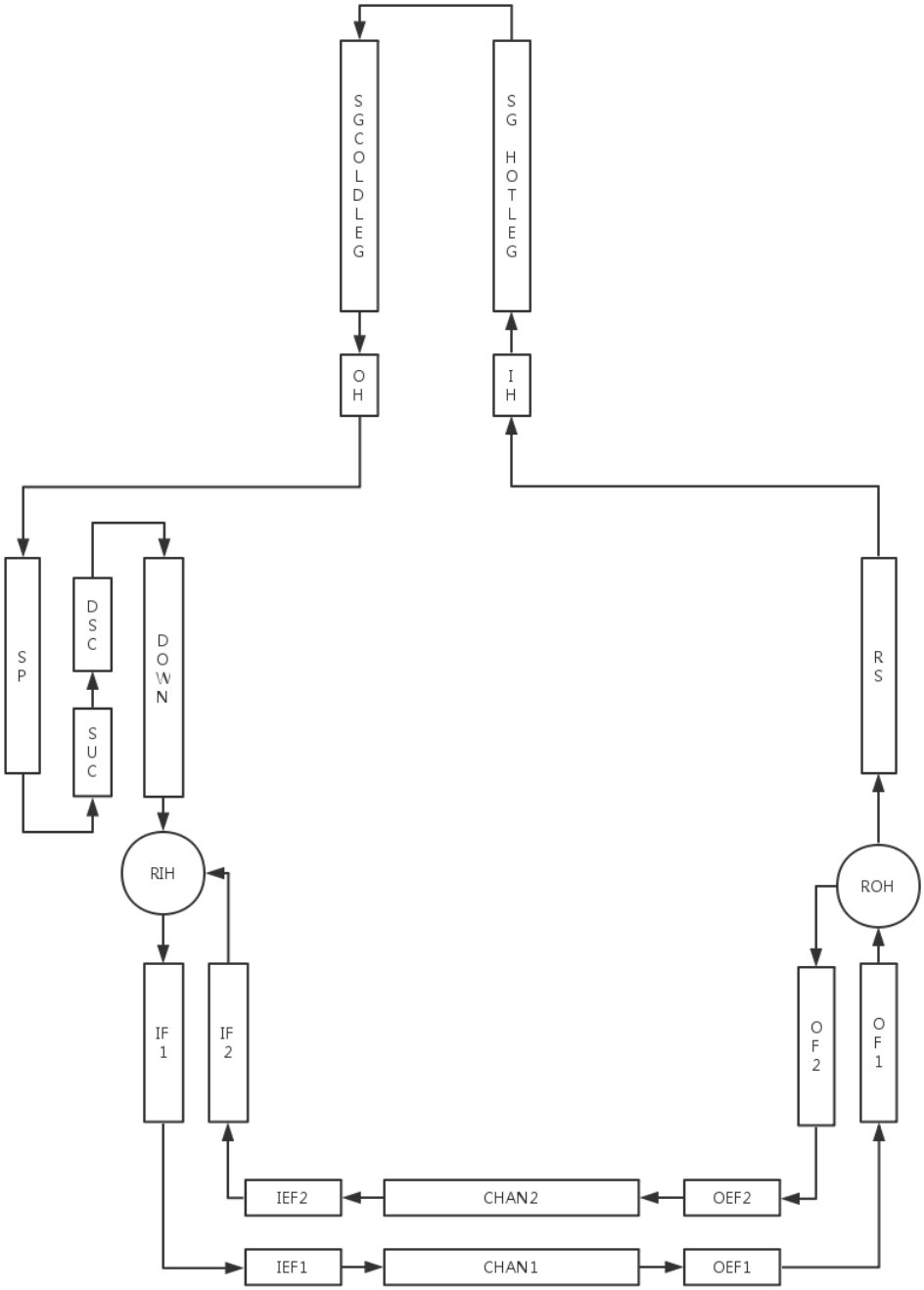

Figure 4.3: Figure-of-zero loop for simulation

1. Sections above the headers:

   - SG (Steam Generator): a lumped inverted U-tube is used to represent all inverted U-tubes in SG, and this module is divided into two parts of hot and cold legs by the bend at the very top of U-tube.
   - IH & OH (Inlet Head & Outlet Head of SG): two cylinder pipes are used to represent two quarter-sphere chambers at the bottom of SG.
   - SP (pipes between SG outlet and the inlet of pump), SUC (pump suction), DSC (pump discharge), DOWN (pipes between pump outlet and inlet of RIH), RS (Riser: pipes between outlet of ROH and inlet of SG inlet head).
   - RIH (Reactor Inlet Header) & ROH (Reactor Outlet Header).

2. Sections below the headers:

   - The piping system below the headers is separated into two parallel lines, CHAN1 line and CHAN2 line, to represent two different flow paths when reversal occurs. CHAN1 line contains IF1, IEF1, CHAN1, OEF1 and OF1, and this line is to represent pipes within which coolant flows in normal forward direction. CHAN2 line consists of OF2, OEF2, CHAN2, IEF2 and IF2, which present pipes transporting reversed flow when flow reversal happens.
   - IF (Inlet Feeders) & OF (Outlet Feeders): a lumped pipe is used to simulate a group of feeder pipes with different geometry parameters in one pass.
   - IEF (Inlet End Fittings) & OEF (Outlet End Fittings): a lumped cylinder

pipe is used to represent the structure of End Fittings connecting different channels in one pass.

- CHAN (Fuel Channels): a lumped fuel channel with total power and the equivalent hydraulic diameter is used to represent all channels in one flow pass. CHAN1 includes all forward-direction channels, while CHAN2 contains all reversed channels.

The details of each module and the corresponding simulation techniques are introduced in following paragraphs.

Parallel Average Algorithm

In CANDU HTS, there are a lot of paralleled pipes to transport coolant. It is cumbersome and unnecessary to model them individually in the simulation. So in realistic operation, a lumped pipe with the equivalent thermal hydraulic properties is used to represent these paralleled pipes. A parallel average algorithm has been developed to lump the pipes into one equivalent pipe with equivalent thermal hydraulic properties. The detailed method is as below:

$$V_{total} = \sum_{i=1}^{n} V_i = \sum_{i=1}^{n} A_i L_i \tag{4.34}$$

$$\overline{L} = \frac{1}{n} \sum_{i=1}^{n} L_i \tag{4.35}$$

$$A_{equivalent} = \frac{V_{total}}{\overline{L}} \tag{4.36}$$

$$\overline{\Delta z} = \frac{1}{n} \sum_{i=1}^{n} \Delta z_i \tag{4.37}$$

$$w_{total} = \sum_{i=1}^{n} w_i \tag{4.38}$$

$$G_{m,equivalent} = \frac{w_{total}}{A_{equivalent}} \tag{4.39}$$

$$Q_{total} = \sum_{i=1}^{n} Q_i \tag{4.40}$$

where:

V is the volume of coolant, V_{total} is the total volume of the paralleled pipes;

L is the length of pipe, $\overline{L}$ is the average length of the paralleled pipes;

A is the area of cross section of flow pass, $A_{equivalent}$ is the equivalent area of flow cross section;

Δz is the elevation difference of the pipe, $\overline{\Delta z}$ is the average elevation difference of the paralleled pipes;

w is the flow rate through the pipe, w_{total} is the total flow rate through all paralleled pipes;

$G_{m,equivalent}$ is the equivalent flow flux of the paralleled pipes;

Q is the power deposited in or transferred out of the coolant in the pipe, Q_{total} is the total power deposited in or transferred out of the coolant in paralleled pipes.

These average methods can simplify several paralleled pipes into a lumped pipe with equal power and flow rate, as well as equivalent thermal hydraulic properties.

Nodalization

Fig. 4.3 illustrates the loop represented by the form of modules. In actual numerical calculation, each module is subdivided into several nodes. These nodes represent the volumes that contain the working fluid, which carries the thermal hydraulic details of mass and energy of the coolant, e.g., density and enthalpy. So it is a natural result that the conservation equations of mass and energy are applied on these nodes. Flow, on the other hand, is driven by the pressure differential along the flow path. It is transported around the loop through different nodes, i.e., it is the links between nodes. This makes it naturally follow the conservation equation of momentum. In conclusion, in numerical calculation, mass and energy conservation equations are applied to nodes, and momentum information is carried by the flow that links nodes. This kind of lumped simulation approach is called node-link method. It is used in this report to build a circulation model.

Apply conservation equations of mass, energy and momentum introduced in Section 4.1.2 to the loop represented by the node-link structure in Fig. 4.3, some thermal hydraulic information about mass, enery and momentum can be obtained for the loop:

- For Mass:

  Apply Eq. 4.7 to different locations in the loop, the specific descriptions of mass

conservation for different locations is obtained.

In the RIH and ROH, where the flows from different branches merge together and are redistributed, the mass conservation equation is as below:

$$W_1 - W_2 - W_{SG} = 0 \tag{4.41}$$

where:

W_1 is the flow rate along CHAN1 flow branch;

W_2 is the flow rate along CHAN2 flow branch;

W_{SG} is the flow rate along SG flow branch;

In all pipes and nodes belonging to the same flow branch, the flow rates through them are certain and constant.

- For Energy:

  For the connection point of different flow branches, such as RIH and ROH, the energy equations are as below:

  In ROH:

$$W_1 h_{OF1} = W_2 h_{ROH} + W_{SG} h_{ROH} = (W_2 + W_{SG}) h_{ROH} \tag{4.42}$$

  where:

  W_1 is the flow rate in CHAN1 branch;

W_2 is the flow rate in CHAN2 branch;

W_{SG} is the flow rate in SG branch;

h_{OF1} is the enthalpy in the last node of OF1 section;

h_{ROH} is the enthalpy in ROH section.

In RIH:

$$W_1 h_{RIH} = W_2 h_{IF2} + W_{SG} h_{DN} \tag{4.43}$$

where:

h_{RIH} is the enthalpy in RIH section;

h_{IF2} is the enthalpy in the last node of IF2 section;

h_{DN} is the enthalpy in the last node of DN section;

- For Momentum:

  Eq. 4.22 will be used in each node to calculate pressure distribution around the loop in following analysis.

According to the previous experience [6], the number of nodes for a module is determined by the size of the module and its density variation span. It is suggested that the thermal hydraulic properties in the adjacent nodes should not change too much, or it will introduce large bias into calculation due to the rapid change in properties.

As the fluid is transported along the flow path, its properties change over the flow

path. In realistic numerical calculation, the properties within links are set to be the same as the upstream nodal properties. Although this assumption leads to a transport delay on the aspect of fluid properties, the averaged values of properties change slowly in adjacent nodes and do not introduce obvious bias from global view. So this is an acceptable and effective assumption when using many node-link structures in the model.

Table 4.2 collects main geometry parameters of each module in HTS, based on the schematic node-link structure in Fig. 4.3. *No.* is the number of nodes in each module. D_e is the hydraulic diameter for single channel, and A is the lumped area for 120 channels in one flow pass, calculated by parallel average algorithm described in Section 4.2.1. Δz is elevation change in current module. K_1 is form term multiplier for flow change between different modules. K_2 is internal form term multiplier in each module. ϵ is surface roughness of pipe and K_e is relative surface roughness.

Table 4.2: Collection of geometry parameters of modules in HTS

Modules	Length	$No.$	D_e	A	Δz	K_1	K_2	ϵ	$K_e = \frac{\epsilon}{D_e}$
	m		m	m^2	m	$\frac{kPa}{kPa}$	$\frac{kPa}{kPa}$	m	$\frac{m}{m}$
RIH	-	1	-	-	-	-	-	-	-
IF	13.89	9	0.0428	0.3241	7.4265	1.75	1.2021	4.57E-05	1.07E-03
IEF	4.46	1	0.0426	0.4105	0	0.4	0	4.57E-05	1.07E-03
CHAN	6	12	7.4E-03	0.4107	0	1	8.6251	8.00E-07	1.08E-04
OEF	4.46	1	0.0426	0.41053	0	0.78	0	4.57E-05	1.07E-03
OF	17.3635	3	0.0513	0.4535	7.3048	0.4	0.8281	4.57E-05	8.92E-04
ROH	-	1	-	-	-	-	-	-	-
RS	5.6232	3	0.4889	0.1877	3.44	0	0	4.57E-05	9.35E-05
IH	1.24	1	1.3548	1.44	1.147	0	0	4.57E-05	3.37E-05
SG	21.51	13	0.01475	0.6774	10.755	1.1	1.7	1.50E-06	1.02E-04
OH	1.24	1	1.3548	1.44	1.147	0.5	0	4.57E-05	3.37E-05
SP	18.615	2	0.5318	0.2221	-0.9	0.3	0	4.57E-05	8.60E-05
SUC	0.686	1	0.5318	0.2221	0.686	1.1	0	4.57E-05	8.60E-05
Pump	-	1	-	-	-	14.7	-	-	-
DSC	0.686	1	0.509	0.2035	0.686	0	0	4.57E-05	8.98E-05
DOWN	3.79	3	0.443	0.1541	3.79	1.3	0	4.57E-05	1.03E-04

Code Structure

Pressure and enthalpy are chosen as the input parameters of the equation of state across the loop, and they are passed on from node to node to calculate the corresponding thermal hydraulic properties for each node-link structure. The thermal hydraulic properties of light water are used to replace that of heavy water in the simulation. Since they have little difference in current working conditions, it is an acceptable assumption for this work. A MATLAB thermal hydraulic package, XSteam, is used in the code to calculate the light water properties of current node, based on the outlet pressure and enthalpy inherited from the upstream node. This package is compiled on the basis of IAPWS IF-97 standard.

A series of MATLAB codes have been programed to assist the calculation in this study, the structure of main code can be summarized as below:

1. Boundary conditions:

   Inlet pressure: P_{in};

   Inlet enthalpy: H_{in};

   They are inherited from the upstream node or the initial boundary assumption.

2. Water properties:

   Saturation liquid and vapor enthalpy at current pressure: H_l and H_v;

   Saturation liquid and vapor density at current pressure: ρ_l and ρ_v;

   Saturation liquid and vapor specific volume at current pressure: ν_l and ν_v;

   Saturation liquid and vapor viscosity at current pressure: μ_l and μ_v;

3. Heat conditions:

   Power injected into the current node: dQ;

4. Flow properties:

   Flow rate: w;

   Flow flux: G_m;

5. Geometry properties:

   Length of the current node: dL;

   Cross section area of the current node: A;

   Hydraulic diameter of the current node: D_e;

   Elevation difference of the current node: Δz;

   Tube surface roughness: ϵ;

6. Calculation process:

   (a) Enthalpy of current node:

$$H_{out} = H_{in} + \frac{\Delta Q}{w} \tag{4.44}$$

(b) Heat quality of current node:

$$x_e = \frac{H_{out} - H_l}{H_{fg}} \tag{4.45}$$

(c) Flow quality of current node:

$$x = \begin{cases} 0 & x_e \leq 0 \\ x_e & 0 < x_e < 1 \\ 1 & x_e \geq 1 \end{cases} \tag{4.46}$$

(d) Void fraction:

$$\alpha = \begin{cases} 0 & x = 0 \\ (1 + \frac{1-x}{x}\frac{\rho_v}{\rho_l})^{-1} & x > 1 \end{cases} \tag{4.47}$$

Note that, for two-phase flow

$$\alpha = (1 + \frac{1-x}{x}\frac{\rho_v}{\rho_l}S)^{-1} \tag{4.48}$$

where:

S=V_g/V_l, is slip ratio of two-phase flow. Since this report adopts HEM assumption, the velocities of two phases are the same, so S=1.

(e) Density of two-phase mixture:

When flow is subcooled, the density of coolant in the node is determined by XSteam package, judged by the pressure in the upstream node and the

enthalpy in the current node.

When flow has been saturated and two-phase flow has occurred in the pipe, the density of mixture is calculated by the method for HEM, using Eq. 4.1.

(f) Specific volume of two-phase mixture:

Following the similar way for calculation of density, the calculation of specific volume for current node is as below:

When flow is subcooled and no void appears, specific volume is calculated by XSteam, using the pressure in the upstream node and the enthalpy in the current node.

When flow has been saturated two-phase flow, HEM method is applied to the node by using Eq. 4.2.

(g) Viscosity of two-phase mixture:

Following the similar way as for above two properties, viscosity is calculated by XSteam package if the flow is subcooled. Eq. 4.3 is used to calculate the viscosity if it is saturated two-phase flow.

(h) Mass inventory:

The mass inventory is one of key system parameters that are being investigated in the study. The inventory in each node is calculated by using the density and the volume of each node, just as below:

$$invt = \rho_m AdL \tag{4.49}$$

The system total inventory is the sum of inventories in all nodes, as shown in Eq. 4.50.

$$invt_{total} = \sum_{i} invt_i \tag{4.50}$$

The simulation is divided into two stages: First, normal operation boundary conditions are applied to calculate the key parameters of system during normal operation case. These parameters are used as reference values in subsequent calculation. Second, the accident scenario is investigated by changing boundary conditions, and the newly-obtained parameters are compared with the results in normal operation to understand the influence of the accident to HTS thermal hydraulic characteristics.

(i) Reynolds Number:

Re is a dimensionless quantity to define flow conditions, and it is calculated as below:

$$Re = \frac{G_m D_e}{\mu_m} \tag{4.51}$$

(j) Friction factor of tube surface:

Friction factor is determined by the flow conditions in the pipe. If it is in laminar flow range, it is calculated as below:

$$f = \frac{64}{Re} \qquad Re < 3000 \tag{4.52}$$

If it is in turbulent flow range, friction factor is calculated by Colebrook-White equation.

$$\frac{1}{\sqrt{f}} = -2log_{10}(\frac{\epsilon}{3.7De} + \frac{2.51}{Re\sqrt{f}}) \tag{4.53}$$

where:

ϵ is tube surface roughness.

(k) Two-phase Friction Multiplier:

The correlation below is applied in the model

$$\Phi_{lo}^2 = (\frac{\rho_l}{\rho_v} - 1)x + 1 \tag{4.54}$$

(l) Pressure Drop Calculation:

Pressure drop is calculated by the derivation results of momentum conservation equation, as mentioned in Section 4.1.2.

- Acceleration term:

$$\Delta P_{acc} = G_m^2 \nu_{out} - G_{m,up}^2 \nu_{in} \tag{4.55}$$

- Friction term:

$$\Delta P_{fric} = \Phi_{lo}^2 \frac{fdL}{D_e} \frac{G_m^2}{\rho_l} \tag{4.56}$$

- Local form term:

$$\Delta P_{form} = \Phi_{lo}^2 K \frac{G_m^2}{\rho_l} \tag{4.57}$$

- Gravity term:

$$\Delta P_{grav} = \rho_m g \Delta z \tag{4.58}$$

- Total pressure drop in current node:

$$\Delta P = -\Delta P_{acc} - \Delta P_{fric} - \Delta P_{form} - \Delta P_{grav} \tag{4.59}$$

- Outlet pressure:

$$P_{out} = P_{in} + \Delta P \tag{4.60}$$

Repeat this calculation process for each node in the loop, thermal hydraulic features and their distributions within HTS will be obtained. And these parameters are used in subsequent analysis to investigate the flow reversal behavior of HTS.

4.2.2 Module Details

This part will introduce the special features of different modules in the loop. The detailed values are input into the corresponding codes. These parameters are from CANDU technology manual [3] and other sources in published documents.

Fuel Channel section

There are 120 channels in one flow pass, and all of them have unidirectional forward flows under normal operation condition. In this report, the simulation starts with the assumption that all flows are in normal forward-direction at the beginning of simulation. With ongoing depressurization of HTS and decrease of coolant inventory, channels in some rows will reverse. These reversed channels are lumped as CHAN2 branch in the model. The rest forward-direction channels are lumped as CHAN1

branch, as shown in Fig. 4.3.

CHAN1 and CHAN2 branches have different lumped elevations and power injection rates, since the positions and numbers of channels contained in these two branches are different. The numbers of channels contained in CHAN1 or CHAN2 are determined by the number of rows that flow reversal occurs. If only row A is reversed, all channels in row A are counted into CHAN2 branch, while the rest of channels are counted into CHAN1 branch. If row A and B are reversed, all channels in these two rows are treated as CHAN2 branch, while the rest channels are counted into CHAN1 branch, etc.

- Elevation Position

  To determine the elevation positions of CHAN1 and CHAN2, an approach is applied that is similar to the concept of center of mass, as shown in Eq. 4.61.

$$z_{CHAN} = \frac{\sum_i w_i z_i}{\sum_i w_i} \tag{4.61}$$

  where:

  z_{CHAN} is the elevation position of CHAN1 or CHAN2;

  z_i is the elevation position of one of channels in current branch;

  w_i is the flow rate in corresponding channel;

  Subscript i is the label of channel in CHAN1 or CHAN2 branch;

- Power Profile

  Since the powers in all channels decay in the same way, as shown in Fig. 1.2, they

have the same form of power profile. The power profile within the CANDU core is complex, in this analysis, a cosine distribution is adopted as an approximation:

$$q(z) = q_0 \cos(\frac{\pi z}{L_{core}}) \qquad z \in [-\frac{L_{core}}{2}, \frac{L_{core}}{2}] \tag{4.62}$$

where:

L_{core} is the length of the core;

$q(z)$ is linear power at specific point of core;

q_0 is the peak value of linear power, and it is different for CHAN1 and CHAN2.

- Hydraulic Diameter

  In this report, hydraulic diameter is calculated as below:

$$D_e = \frac{4A_{CHN}}{P_e} \tag{4.63}$$

where:

$A_{CHN} = 0.25\pi(D_{PT}^2 - 37D_{FE}^2)$, is the flow area of sub-channel cross section for one channel;

$P_e = \pi(D_{PT} + 37D_{FE})$, is the wetted perimeter of sub-channel cross section for one channel;

D_{PT} is the diameter of pressure tube, and D_{FE} is the diameter of fuel element.

Feeders

As introduced in Section 2.6, the structure and layout of feeders are complicated. To simplify the model, 4 specific inclined straight pipes (IF 1 & 2 and OF 1 & 2)

are applied to represent all feeder pipes connected to CHAN1 and CHAN2 line on both ends, as shown in Fig. 4.4. The lengths, slopes and cross section areas of these four lumped feeders are different from one another as a result of complexity of feeder geometry structure.

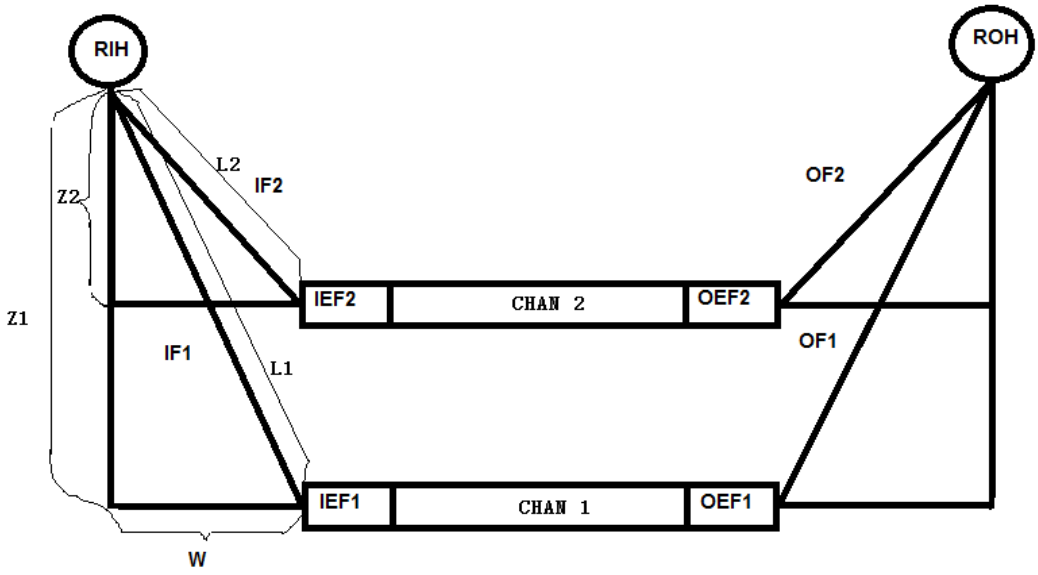

Figure 4.4: All feeder pipes are lumped into four inclined pipes.

As shown in Fig. 4.4, the width W is fixed, if the lumped channel elevation positon $z1$ and $z2$ are calculated using Eq. 4.61, the lengths of lumped feeders, L1 and L2, can be calculated. The same method is used for the other side, and all main geometry parameters for feeders are available.

Steam Generator

Based on the heat transfer process discussed in Section 4.1.3 and the vapor-lock phenomena introduced in Section 4.1.4, a module of inverted U-Tubes is constructed to simulate two-phase flow pressure drop within steam generator under small LOCA conditions.

1. Heat Transfer Capability

   As described in Section 4.1.3, the heat transfer in SG involves multiple processes covering conduction, single-phase and two-phase convection, and fouling. This makes it difficult to find all proper equations or correlations to describe these processes in an accurate mathematic way, so semi-empirical assumption is adopted in the model following the approach of Soedijono et al[22]:

   Since Class III power is maintained in the assumed initiating events, so auxiliary boiler feed pumps supplied by Class III power can still work normally after loss of Class IV power. It supplies feedwater to the secondary side of SG when main boiler feed pumps are tripped due to loss of Class IV power. So the design heat removal capability of SG under decay heat conditions is maintained, and it is assumed to be large enough to remove all decay heat generated in channels after reactor trip. The high-temperature flow entering into SG can be cooled down in a short portion of boiler tube inlet. Therefore it is assumed that the enthalpies of nodes within SG are the same as the saturation liquid enthalpy at the secondary-side pressure.[22] With further depressurization of primary loop, there is possibility that the pressure at the very top of SG inverted U-tubes is slightly lower than the pressure on the secondary side. They make it possible

that vapor lock can occur at the very top of SG. However, the majority of primary side is still not superheated to local pressure.

It should be noted that, although Class III power is available, ECI system supported by Class III power can still not be initiated due to random failures. This assumption is adopted in this analysis, so there is no crash cooldown in SG either.

The assumptions above are acceptable as they are just applied to the calculation with decay heat. In addition, they avoid the uncertainty in choosing proper correlations for various flow regimes, and accelerate the calculation.

2. Vapor Lock Model

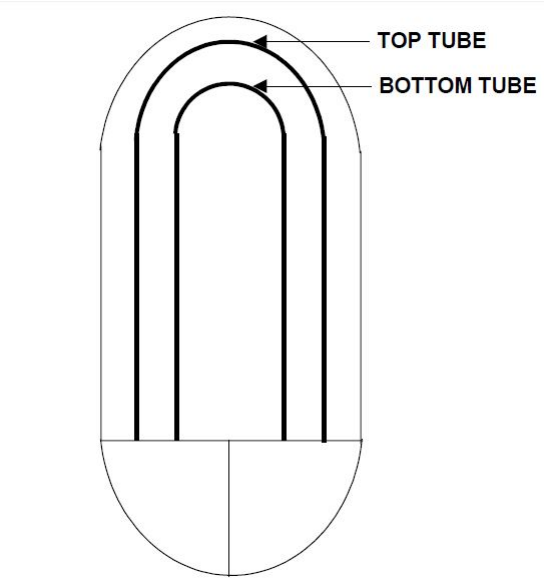

Figure 4.5: The cross section of boiler tubes in SG[22]

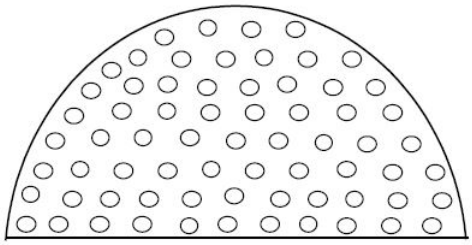

Figure 4.6: The cross section of boiler U-bend at the very top of SG[22]

As discussed in Section 4.1.4, the top of inverted U-tubes have the lowest pressure within the primary heat transfer loop. Fig. 4.5 and Fig. 4.6 show the cross sections of boiler tubes and the boiler U-bend at the very top of SG respectively. With the decrease of inventory and the depressurization of HTS, the pressure there will be slightly lower than the saturation pressure of the secondary side, so cold flashing may occur at the top of inverted tubes. This void expands and finally blocks some inverted U-tubes, and results in vapor-lock in these tubes.

The number of tubes that are vapor locked depends on the pressure at the very top of inverted U-tubes on the primary side (P_{top}). Suppose N_{block} is the number of tubes that are vapor locked as a fraction of total number of tubes, so $0 \leq N_{block} \leq 1$. The relation between N_{block} and P_{top} is as below:

If $P_{top} > P_{sec}$, $N_{block} = 0$;

If $P_{top} < P_{sec} - \Delta P_{tb}$, $N_{block} = 1$;

where:

P_{sec} is secondary-side pressure, and it is set to be 5.070 MPa for CANDU 9 in

this analysis;

$\Delta P_{tb} = \rho_{top} g \delta h_{tb}$, ρ_{top} is the two-phase mixture coolant density at the top of inverted U-tubes, g is the gravitational acceleration, and δh_{tb} is elevation difference between the very top and the very bottom inverted U-tubes, and it is assumed to be 0.7 m in the analysis.

The relations above set the boundary conditions of P_{top} and N_{block}. As shown in Fig. 4.5, if the pressure at the very top of the primary side is higher than the pressure on the secondary side, vapor lock will not occur in SG. If the pressure at the top of the primary side is lower that of the secondary side by a gap that is larger than $\rho_{top} g \delta h_{tb}$, i.e., even the pressure of the very bottom inverted U-tube is still lower than the pressure of the secondary side, all inverted U-tubes will be blocked at the very top of SG and no flow can go through SG. This total vapor-lock situation means the flow path through SG has disappeared.

It should be noted that, in the SG, the pressure of the majority part of the primary side should always be larger than the pressure on the secondary side. This assures that the overall primary-side saturation temperature is higher than the secondary-side saturation temperature, and a positive heat transfer direction can be maintained within SG.

For $P_{sec} - \Delta P_{tb} \leq P_{top} \leq P_{sec}$, the value of N_{block} is determined by the geometry structure at the top of inverted U-tubes, as shown in Fig. 4.6. This geometry structure is similar in both Pickering SG and CANDU9 SG, except the number

of boiler tubes. Table 4.3 shows the relation of N_{block} and P_{top} in the Pickering SG, which has totally 2559 inverted U-tubes within one SG. ΔP_{tb} is the static pressure difference from top to bottom that is set to be 6.0 kPa for a Pickering SG, and the secondary-side pressure is 4.6 MPa.[22]

Table 4.3: No. of vapor locked tubes vs. Pressure difference at the top of SG[22]

Top Pressure Difference (kPa)	No. of Tubes Vapor-Locked	N_{block}
1.0	225	0.0879
2.0	577	0.2255
3.0	1013	0.3959
4.0	1505	0.5881
5.0	2030	0.7933
6.0	2559	1.0000

Fig. 4.7 shows the relation between P_{top} and N_{block}, and the boundary conditions are as below:

$P_{top} > P_{sec}$ (4600 kPa), $N_{block} = 0$;
$P_{top} < P_{sec} - \Delta P_{tb}$ (4600 kPa - 6.0 kPa), $N_{block} = 1$.

By using mechanistic method, a relation between N_{block} and P_{top} is obtained.It is found that the form of second order polynomial of P_{top} has a good agreement with the trend and magnitude of data points. So it is supposed that the relation of N_{block} and P_{top} has a form of second order polynomial, therefore a

mathematical equation is derived based on this assumption, as shown in Eq. 4.64. It is assumed to be available to all SGs with similar inverted-U-tube geometry structure. According to Reference [22], this equation is used to scale the RD-14M data to the CANDU9 SG.

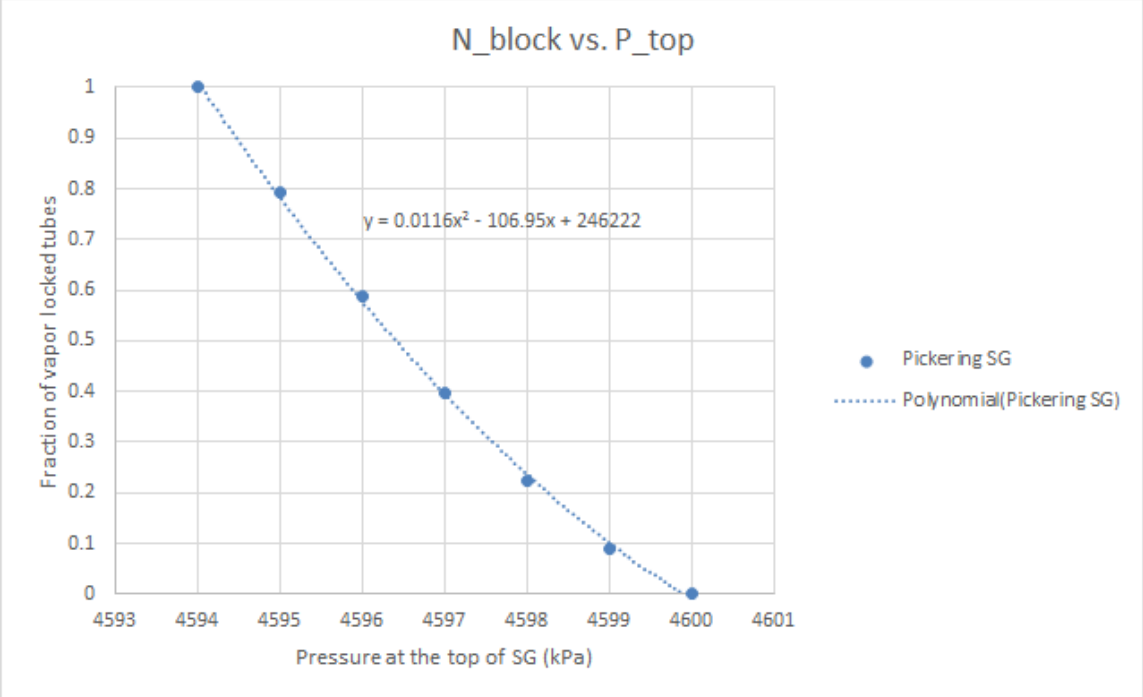

Figure 4.7: N_{block} vs. P_{top} of Pickering SG[22], and a polynomial trend line is fitted based on Pickering SG data to be utilized for CANDU9.

$$N_{block}(P_{top}) = \frac{1}{\Delta P_{tb}^2}(P_{top} - P_{sec})^2 \tag{4.64}$$

With the occurrence of vapor lock, the flow area that is available for coolant transportation decreases, and subsequently flow resistance increases, as shown

in Eq. 4.65.

$$A_{available} = (1 - N_{block})A_{initial} \tag{4.65}$$

Pumps

As discussed in Section 2.9, after loss of Class IV power, PHTP can not provide driving force to forced circulation cooling. Instead, it actually adds flow resistance to the loop as a result of the friction pressure drop within the pump. To calculate the pressure drop caused by the tripped PHTP, an extra pressure drop term , ΔP_{pump}, is added into the loop, as shown in Eq. 4.66, where a specific multiplier factor, K_{pump}, is assigned to the equation.

$$\Delta P_{pump} = K_{pump}\frac{G_m^2}{\rho_m} \tag{4.66}$$

This completes the construction of HTS model. All important details about the model have been introduced in previous sections. This model is to be used to simulate HTS and to investigate the flow reversal phenomena after the initiating accidents.

Flow Reversal Criterion

As described in Section 3.1.2, in the analysis of pressure and flow distributions under two-phase natural circulation conditions, a quasi-steady criterion is used to decide which channels will reverse with the evolution of HTS conditions: the RIH-to-ROH pressure differential must be negative enough to counterbalance the forward driving

force resulting from the density gradient between inlet and outlet feeders. Mathematically, the criterion is expressed as below:

$$P_{ROH} - P_{RIH} > \int_{z,IF} \rho_{IF}(z) g dz - \int_{z,OF} \rho_{OF}(z) g dz \tag{4.67}$$

where:

P_{ROH}, P_{RIH} are the pressures at outlet header and inlet header respectively;

$\rho_{IF}(z), \rho_{OF}(z)$ are the fluid densities at the elevation position z within inlet feeders and outlet feeders;

g in gravitational acceleration.

Rearrange Eq. 4.67, it becomes as below:

$$\Delta P_{HH} < \Delta P_{rev} \tag{4.68}$$

where:

$\Delta P_{HH} = P_{RIH} - P_{ROH}$, RIH-to-ROH pressure differential in the loop;

$\Delta P_{rev} = \int_{z,OF} \rho_{OF} g dz - \int_{z,IF} \rho_{IF} g dz$, the minimum header-to-header pressure differential required to reverse flow.

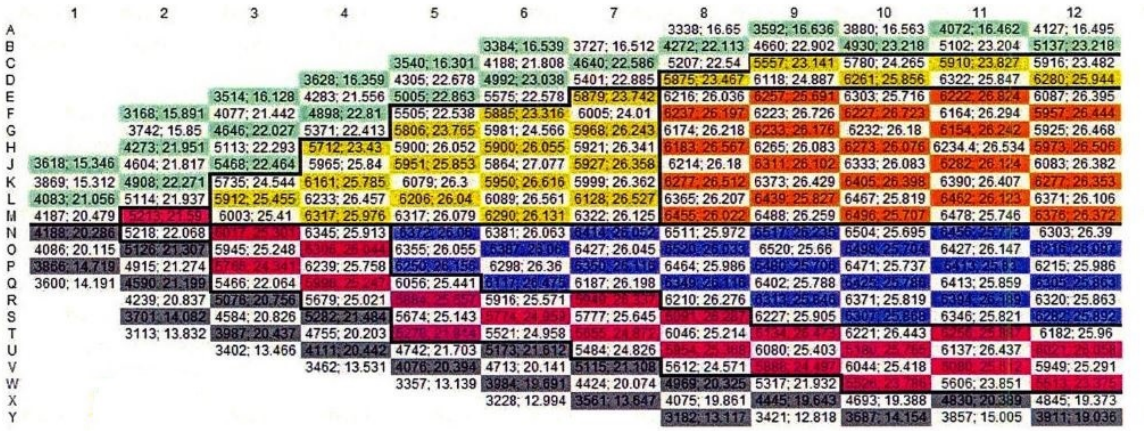

Figure 4.8: 240 channels in one HTS loop[21]

Fig. 4.8 shows 240 channels in one CANDU9 HTS loop, and two flow passes within one loop are distinguished by shading in the diagram. It can be seen that all channels are laid out in 24 rows in vertical direction(note that letter "Y" is not adopted in enumeration) and 12 columns in horizontal direction. The configuration of the other loop is mirror-symmetric to that of this loop in horizontal direction. In this analysis, the pass with shading is adopted, so row A has 2 channel, row B has 4 channels, etc.

Following Eq. 4.68, the criterion can be stated as follows: When ΔP_{HH} is larger than ΔP_{rev}, the flow in the corresponding channels will have flow in the forward direction. When $\Delta P_{HH} < \Delta P_{rev}$, the flow in the corresponding channels will reverse. Based on the definition of ΔP_{rev} in Eq. 4.68, ΔP_{rev} is determined by density difference in hot and cold legs, as well as the elevation change of channels. For example,

row A in Fig. 4.8 has the smallest elevation change from fuel channel to headers, so it will have a relatively smaller ΔP_{rev} compared with other rows in reactor.

Normally, Eq. 4.68 can be fulfilled when vapor lock occurs in SG. As it requires a small gap between ΔP_{HH} and ΔP_{rev} to overcome the original inertial effect in reversing flow direction, a value at the order of 1 kPa is set in this model, i.e., if ΔP_{HH} is more negative than ΔP_{rev} by the magnitude of about 1 kPa, it is assumed that the corresponding channel row has fulfilled the criteria stated in Eq. 4.68, and all the channels in this row will reverse.

4.2.3 Types of Calculation

To verify the efficiency of the quasi-steady-state HEM model and to investigate the pressure and flow distribution before and after flow reversal, the calculations are performed for three different cases: normal operation case, no reversal case and reversal case. In the simulation model, channel powers, RIH pressure and secondary side pressure are chosen as thermal hydraulic boundary conditions.

Benchmark of Normal Operation

In this case, the parameters under normal full power operations are applied to the model. PHTP is assigned a normal positive driving head. An empirical primary heat transfer coefficient value is assigned to Eq. 4.24 to calculate the lumped heat transfer

coefficient for SG, accompanied with other conduction, convection and fouling parameters, and a resultant heat balance is maintained.

The function of this step is to calibrate the model and to verify its efficiency. After this step, a benchmark is built for the subsequent calculations.

The Case with No Reversal

In order to investigate HTS thermal hydraulic behavior, a calculation scheme is designed as Fig. 4.9. In this case, since all channels are in normal forward direction and no reversal occurs, CHAN2 line in Fig. 4.3 is not used in the calculation, and all channels are lumped by CHAN1 line. The calculation is performed by iteration around the figure-of-zero loop, until the assumed flow can match with the designed pressure. After this step, the thermal hydraulic behavior before the flow reversal can be obtained in HTS.

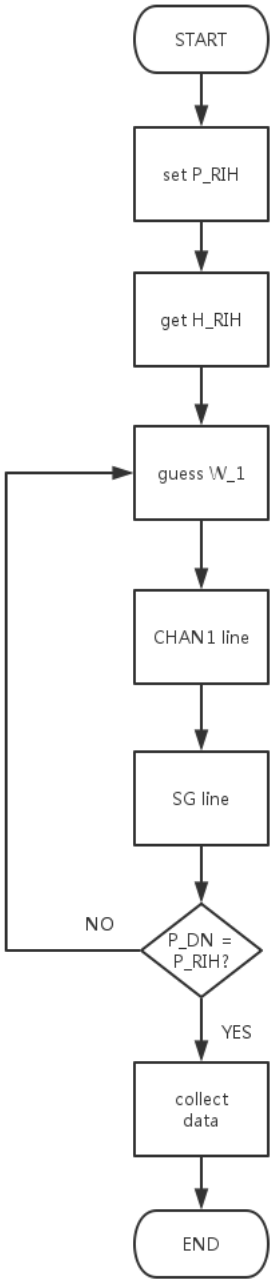

Figure 4.9: Calculation procedures for no reverse case

The Case with Reversal

When flow reversal occurs in some high elevation channel rows, all channels are divided into two groups: normal forward direction and reversed direction. They are represented by CHAN1 line and CHAN2 line respectively in the model, as shown in Fig. 4.3. An iteration scheme is designed as shown in Fig. 4.10, and the calculation is performed around two loops. The first one is from RIH to RIH via CHAN1 line, ROH and SG line. The second one is from RIH to RIH via CHAN1 line, ROH and CHAN2 line. The calcualtions are iterated until a converged quasi-steady-state solution is achieved. Based on these calculations, the thermal hydraulic features of HTS can be investigated when flow reversal happens in some channel rows.

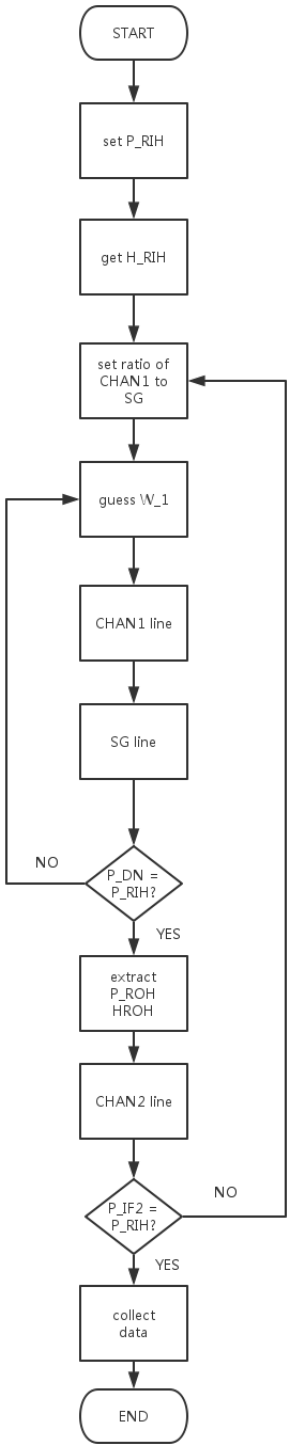

Figure 4.10: Calculation procedures for flow reversal

Chapter 5

Results and Discussion

5.1 HTS parameters with decreasing inventory

Due to the assumed small LOCA accident scenario, the HTS keeps losing coolant inventory with time. As a result of the decreasing inventory, the various thermal hydraulic parameters undergo different variation trends in the primary loop. On the other hand, these parameters are somewhat interconnected with each other, as discussed in Section 4.1.1 and 4.2.1, so to some extent, the change of one parameter may influence the behavior of other parameters. The following paragraphs analyze and discuss the variations of these thermal hydraulic parameters.

5.1.1 Depressurization Process

The thermal hydraulic behavior of PHTS are investigated with the model introduced in Chapter 4. Different system parameters are predicted as a function of channel powers, RIH pressure and the secondary side pressure. The decay heat level is dependent on the time elapsed from reactor trip. In this section, a reference decay power is set to be 1.5% of full power (FP). Although there is no obvious beginning point or ending point in coolant circulation, RIH is chosen as the hypothetical start point of loop calculation. Therefore RIH pressure is naturally adopted as one of initial boundary conditions. In addition, RIH pressure is a good reflection of PHTS pressure level. The secondary side design pressure is 5.070 MPa for CANDU9 reactor. It will decide the secondary side saturation temperature, and subsequently the primary-secondary temperature difference and the heat transfer capability.

As indicated in Fig. 5.1, the HTS inventory is calculated for each input RIH pressure on the curve. With RIH pressure decreasing from 11.300 to about 5.130 MPa, which is slightly higher than the secondary side pressure of 5.070 MPa, the HTS inventory decreases from 100.0% of normal inventory level to 76.7% of normal inventory level. As discussed in item 6(h) in Sectioin 4.2.1, normal inventory level is obtained from the calculation type of normal reactor operation conditions described in Section 4.2.3, while the subsequent inventory levels are expressed as the fractions of normal inventory.

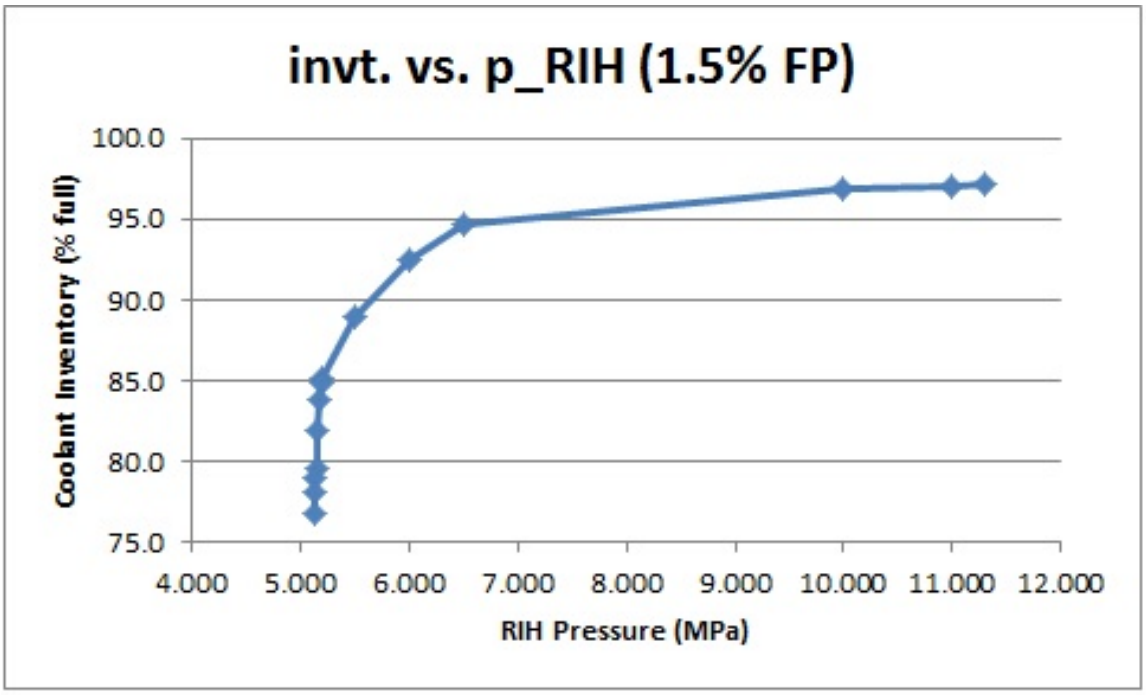

Figure 5.1: HTS coolant inventory keeps decreasing with RIH pressure decreasing.

It can be seen from Fig. 5.1, before RIH pressure falls below 6.500 MPa, coolant inventory does not decrease significantly. In another word, a small loss of coolant inventory can lead to a large decrease in RIH pressure during this period. However, after RIH pressure decreases below 6.500 MPa, inventory decreases sharply with each small step of depressurization. Conversely, loss of inventory has little influence on RIH pressure level.

Fig. 5.2 shows the variation of ROH pressure with coolant inventory decreasing, while Fig. 5.3 shows the trend of the pressure at the top of SG inverted U-tubes as a function of inventory. It can be seen that, with coolant inventory decreasing, the

primary loop has been constantly depressurized. Similar to RIH, the depressurization processes in ROH and at the top of SG have different sensitivities to the loss of inventory. With inventory decreasing from 96.9% to 94.7% of the initial value, the pressure at ROH decreases from 10.002 MPa to 6.505 MPa, while the pressure at the top of inverted U-tubes declines from 9.892 MPa to 6.395 MPa. During this stage, the fluid in the loop is still single-phase incompressible liquid. A small loss of inventory can lead to a large depressurization. When inventory is continuously reduced, vapor occurs, and it makes fluid two-phase compressible flow. This decreases the HTS sensitivity to the loss of inventory, so curves become flat when inventory decreases below 83.9% in Fig. 5.2 and Fig. 5.3.

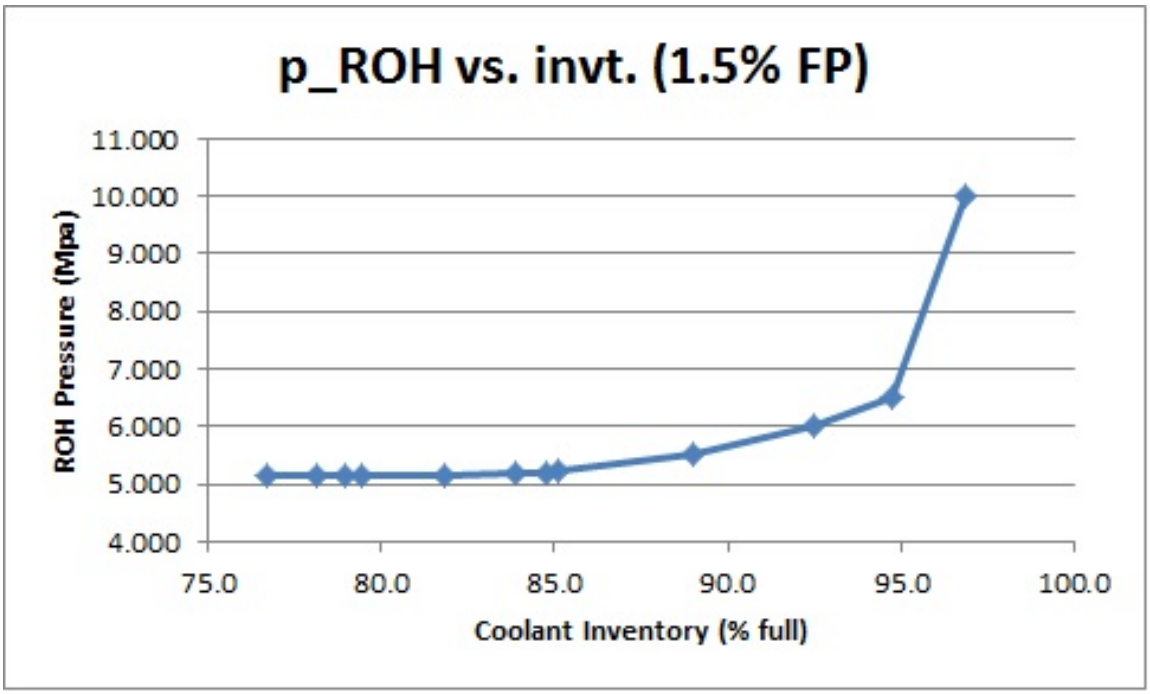

Figure 5.2: Pressure in ROH keeps decreasing with inventory decreasing

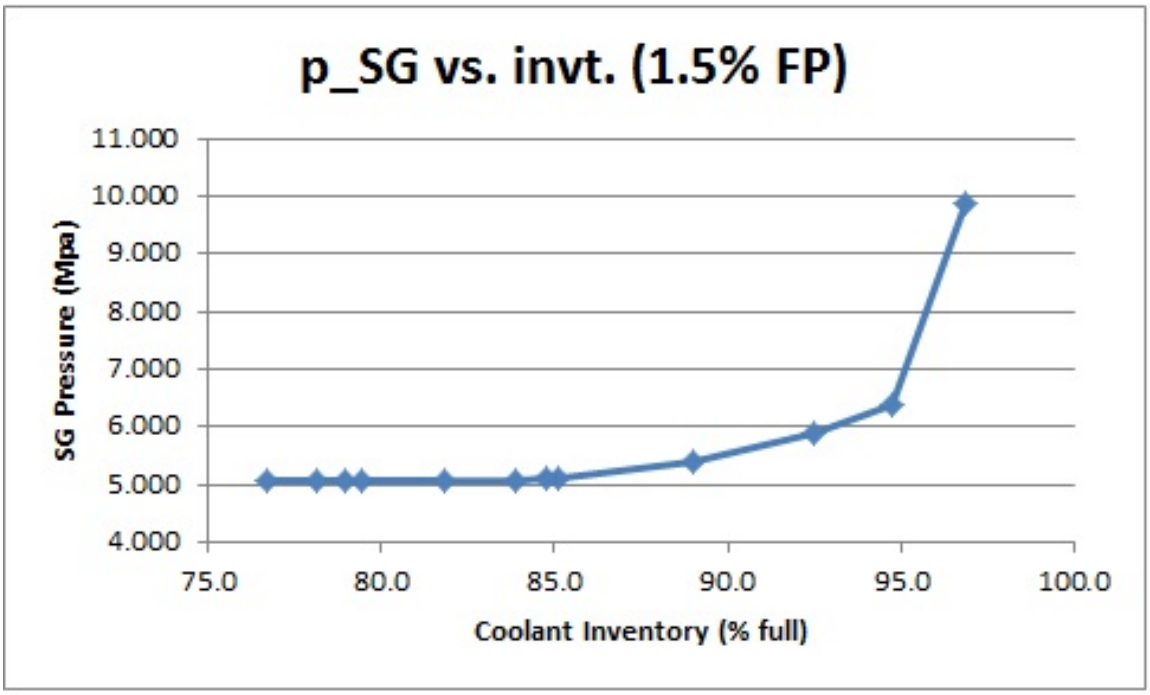

Figure 5.3: Pressure at the top of SG keeps decreasing with inventory decreasing

It should be noticed that, with depressurization ongoing, the primary side pressure approaches the secondary side pressure. This reduces the saturation temperature difference between the primary side and the secondary side.

5.1.2 Vapor Lock Phenomenon and Consequences

Vapor-Locked Boiler Tubes, N_{block}

As defined in item 2(Vapor Lock Model) in Section 4.2.2, N_{block} is the number of vapor-locked inverted U-tubes in SG, and is normalized as the fraction of total number of tubes. Fig. 5.4 shows its variation with decreasing inventory. There is no vapor

lock in SG until HTS inventory declines to the level below 83.9% of full inventory. As indicated in Fig. 5.3, when inventory decreases from 83.9% to 81.8%, the pressure at the top of SG has dropped from 5.079 MPa to 5.066 MPa, which is lower than the secondary side saturation pressure of 5.070 MPa. Therefore the primary side becomes superheated and the coolant at the top of SG evaporates and results in the appearance of vapor lock.

It should be noted that, it is only the pressure at the very top of SG inverted U-tubes and at its adjacent sections that are lower than the secondary side pressure of 5.070 MPa. The pressure at rest majority part of SG is still higher than the secondary side pressure(i.e., the local temperature difference is still positive from the primary side to the secondary side), so there is no cold fleshing in this part of SG.

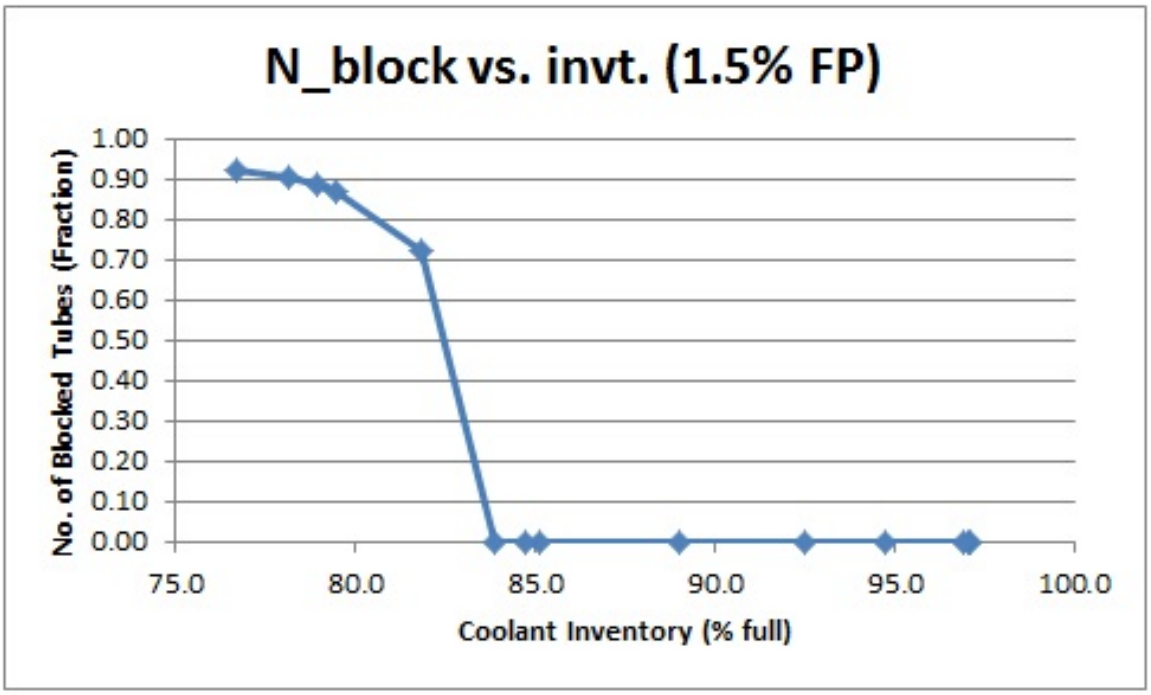

Figure 5.4: Vapor lock occurs when inventory decreases below 83.9%.

It can be seen from Fig. 5.4, when vapor lock initially occurs at the top of SG, it expands promptly and occupies 0.72 of the inverted U-tubes with a small further loss of inventory (from 83.9% to 81.8%). Afterwards, N_{block} increases in a relatively flat manner and approaches gradually to 1, until final total vapor lock of SG flow branch.

Density-Dominated Phase and Resistance-Dominated Phase

Fig. 5.5 shows the variation of flow rate in CHAN1 branch ($w1$) as a function of decreasing inventory. As indicated in the diagram, when inventory starts to decrease from the beginning, $w1$ increases initially due to the large density difference between

cold and hot legs. When the inventory falls down below 83.9%, $w1$ inverts the trend and starts to decrease.

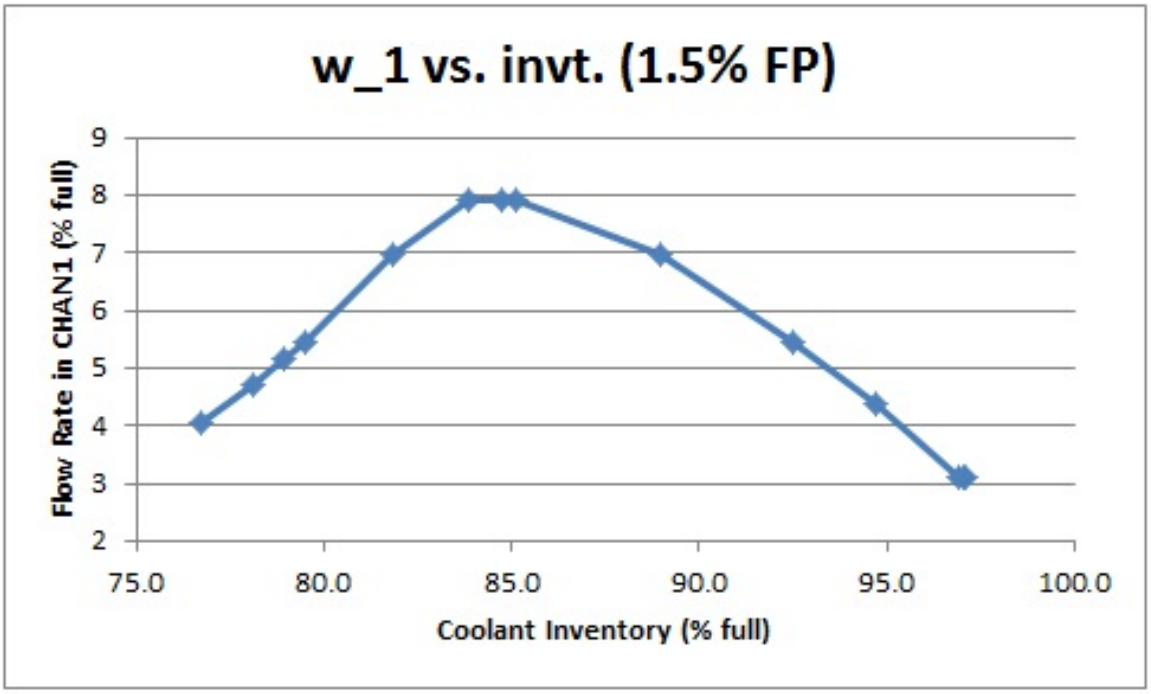

Figure 5.5: Flow rate in the loop increases first, and then decreases.

This might be the results of the competition between density driving head and flow resistance around the loop. In the first phase, as a result of decreasing inventory and the relatively stable channel power, the flow quality (x_{ROH}) and void fraction (α_{ROH}) of coolant fluid increase monotonically when flows leave the channels, as shown in Fig. 5.6 and 5.7. This will lower the density of fluid in the hot leg of the loop and increase the density difference between the cold and hot legs. Fig. 5.8 shows the declining mixture-density in ROH as the inventory decreases in the loop. Since the

density difference between the hot and cold legs is the driving force for natural circulation, flow rate increases as a result of increasing density difference. So this phase is identified as density-dominated phase.

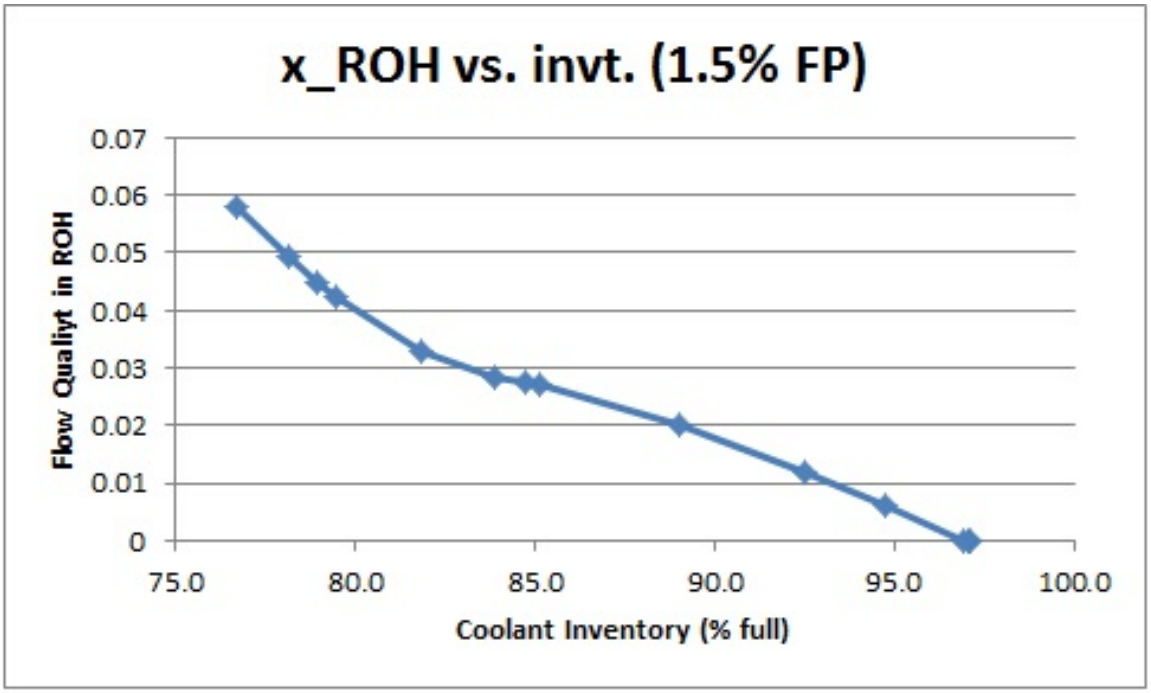

Figure 5.6: Flow quality of fluid in ROH

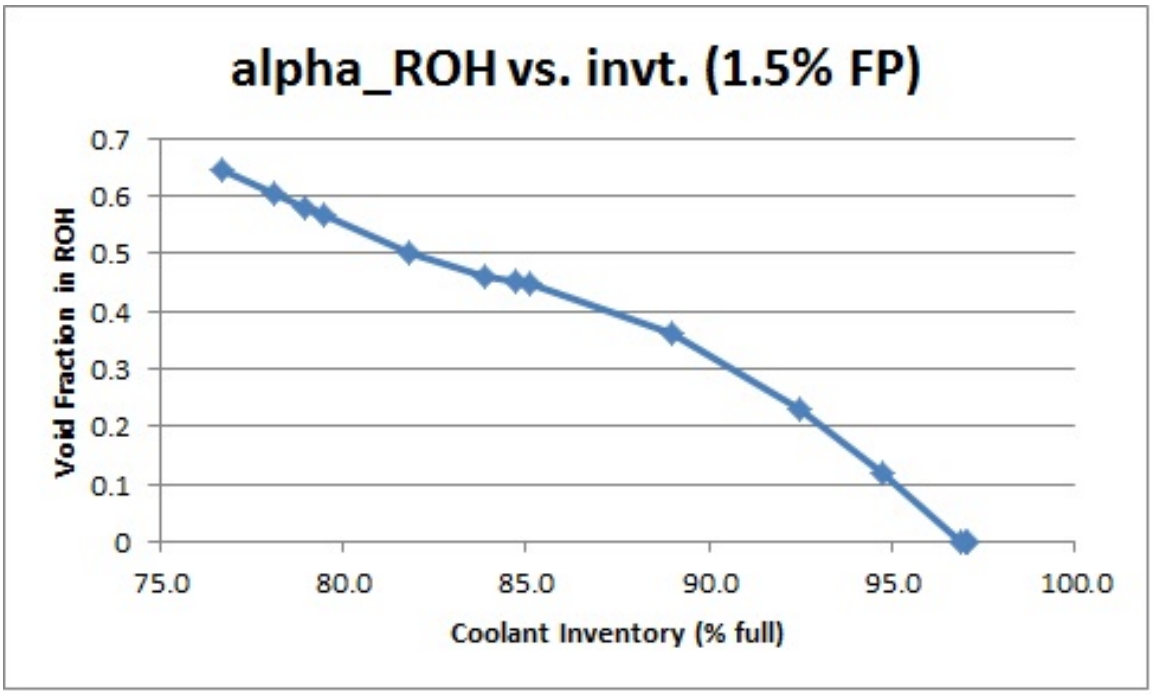

Figure 5.7: Void fraction of fluid in ROH

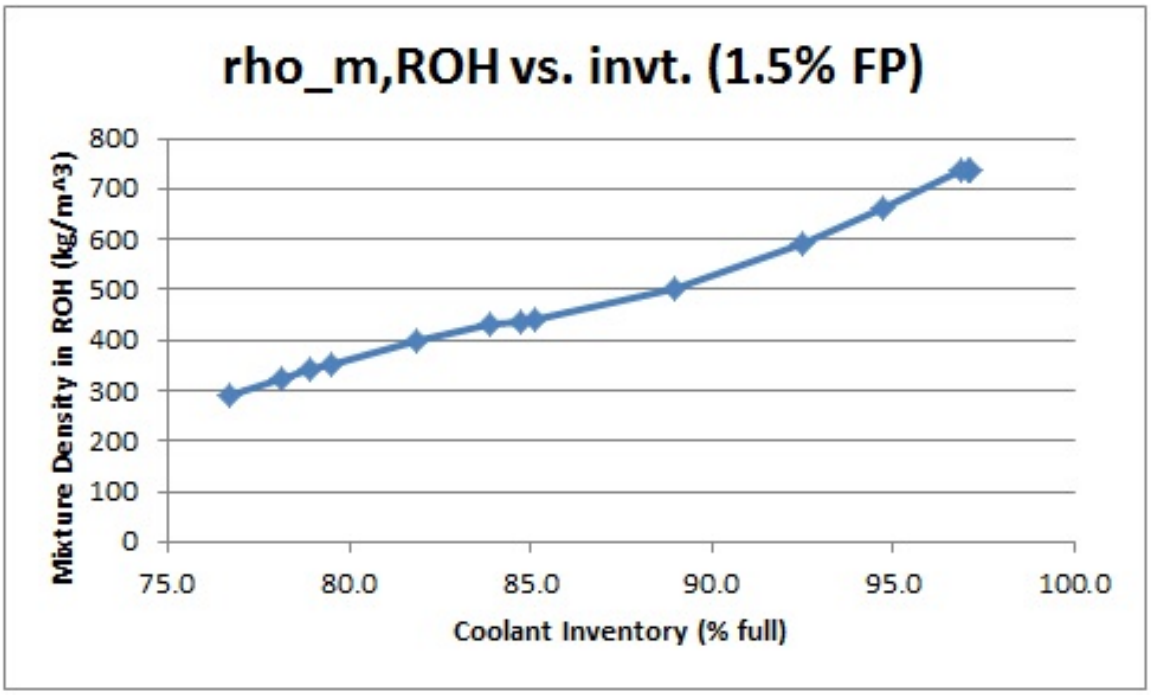

Figure 5.8: Void fraction of fluid in ROH

When inventory falls below 83.9%, vapor lock occurs at the top of SG, as discussed in previous paragraphs. The expansion of void and the blockage of the inverted U-tubes in SG, significantly increase the flow resistance across SG, so flow rate around the loop starts decreasing after the appearance of vapor lock. So this phase is identified as resistance-dominated phase.

Enthalpy in ROH, H_{ROH}

As a result of the inverted U-shape trend of flow rate(Fig. 5.5), the enthalpy in ROH has a U-shape trend, as illustrated in Fig. 5.9. As shown in Eq. 4.44, outlet enthalpy

of channels is determined by inlet enthalpy, channel power and flow rate through the channels. Since there is little variation in inlet enthalpy, which is close to the secondary side saturation enthalpy, the first term on the right-hand side of Eq. 4.44 will not change too much when inventory decreases. The channel power is the fixed boundary condition in the model. Therefore, outlet enthalpy largely depends on the flow rate on the denominator of second term on the right-hand side of Eq. 4.44. This makes outlet enthalpy have the opposite trend to that of flow rate.

$$H_{out} = H_{in} + \frac{\Delta Q}{w} \tag{4.44}$$

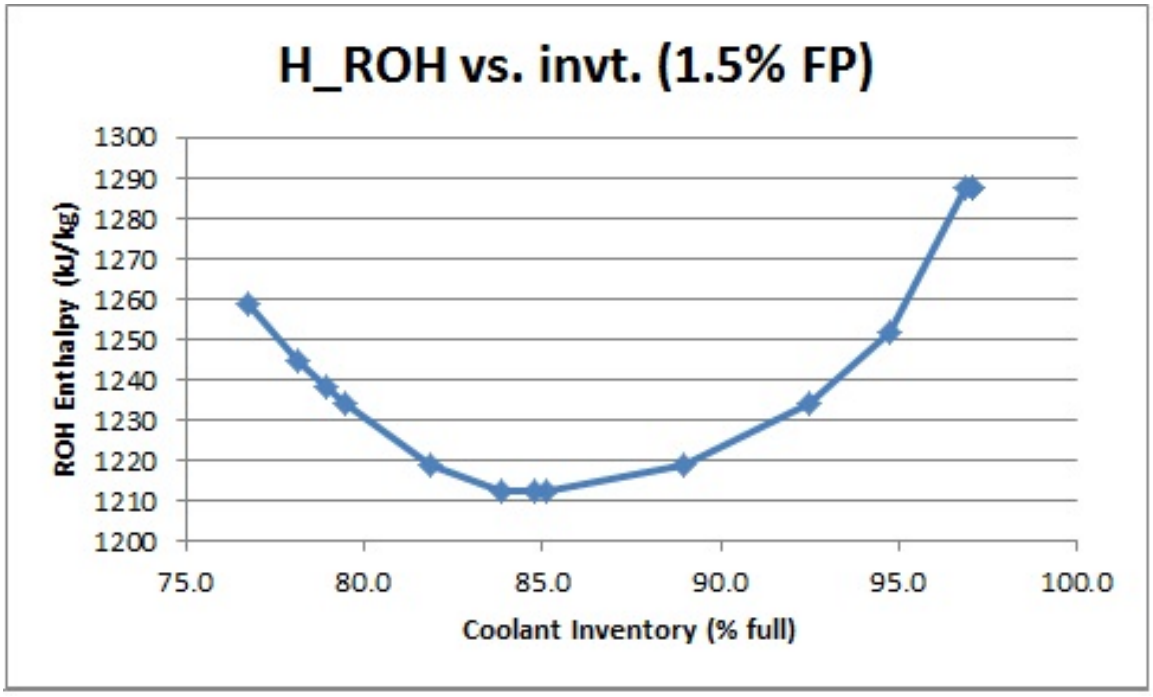

Figure 5.9: ROH enthalpy has an inverted U-shape trend with inventory decreasing.

Thermal Quality in ROH, x_{eROH}

$$x_e(p) = \frac{H_{out} - H_l(p)}{H_{fg}(p)} \tag{4.45}$$

Local thermal quality in ROH (x_{eROH}), as defined in Eq. 4.45, is determined by local enthalpy and local pressure. It can be seen in Fig. 5.10, as inventory decreases, thermal quality increases monotonically. It increases sharply until inventory touches 94.7%, after that it increases gently. This is due to the influence from local pressure. Before the inventory falls below 94.7%, the loop is depressurized rapidly, after that local pressure enters into a relatively flat stage, as shown in Fig. 5.2.

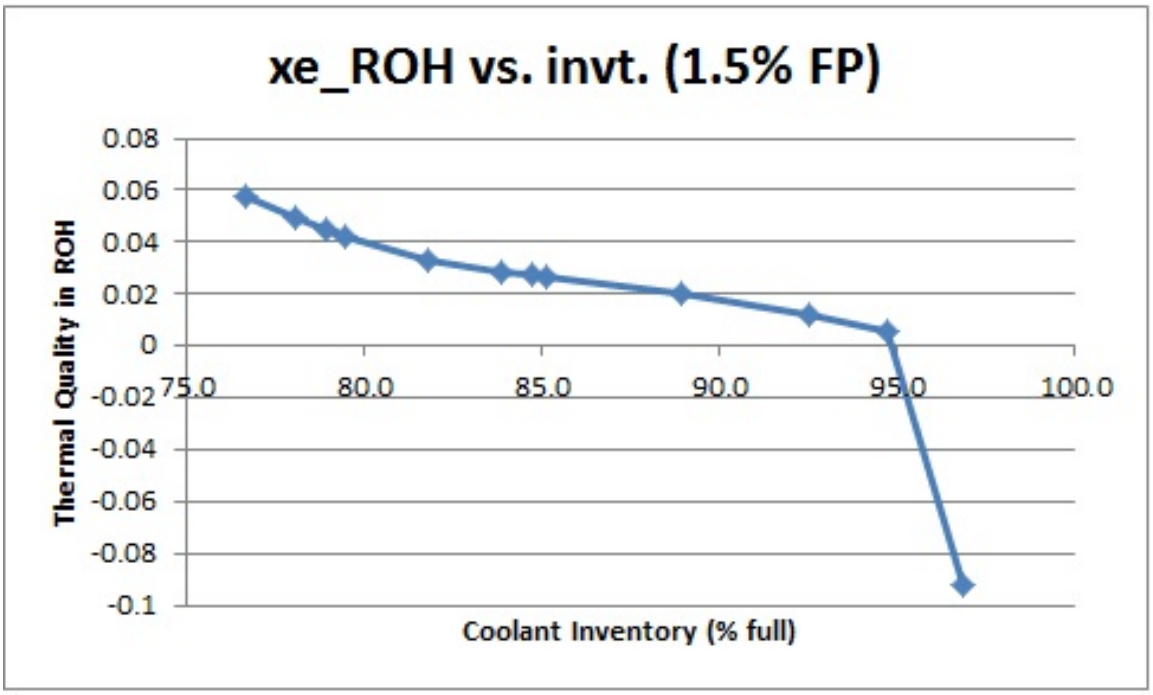

Figure 5.10: Thermal quality of fluid at ROH

Average Temperature of Headers, T_{ave}

The average temperature of fluid in RIH and ROH is analyzed by the model as below. Fig. 5.11 shows that the average temperature decreases as inventory decreases. This is due to the depressurization of HTS with loss of coolant inventory. The integrity of SG function is also important to the temperature of the primary side: Based on the assumption that SG maintains enough decay heat removal capability in this study, it can transfer all decay heat from the primary side to the secondary side. This will avoid the HTS heat-up phenomena that may happen in Station Blackout (SBO) accident because of the lack of SG heat removal capability, so T_{ave} can keep decreasing with inventory decreasing.

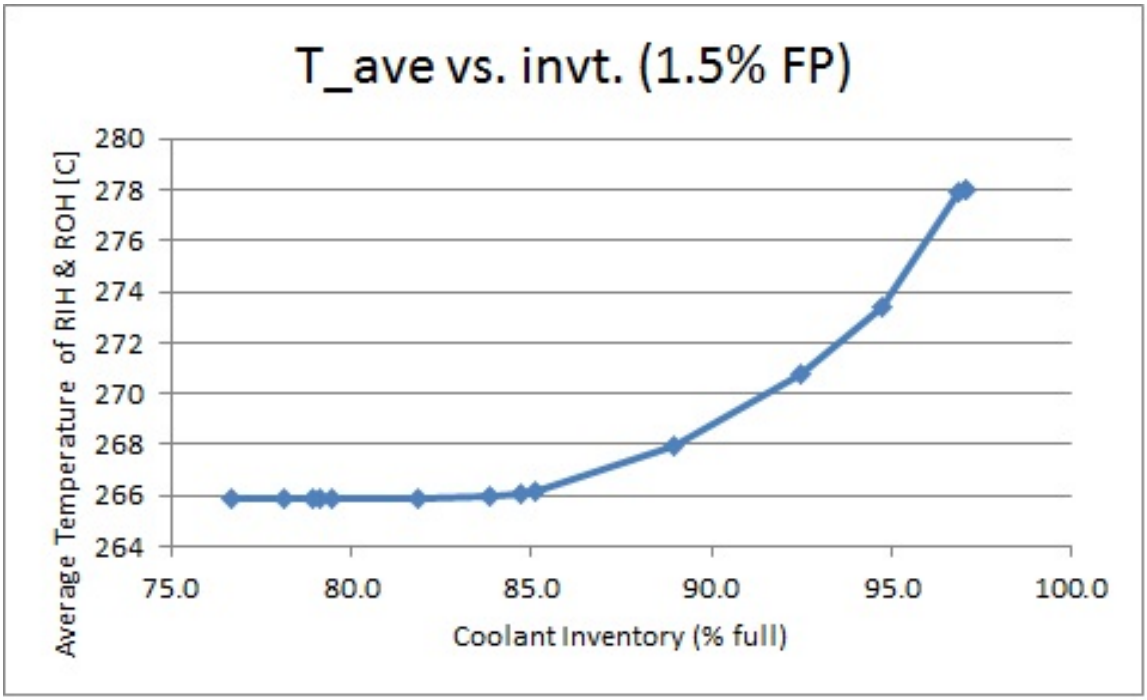

Figure 5.11: Average temperature of fluid in RIH and ROH

However, it should be noted that void fraction increases as a result of depressurization, and this may increase the danger of Critical Heat Flux (CHF). This phenomena is not discussed in this report.

5.2 Flow Reversal Phenomena

5.2.1 Reversal Preference

Fig. 5.12 shows RIH-to-ROH pressure difference predicted by the model when coolant inventory decreases from the initial conditions. In this simulation, the flows in all channels are set to be in normal forward direction (i.e., before the flow reversal). As labelled by ***DP_HH*** in the diagram, ΔP_{HH} is kept negative across the whole span of decreasing inventory, since the pressure at ROH is larger than that at RIH to drive flow over SG without any external pump driving force. With inventory decreasing, RIH-to-ROH pressure difference keeps decreasing and becomes more negative. It can be seen that the slope of curve ***DP_HH*** becomes sharper after the inventory falls below 83.9%, at which vapor lock first occurs at the very top of SG inverted U-tubes, as illustrated in Fig. 5.4. The appearance of vapor lock increases the flow resistance across SG, and forms a larger pressure drop from ROH to RIH. With the further expansion of vapor lock, its effect on ***DP_HH*** is amplified.

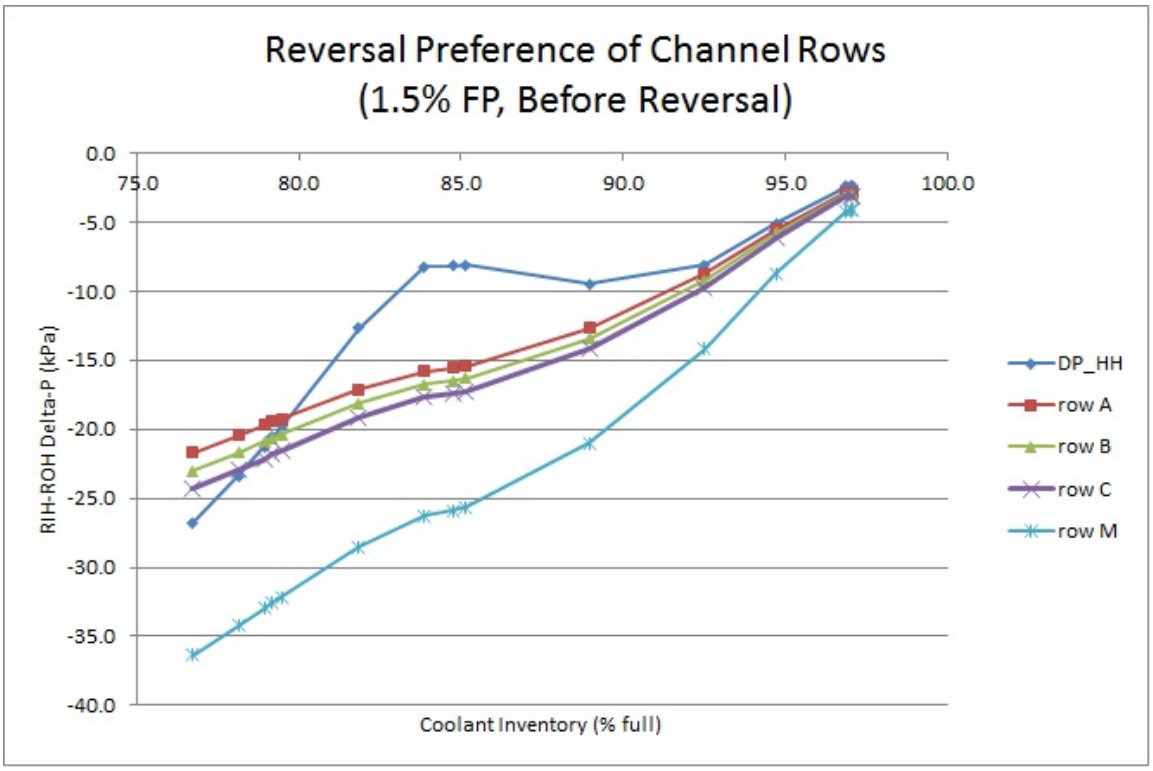

Figure 5.12: ΔP_{HH} vs. ΔP_{rev} when all channels are unidirectional

Also shown in Fig. 5.12 are the corresponding pressure differences that are required to reverse the flows in channel row A, B, C and M, as shown in Fig. 4.8. As defined in Eq. 4.68, ΔP_{rev} is more negative than ΔP_{HH} initially, as illustrated in Fig. 5.12, so flows in related channels cannot reverse in this situation. With the ongoing of loss of coolant inventory and the occurrence of vapor lock in SG, ΔP_{HH} becomes more negative than ΔP_{rev}. The curves of different ΔP_{rev} for different channel rows intersect with the curve of ΔP_{HH}, as indicated in Fig. 5.12. These intersection points label the inventory levels at which the flows in the corresponding channel rows will reverse direction. The earlier the intersection point shows up, the higher reversal

preference the corresponding row has. Therefore, the top channels in row A in Fig. 4.8 have the highest preference to reverse, since ΔP_{rev} of row A is the smallest one due to the shortest elevation difference of feeders and the lowest local pressure among all rows of channels. The subsequent rows are from row B to row C, etc., as indicated in Fig. 5.12. It should be noted that the curve of ΔP_{rev} for row M, which is close to the vertical centreline of all rows in Fig. 4.8, does not have intersection with the curve of ΔP_{HH} in Fig. 5.12. This means row M has a really low reversal preference, and will not reverse when loss of inventory proceeds to this level.

According to Fig. 5.12 and the analysis above, the flow reversal phenomenon will first appear in row A at the inventory level of about 79.5%.

5.2.2 Proceeding of Flow Reversal

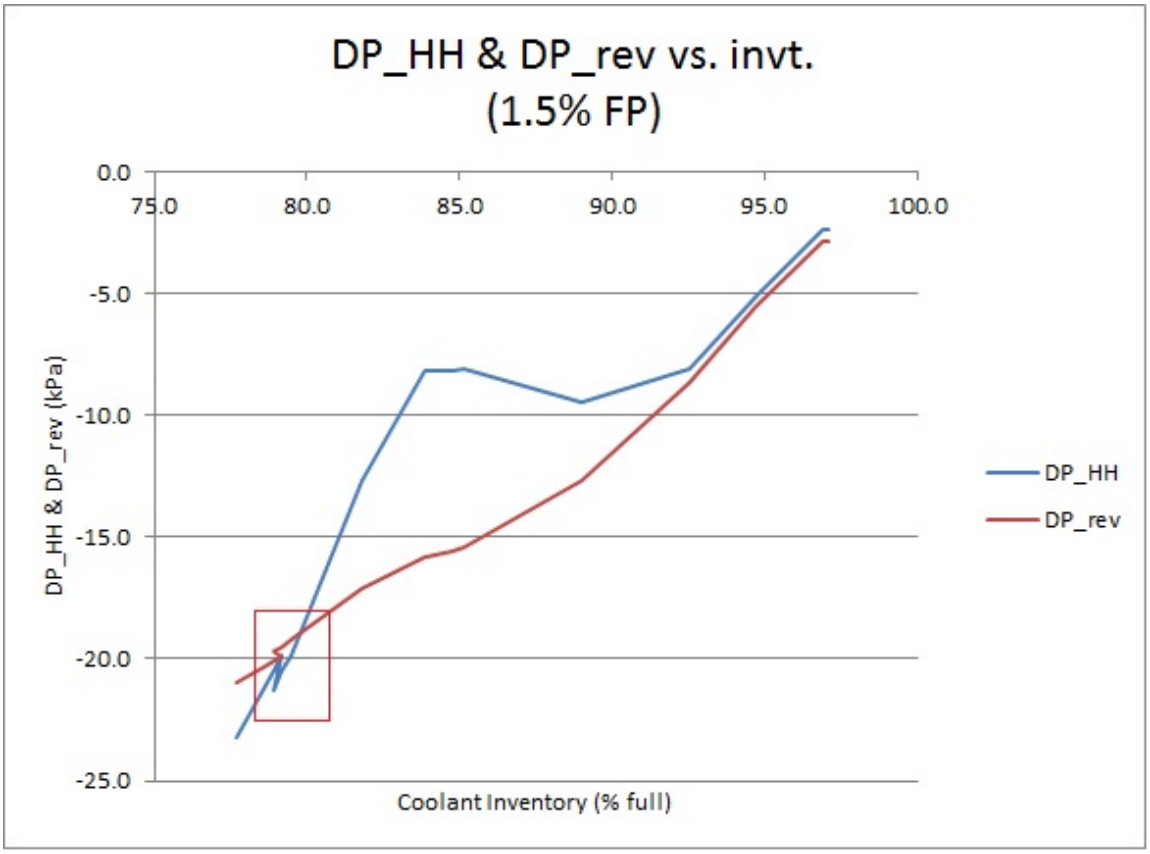

Figure 5.13: ΔP_{HH} vs. ΔP_{rev} after the appearance of flow reversal

Fig. 5.13 illustrates the relationship between ΔP_{HH} and ΔP_{rev} from the inventory level at which all rows are unidirectional, to the level at which more and more rows reverse flow direction. Based on the results of simulation, when inventory falls below 79.5%, flow reversal occurs in row A, and then the combination of row A and B fulfills the flow reversal criteria when inventory falls to 78.6%.

As shown by the red box in Fig. 5.13, the first time flow reversal happens, i.e., when flow reverses in row A, the HTS goes through an adjusting process. There is a short period of fluctuation. As shown in Table 5.1, when inventory is fixed at 79.2%, ΔP_{rev} for row B is -20.1 kPa before the reversal, while it becomes -19.9 kPa after the reversal. The similar phenomena happen when inventory is 78.9%. This means flow reversal in row A lowers the required pressure difference to reverse flow in row B. This is probably because low-density coolant in ROH flows back to RIH via CHAN2 branch by bypassing heat sink SG(Fig. 4.3), and this low-density coolant flows into the cold leg of inlet feeders and reduces the density of fluid in the cold leg, so due to Eq. 4.68, ΔP_{rev} decreases in absolute value. Flow reversal also has influence on the pressure at RIH. As shown in Table 5.1, flow reversal increases the pressure in RIH slightly. Flow reversal creates a new flow path bypassing SG that has a high flow resistance after vapor-lock, and decreases the pressure drop from ROH to RIH. As a result, pressure in RIH can be increased a little.

Table 5.1: Reversal in row A has an influence in $\Delta_{P_{rev}}$ in row B.

Items	Before Reversal		After Reversal	
Inventory (%)	$\Delta_{P_{rev}}$ for row B (kPa)	P_{RIH}	$\Delta_{P_{rev}}$ for row B (kPa)	P_{RIH}
79.2	-20.1	5.139	-19.9	5.140
78.9	-20.3	5.138	-20.1	5.139

Another thing that should be noted is that, in this study, the simulation just provides pressure and flow variations before row C reverses direction. When more and more rows reverse, it becomes more and more difficult to find the appropriate flow

rates for different flow loops to make the iteration process converge. There is a significant increase in time cost for numerical calculation, so the subsequent simulation is terminated.

Tables below summarize various HTS thermal hydraulic characters with continuous depressurization. Table 5.2 collects the number of reversed rows and channels, as well as N_{block} with RIH pressure decreasing. Table 5.3 shows the variations of flow rates in CHAN1,SG and CHAN2 branches. Table 5.4 summarizes the enthalpies in IF2 outlet, DN outlet, RIH and ROH with ongoing depressurization. Table 5.5 shows the heat addition in CHAN1 and CHAN2 branches, as well as heat removal in SG branch, and a heat balance bias is calculated in the table as well.

Table 5.2: Number of reversed rows and channels with decreasing RIH pressure, and vapor-locked boiler tubes

P_{RIH}	reversed rows	No. of reversed channels	N_{block}
Mpa			
11.300	0	0	0.00
11.000	0	0	0.00
10.000	0	0	0.00
6.500	0	0	0.00
6.000	0	0	0.00
5.500	0	0	0.00
5.200	0	0	0.00
5.190	0	0	0.00
5.170	0	0	0.00
5.150	0	0	0.72
5.140	0	0	0.87
5.139	0	0	0.88
5.138	0	0	0.88
5.140	A	2	0.87
5.139	A	2	0.88
5.138	A	2	0.88
5.135	A+B	6	0.90

Table 5.3: Flow rates in CHAN1, SG and CHAN2 branches

P_{RIH}	flow rate in CHAN1		flow rate in SG		flow rate in CHAN2	
	of normal flow	value	of flow in CHAN1	value	of flow in CHAN1	value
MPa	%	kg/s	%	kg/s	%	kg/s
11.300	3.1	82.3	100.000	82.3	0.000	0.0
11.000	3.1	82.3	100.000	82.3	0.000	0.0
10.000	3.1	82.3	100.000	82.3	0.000	0.0
6.500	4.4	116.3	100.000	116.3	0.000	0.0
6.000	5.5	145.8	100.000	145.8	0.000	0.0
5.500	7.0	185.9	100.000	185.9	0.000	0.0
5.200	7.9	211.5	100.000	211.5	0.000	0.0
5.190	7.9	211.4	100.000	211.4	0.000	0.0
5.170	7.9	211.5	100.000	211.5	0.000	0.0
5.150	7.0	186.2	100.000	186.2	0.000	0.0
5.140	5.5	145.6	100.000	145.6	0.000	0.0
5.139	5.3	141.6	100.000	141.6	0.000	0.0
5.138	5.2	137.6	100.000	137.6	0.000	0.0
5.140	5.5	145.8	98.833	144.1	1.167	1.7
5.139	5.3	141.6	98.792	139.9	1.208	1.7
5.138	5.2	137.5	98.750	135.8	1.250	1.7
5.135	4.7	125.2	98.667	123.5	1.333	1.7

Table 5.4: Enthalpies in different locations of loop

P_{RIH}	$H_{IF2,out}$	$H_{DN,out}$	H_{RIH}	H_{ROH}
MPa	kJ/kg	kJ/kg	kJ/kg	kJ/kg
11.300	0	1164	1164	1288
11.000	0	1164	1164	1288
10.000	0	1164	1164	1288
6.500	0	1164	1164	1252
6.000	0	1164	1164	1234
5.500	0	1164	1164	1219
5.200	0	1164	1164	1212
5.190	0	1164	1164	1212
5.170	0	1164	1164	1212
5.150	0	1164	1164	1219
5.140	0	1164	1164	1234
5.139	0	1164	1164	1236
5.138	0	1164	1164	1238
5.140	1378	1164	1166	1235
5.139	1380	1164	1166	1237
5.138	1381	1164	1166	1239
5.135	1393	1164	1166	1246

Table 5.5: Heat injected in CHAN1 and CHAN2, and removed in SG

P_{RIH}	Q_{CHAN1}	Q_{CHAN2}	Q_{inject}	Q_{remove}	$\Delta Q = (Q_{inject}\text{-}Q_{remove})/Q_{remove}$*100%
MPa	kw	kw	kw	kw	%
11.300	10160	0	10160	10160	0.00
11.000	10160	0	10160	10160	0.00
10.000	10160	0	10160	10160	0.00
6.500	10160	0	10160	10160	0.00
6.000	10160	0	10160	10160	0.00
5.500	10160	0	10160	10160	0.00
5.200	10160	0	10160	10160	0.00
5.190	10160	0	10160	10160	0.00
5.170	10160	0	10160	10160	0.00
5.150	10160	0	10160	10160	0.00
5.140	10160	0	10160	10160	0.00
5.139	10160	0	10160	10160	0.00
5.138	10160	0	10160	10160	0.00
5.140	10066	245	10311	10160	1.49
5.139	10066	245	10311	10160	1.49
5.138	10066	245	10311	10160	1.49
5.135	10066	245	10311	10160	1.49

5.3 The influence of decay heat on reversal

Channel power is one of three thermal hydraulic boundary conditions applied in this model. It plays a significant role in influencing the thermal hydraulic behavior in the simulation. Fig. 5.14 shows the variations of ΔP_{HH} and ΔP_{rev} with decreasing coolant inventory, when decay heat of fuel channels is set as 1.0% of FP, compared to 1.5% of FP used in Fig. 5.12.

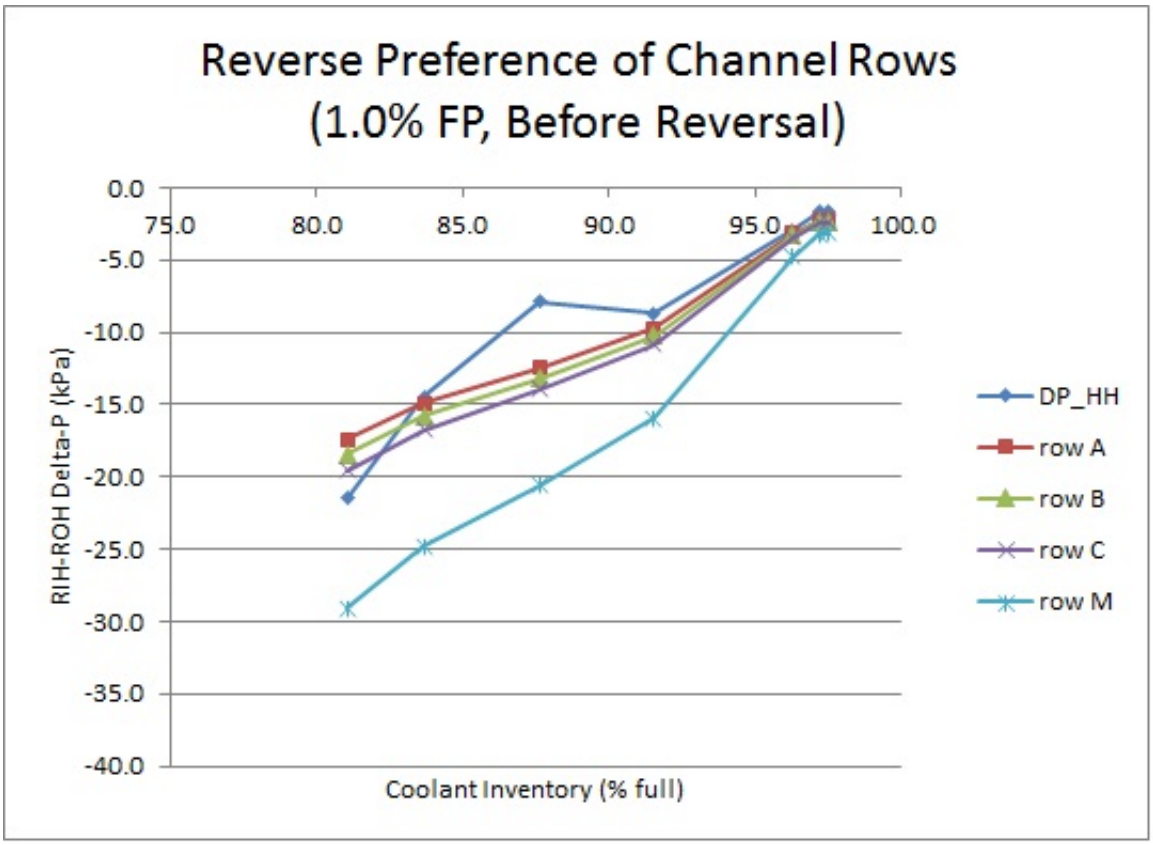

Figure 5.14: ΔP_{HH} vs. ΔP_{rev} when decay heat is 1.0% FP

As illustrated in Fig. 5.14, ΔP_{HH} and ΔP_{rev} still have negative values and declining trends when inventory keeps decreasing, but the positions of intersection points of curves are different. When decay heat is 1.0% of FP, flow reversal occurs in row A when inventory is about 83.3%, instead of 79.5% in 1.5% FP case. The inventory level at which flow reverses is brought forward.

On the one hand, the lower decay heat contributes to the depressurization of the primary loop, and accelerates the appearance of vapor lock at the very top of SG inverted U-tubes. This makes RIH-ROH pressure difference decrease earlier. On the other hand, lower decay heat leads to the lower hot leg temperature and smaller densiyt difference between the legs. This decreases the driving force of the forward-direction flow, so the occurrence of flow reversal is brought forward. Fig. 5.15 compares the pressures at the very top of SG inverted U-tubes for 1.5% FP and 1.0% FP as a function of inventory. As shown in the diagram, the curve for 1.0% FP has a sharper slope and reaches the inflection point earlier than that for 1.5% FP, so this means depressurization rate is faster in 1.0% FP case than in 1.5% FP case. This is probably due to the lower temperature as a result of the lower decay heat.

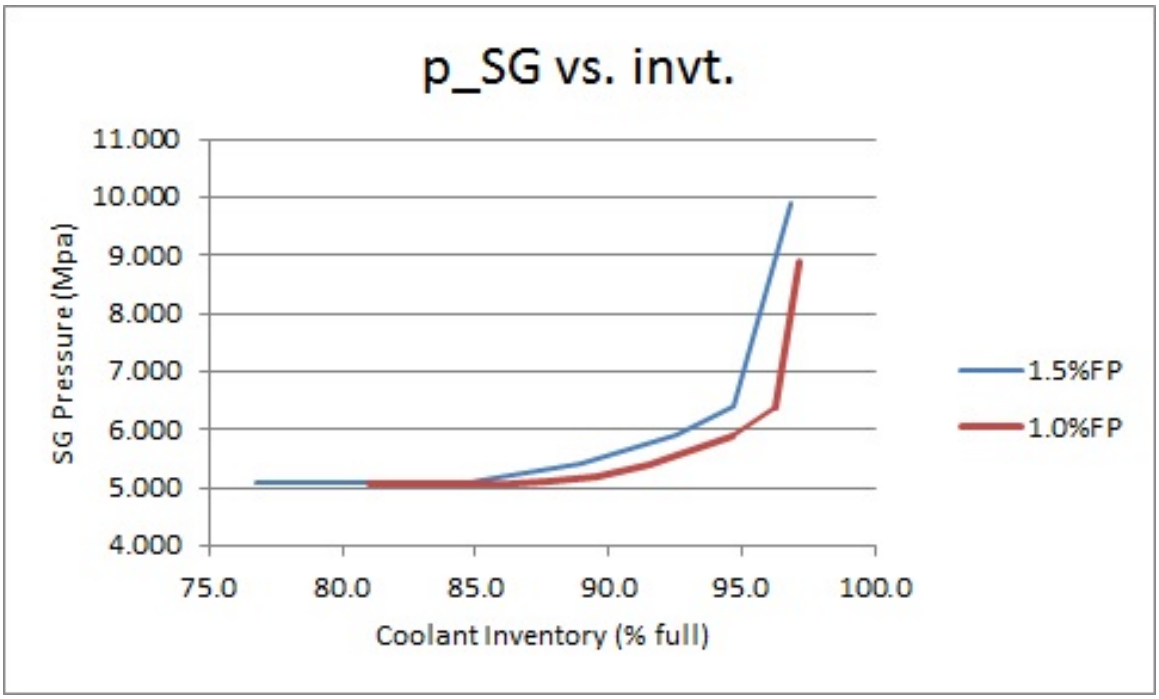

Figure 5.15: $P_{SG,top}$ vs. Inventory for 1.5% FP and 1.0% FP

Fig. 5.16 compares N_{block} variations for different channel power levels. With inventory decreasing, vapor lock occurs earlier for 1.0% FP than for 1.5% FP. This means low channel power is more sensitive to the loss of coolant inventory.

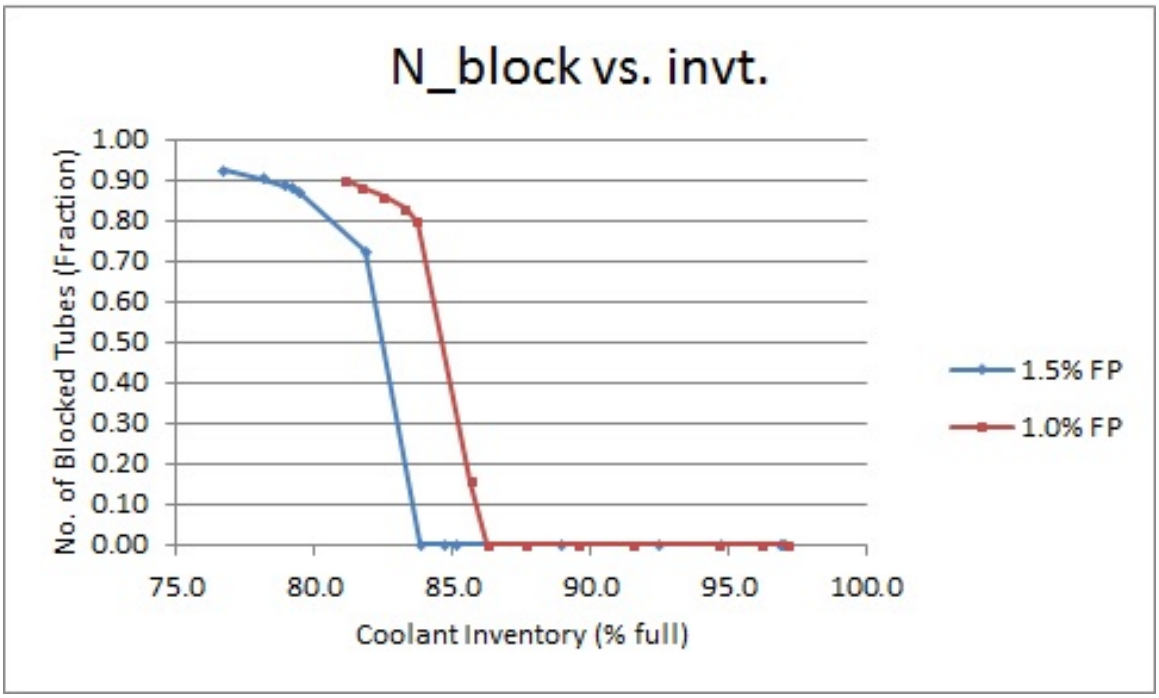

Figure 5.16: N_{block} vs. Inventory for 1.5% FP and 1.0% FP

The comparisons of results between 1.5% FP and 1.0% FP indicate the significance of initial power level. Since the channel power follows an exponential decay trend after reactor trip, the initial power and the time elapsed from reactor trip decide the power level afterwards. And they can further influence HTS thermal hydraulic behavior when coupled with coolant inventory. Therefore, the initial condition of channel power is very important in this kind of accident safety analysis.

Chapter 6

Conclusion and Future Work

6.1 General Conclusion

A quasi-steady state HEM thermal hydraulic model has been built to simulate the thermal hydraulic behavior of CANDN 9 PHTS under the initiating events of small LOCA with loss of Class IV power and the failure of ECI. The variations of pressure, flow and other thermal hydraulic parameters have been investigated with this model. In addition, a study in flow reversal and its subsequent consequences has been conducted as well, and it provides a good insight into the flow reversal phenomena. Several conclusions have been drawn from the analysis:

1. The model can simulate and reflect the thermal hydraulic behavior of CANDU 9 under the assumed initiating events.

2. The loss of coolant inventory and the subsequent depressurization have significant influences on the HTS thermal hydraulic behavior. The depressurization of HTS results in the generation of void at the very top of boiler tubes in SG. The

expanding void blocks an increasing number of inverted U-tubes and increases the flow resistance in SG flow path. This phenomenon is called vapor lock.

3. The occurrence of vapor lock increases the pressure drop from ROH to RIH across SG. A negative RIH-to-ROH pressure difference has formed as a result of vapor lock and the large pressure drop in SG. The model predicts an increasingly negative RIH-to-ROH pressure differential with reduced inventory and amplified vapor lock effect.

4. The occurrence of flow reversal has been predicted as a result of counter force balance, when the negative RIH-to-ROH pressure difference overcomes the initial driving head due to density difference between the hot leg and the cold leg.

5. The reversal preference of fuel channel rows, i.e., which row has largest potential to reverse with inventory decreasing, has been investigated by the model. It is found that channels in row A have the highest reversal preference, then followed by the ones in row B, and in that order subsequently.

6. The flow reversal occurs first in row A when inventory decreases to about 79%, with following boundary conditions: decay heat is 1.5% FP and secondary side pressure is 5.07 MPa.

7. The decay heat level, one of boundary conditions used in the model, has a significant influence on HTS thermal hydraulic behavior. The decrease in channel power accelerates the depressurization process and brings forward the occurrence of flow reversal in fuel channels.

6.2 Future Work

The study has completed its initial target to investigate the thermal hydraulic behavior under the circumstance of assumed accident scenarios. However, to better understand the thermal hydraulic variations in HTS and to improve the accuracy of the prediction by the models, more work can be done in the future.

Although it can well analyze the trends and obtain approximate magnitudes of values, the quasi-steady state model used in this study is still simple, and many improvements can be made on this model.

First, since a simplified SG module is applied in this simulation, the detailed thermal hydraulic information in SG is lost in calculation process. To get this information, a more complicated SG module with more appropriate and accurate heat transfer correlations can be used in the future. On the other hand, the case in which the flow over SG is zero(i.e., all boiler tubes are vapor locked) is not considered in the simulation. An extra model should be developed to simulate the heat transfer mode of reflux condensation by boiler tubes: The heated lower-density coolant arises up to SG while cooled higher-density coolant flows back to channels due to buoyancy force. The reflux occurs within one leg of the HTS in the absence of flow over the top of SG.

Second, the flow conditions and pressure losses within headers and feeders are not very explicit, as the geometry conditions in these sections are complicated and it is difficult to get the accurate pressure drop in these sections based on current model.

More geometry details can be added to optimize the model.

Third, since this is a quasi-steady state model, it is inherently short of information about time, so transient state problems can not be directly analyzed by the model. To make the model more powerful, a transient state model can be built in the future with time-dependent factors taken into account.

Fourth, as the model is based on HEM, the details such as subcooled boiling have been ignored during the calculation. This may weaken the accuracy of the results. To improve the validation of the model, some heterogeneous options can be added in the model.

Appendix A

RD-14M Test Facility

RD-14M is a multiple-channel integral thermal hydraulic test facility that is designed with full-elevation and full-scale of CANDU PHTS. As shown in Fig. A.1, it arranges components in a figure-of-eight heat transport circuit, and can produce similar mass transit times and pressure gradient as it is in CANDU HTS under forced or natural circulation conditions.

Many tests have been conducted on this facility and its predecessors, RD-12 and RD-14, and the tests results have been used for various functions including code validation, reactor safety analysis and flow stability modelling, etc. For example, Ingham et al [15][16] investigated the natural circulation in CANDU with RD-14M, Wan et al [26] studied the onset of flow reversal in RD-14M to test the criteria to determine the occurrence of flow reversal. The test results in RD-14M are important landmarks in thermal hydraulic analysis.

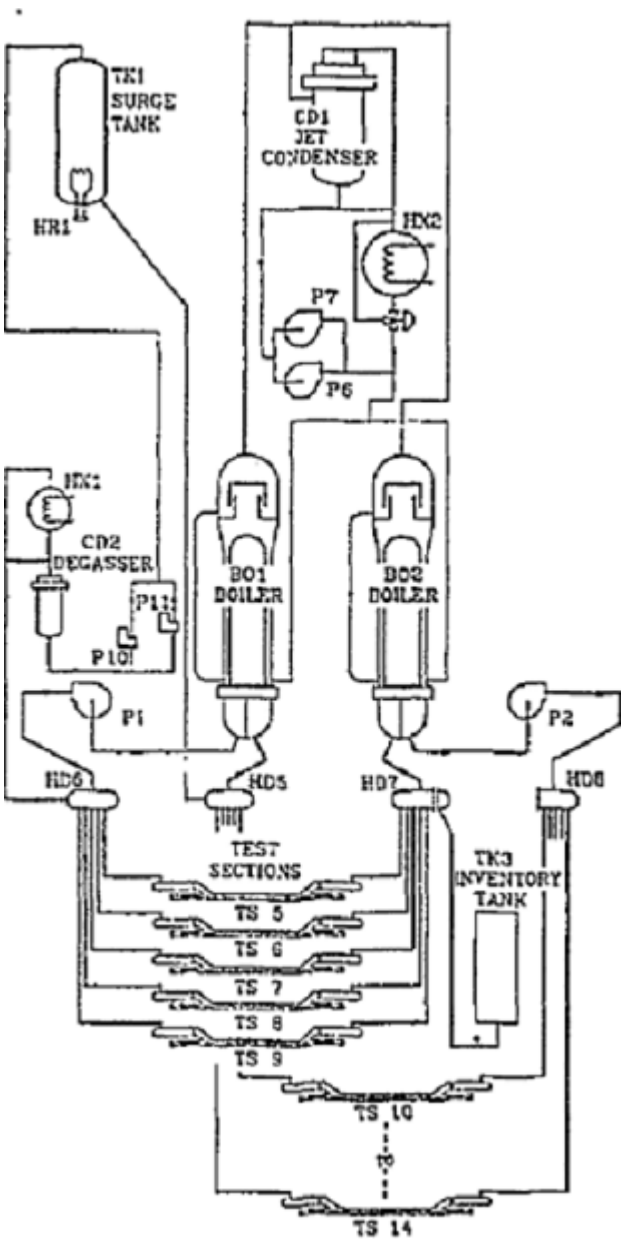

Figure A.1: Schematic of RD-14M [15]

Bibliography

[1] K. H. Ardron, V. S. Krishnan, G. R. McGee, J. W. D. Anderson, and E. H. Hawley. Two-phase natural circulation experiments in a pressurized water loop with figure-of-eight symmetry. In *International Atomic Energy Agency, Vienna (Austria). Technical Committee on Thermal Reactor Safety Research*, pages 99–113, jul 1984.

[2] M. Awad and Y. Muzychka. Effective property models for homogeneous two-phase flows. *Experimental Thermal and Fluid Science*, 2008.

[3] G. T. Bereznai and G. Harvel. Introduction to candu systems and operation. 2011.

[4] S. M. Corporation. Incoloy alloy 800. URL `http://www.specialmetals.com/assets/documents/alloys/incoloy/incoloy-alloy-800.pdf`.

[5] F.B.P.Tran and W. Garland. Modelling of two phase flow instability under natural circulation conditions using nodal transmission matrices. In *12th Simulation Symposium of Reactor Dynamics and Plant Control*, Hamilton, Ontario. McMaster University.

[6] W. J. Garland. Nuclear reactor process systems: Thermal hydraulic analysis. Technical report, Department of Engineering Physics McMaster University, 1998.

[7] W. J. Garland and S. H. Pang. Candu-600 heat transport system flow stability. *NUCLEAR TECHNOLOGY*, 75:239–260, dec 1986.

[8] P. Gulshani and H. Huynh. Mmoss-i: A candu multiple-channel thermosyphoning flow stability model. In *15 Annual Conference of CNS*, Saskatoon, Saskatchwan, jun 1995. Canadian Nuclear Society.

[9] P. Gulshani and N. Spinks. A simple stability criterion for candu figure-of-eight flow oscillations. In *International conference on numerical methods in nuclear engineering*, pages 155–175, Montreal (Canada), sep 1983.

[10] P. Gulshani and N. J. Spinks. A candu figure-of-eight flow stability model. *NUCLEAR SCIENCE AND ENGINEERING*, pages 412–424, jun 1984.

[11] P. Gulshani, D. Mori, J. Barkman, H. Huynh, and P. Thompson. Analysis of rd-14m two-phase thermosyphoning experiments and associated cathena simulation results. In *13th Annual Conference of the Canadian Nuclear Society*, volume 2, pages 483–511, Saint John, New Brunswick, jun 1992. Canadian Nuclear Society.

[12] P. Gulshani, H. Huynh, and P. Thompson. A model for computing two-phase pressure drop in vertical u-tube steam generator and its application to thermosyphoning. In G. ARCHINOFF, A. OLIVIA, H. HUYNH, and P. DESBIENS, editors, *FOURTH INTERNATIONAL CONFERENCE ON SIMULATION METHODS IN NUCLEAR ENGINEERING*, volume 1, pages 74–94, MONTREAL,

CANADA, jun 1993. Canadian Nuclear Society and AMERICAN NUCLEAR SOCIETY.

[13] P. Gulshani, H. Huynh, and A. Galia. A candu multiple-channel thermosyphoning flow stability model. In *Canadian Nuclear Society 15th annual conference proceedings*, volume 1, pages 636–656, Montreal, jun 1994. Canadian Nuclear Society.

[14] Holman. *Heat Transfer*. third edition.

[15] P. Ingham, J. Luxat, A. Melnyk, and T. Sanderson. Natural circulation in an integral candu test facility. In *Technical committee meeting on experimental tests and qualification of analytical methods to address thermohydraulic phenomena in advanced water cooled reactors*, pages 201–212.

[16] P. Ingham, T. Borgford, and J. Mallort. two-phase natural circulation experiments in the rd-14m multiple-channel candu thermalhydraulics test facility. 1989.

[17] J. Jiang. *CHAPTER 11 Electrical Systems*. UNENE, aug 2015.

[18] J. C. LUXAT. Thermal-hydraulic aspects of progression to severe accidents in candu reactors. *NUCLEAR TECHNOLOGY*, 167:187–210, jul 2009.

[19] J. Mallory and P. Ingham. Cathena simulation of thermosiphoning in a pressurized-water test facility. *NUCLEAR JOURNAL OF CANADA*, pages 240–249.

[20] S. Osamusali. Tuf validation: Modelling of header-to-header pressure differential under two-phase natural circulation conditions using rd-14m experiments. 2000.

[21] P. SABOURI. Large loca beau analysis of a generic 900 mw candu plant. Applied science, McMaster University, Hamilton, Ontario, Canada, jun 2010.

[22] P. Soedijono, S. Osamusali, A. Tahir, and P. Wan. A mechanistic model to predict phh under two-phase natural circulation flow and comparison against experimental results in rd-14m. In *Twenty Second Annual Conference of the Canadian Nuclear Society*, Toronto, Ontario, Canada, jun 2001. Canadian Nuclear Society.

[23] J. Spencer. Analysis of intermittent buoyancy induced flow in asymmetrically obstructed candu nuclear reactor fuel channels. Master's thesis, McMaster University, 2010.

[24] N. Spinks, A. Wright, M. Caplan, S. Prawirosoehardjo, and P. Gulshani. Thermosyphoning in the candu reactor. In *Fifth International Meeting on Thermal Nuclear Reactor Safety*, volume 1, pages 376–384, Karlsruhe, sep 1984. ENS and KTG and ANS and Nuclear Research Center Karlsruhe.

[25] N. E. Todreas and M. S. Kazimi. *NUCLEAR SYSTEMS I Thermal Hydraulic Fundamentals*, volume 1. 1990.

[26] P. Wan, W. Midvidy, and J. Luxat. Onset of channel flow reversal in rd-14m natural circulation tests. In *13th Annual Conference of the Canadian Nuclear Society*, volume 2, Saint John, New Brunswick, jun 1992. Canadian Nuclear Society.

[27] P. Wan, W. Midvidy, and J. Luxat. Modelling of rd-14m partial-inventory thermosiphoning tests using the ohat code. In G. ARCHINOFF, A. OLIVIA,

H. HUYNH, and P. DESBIENS, editors, *FOURTH INTERNATIONAL CONFERENCE ON SIMULATION METHODS IN NUCLEAR ENGINEERING*, volume 1, pages 95–96, MONTREAL, CANADA, jun 1993. Canadian Nuclear Society and AMERICAN NUCLEAR SOCIETY.

[28] P. Wan, J. Amrouni, J. Anderson, A. Melnyk, and R. Leung. Some ideas on thermosyphoning in a heat transport loop. In *CNS proceedings of the 1997 CNA/CNS annual conference on powering Canada's future*, volume 1,2, page 1122, Canada, 1997. CNA/CNS.